

MUIZENBERG BEACHFRONT UPGRADE – SPECIALIST COASTAL MODELLING

Wave and Sediment Transport Modelling Report

REV.B

22 August 2022



City of Cape Town
Muizenberg, Cape Town, South Africa



CITY OF CAPE TOWN
ISIXEKO SASEKAPA
STAD KAAPSTAD

MUIZENBERG BEACHFRONT UPGRADE – SPECIALIST COASTAL MODELLING

Wave and Sediment Transport Modelling Report

S2135-RP-CE-001-RB

22 August 2022

REV.	TYPE	DATE	EXECUTED	CHECK	APPROVED	CLIENT	DESCRIPTION / COMMENTS
A	A	22/7/2022	LH/SK	PMH	SAL		Draft
B	C	22/08/2022	LH/SK	PMH	SAL		Addressed CCT comments.

TYPE OF ISSUE: (A) Draft (B) To bid or proposal (C) For Approval (D) Approved (E) Void

City of Cape Town
Muizenberg, Cape Town, South Africa



CITY OF CAPE TOWN
ISIXEKO SASEKAPA
STAD KAAPSTAD

TABLE OF CONTENTS.....	I
1. INTRODUCTION	1
1.1 Project background	1
1.2 Terms of reference	2
1.3 Scope of work.....	3
1.4 Assessed return periods.....	4
1.5 Report structure.....	4
2. BATHYMETRIC SURVEY.....	5
2.1 Survey scope	5
2.2 Survey results	5
3. CLIMATE CHANGE.....	7
3.1 Introduction	7
3.2 Basis	7
3.3 Sea level rise.....	7
3.4 Storm surge	8
3.5 Extreme wave height	8
3.6 Summary	9
4. WATER LEVEL ANALYSIS	10
4.1 Measured water levels.....	10
4.2 Storm surge	10
4.3 False Bay wind set-up.....	11
4.3.1 Model description	11
4.3.2 Mesh and bathymetry	12
4.3.3 Boundary conditions.....	14
4.3.4 Results	14
4.4 Extreme water levels.....	16
5. NEARSHORE WAVE CLIMATE.....	18
5.1 Introduction	18
5.2 Model description	18
5.3 Regional wave model	18
5.3.1 Water level	20
5.3.2 Waves	20
5.3.3 Wind	20
5.3.4 Model parameters.....	21
5.4 Nested wave model	21
5.4.1 Mesh and bathymetry	21
5.4.2 Boundary conditions.....	23
5.5 Calibration.....	24
5.6 Modelling period	27
5.7 Results.....	27
5.7.1 Extreme waves	27
5.7.2 Operational waves.....	31
6. NEARSHORE EXTREME WATER LEVELS AND WAVES.....	33
6.1 Joint probability of storm surge and wave height.....	33
6.2 Extreme conditions	37
7. COASTLINE STABILITY	39
7.1 Coastline trends from historical data.....	39
7.1.1 Historical aerial imagery	39
7.1.2 Beach lowering	41
7.1.3 Wetted line analysis	43

7.1.4	Historical beach profile analysis	45
7.1.5	Summary	50
7.2	Coastline recession due to sea level rise.....	50
7.3	Longshore transport modelling.....	52
7.3.1	Model description	52
7.3.2	Model setup	53
7.3.3	Model calibration	55
7.3.4	Results	56
7.3.5	Horizontal profile variability.....	59
7.4	Cross-shore erosion	62
7.4.1	Model description	62
7.4.2	Model setup	63
7.4.3	Profile adjustment.....	65
7.4.4	Results	66
7.5	Impact of proposed seawall on sediment dynamics.....	71
8.	DESIGN WATER LEVELS AND WAVES AT REVETMENT.....	73
8.1	Model description	73
8.2	Model setup	73
8.3	Results.....	75
9.	LOCAL SCOUR	79
9.1	Introduction	79
9.2	Methodology.....	79
9.3	Results.....	81
10.	IMPACT OF CLIMATE CHANGE ON BEACH WIDTH	85
11.	SUMMARY	91
12.	REFERENCES	93
	ANNEXURE A TRITAN SURVEY REPORT	1
	ANNEXURE B CROSS-SHORE EROSION RESULTS	1
	ANNEXURE C EXTREME DESIGN CONDITIONS.....	1

TABLES	Page N°
--------	---------

Table 1-1: Return period and encounter probability.	4
Table 3-1: Climate change applied for each parameter and date.....	9
Table 4-1: Wind set-up correction at Muizenberg compared to Simon’s Town for all modelled wind speeds and directional sectors.....	16
Table 4-2: Extreme still water levels.	17
Table 5-1: Output locations for the extreme and operational wave conditions.....	29
Table 5-2: Extreme nearshore wave climate.	31
Table 6-1: Categories of dependence (Petroligkis, et al., 2016).	33
Table 6-2: Joint return period of storm surge and wave height for zero dependence.	37
Table 6-3: Extreme conditions at -15 m MSL.	38
Table 7-1: Long-term coastline trends based on wetted line analysis.....	45
Table 7-2: Horizontal trends 2010 to 2022 based on beach profile analysis.	50
Table 7-3: Longshore sediment transport results for Profile 8.	59
Table 7-4: Extreme horizontal profile movement.	62
Table 7-5: SBEACH model setup parameters.	63
Table 7-6: Bedrock levels interpreted from geotechnical survey.	65

Table 8-1: Profile 4; design wave and water levels in front of stepped revetment.	78
Table 9-1: Summary of empirical scour estimation methods.	80
Table 9-2: Pre-storm beach level and estimated local scour at the structure toe for the 1, 10, 100 and 475-year storms at Profile 4 in 2026, 2046 and 2076.	82
Table 10-1: Summary of minimum, average and maximum dry beach widths due to climate change.	89

Figure 1-1: Muizenberg Beachfront location and aerial view.	1
Figure 1-2: Muizenberg Beachfront design framework (CCT, 2022a).	2
Figure 2-1: Hydrographic and beach profile scope.	5
Figure 2-2: Survey results.	6
Figure 3-1: Regional relative sea level rise at Cape Town from AR6 (IPCC, In press), showing the median and upper end of the likely range for the SSP2-4.5, SSP3-7.0 and SSP5-8.5 scenarios.	8
Figure 4-1: Measured hourly water levels at Simon’s Town.	10
Figure 4-2: Measured water level, predicted tide and storm surge at Simon’s Town for the entire dataset (top), detail for 2005 (middle) and the November 2005 storm (bottom).	11
Figure 4-3: Bathymetry and computational mesh of the wind set-up model.	13
Figure 4-4: Modelled wind set-up for a southerly wind direction with a 25 m/s wind speed.	15
Figure 4-5: Storm surge at Muizenberg, obtained from measured storm surge at Simon’s Town offset with the difference in modelled wind setup between Simon’s Town and Muizenberg.	16
Figure 4-6: Extreme value analysis of positive storm surge at Muizenberg (baseline date is 1989.5).	17
Figure 5-1: Regional model bathymetry. The magenta dots on the boundary indicate the nodes where hindcast NCEP data was available. Note the colour scale is non-linear.	19
Figure 5-2: Regional model computational mesh. The magenta dots on the boundary indicate the nodes where hindcast NCEP data was available.	20
Figure 5-3: Nested model bathymetry. Note the top colour scale is non-linear.	22
Figure 5-4: Nested model computational mesh.	23
Figure 5-5: Wave refraction plot, demonstrating coupling between regional (top) and nested (bottom) model. Note the colour scale is non-linear.	25
Figure 5-6: Time-series comparison of measured and modelled wave parameters at Monwabisi.	26
Figure 5-7: Scatter and quantile-quantile (Q-Q) comparison of measured and modelled wave parameters at Monwabisi.	26
Figure 5-8: Comparison of measured and modelled wave roses at Monwabisi.	27
Figure 5-9: Wave refraction plot for the 25 January 1981 storm event.	28
Figure 5-10: Scatter plot of H_{m0} and T_p at Point A from 422 storm events. Two partitions, separated at a wave steepness of $s = 1/65$ are shown. Also shown are the H_{m0} - T_p trendlines for each partition.	29
Figure 5-11: H_{m0} EVA plot for the extreme wave climate at -15 m MSL.	30
Figure 5-12: Time-series of operational wave parameters extracted at Point B.	32
Figure 6-1: Scatter plot of 23.9 years of storm surge and wave height pairs at Muizenberg for waves with a steepness of $s < 1/65$	35
Figure 6-2: Scatter plot of 4.8 years of storm surge and wave height pairs at Muizenberg for waves with a steepness of $s > 1/65$	35
Figure 6-3: Dependence parameter χ of storm surge and wave height at Muizenberg for waves with a steepness of $H/L < 1/65$	36
Figure 6-4: Dependence parameter χ of storm surge and wave height at Muizenberg for waves with a steepness of $s > 1/65$	36
Figure 7-1: Historical aerial imagery of Muizenberg in 1935, 1992, 2021 and 2022.	40
Figure 7-2: Illustration of beach lowering procedure (CCT, 2022b).	41

Figure 7-3: Satellite images showing the beach lowering in front of the promenade in February 2017 (top) and along the main beach in March 2017 (bottom).	42
Figure 7-4: Cross-shore lines intercepting the wetted line.	43
Figure 7-5: Estimated long-term wetted line trends for 1935 to 2022.	44
Figure 7-6: Estimated long-term wetted line trends for 1968 to 2022.	44
Figure 7-7: Estimated long-term coastline trends for 2002 to 2022.	44
Figure 7-8: Locations of Profiles A, B and C used in the historical erosion/accretion analysis. Also shown is the proximity of the Tritan beach survey (coloured squares) relative to the profile locations.	46
Figure 7-9: Profile A historical erosion/accretion analysis. Top: profile evolution over time. Bottom: horizontal movement of profile for the 0, 0.5, 1.0, 1.5, 2.0 and 2.5 m MSL levels.	47
Figure 7-10: Profile B historical erosion/accretion analysis. Top: profile evolution over time. Bottom: horizontal movement of profile for the 0, 0.5, 1.0, 1.5, 2.0 and 2.5 m MSL levels.	48
Figure 7-11: Profile C historical erosion/accretion analysis. Top: profile evolution over time. Bottom: horizontal movement of profile for the 0, 0.5, 1.0 and 1.5 m MSL levels.	49
Figure 7-12: Schematic representation of the Bruun Rule, modified after Hands (1983).	51
Figure 7-13: Left: overview of profiles used in coastline stability and phase resolved wave modelling. Right: detail of profiles used for the design conditions of the coastal protection structures.	52
Figure 7-14: Cross-shore Profile 8.	53
Figure 7-15: Median grain diameters of sediment samples taken at Muizenberg.	54
Figure 7-16: Wave rose of H_{rms} at Point B with modelled shoreline angle shown for reference.	55
Figure 7-17: Observed rates of sea level rise at Simon’s Town over the period of 1993-2018 (Allison, et al., 2022). ESA, CMEMS, and CSIRO are three different satellite altimetry products.	56
Figure 7-18: Cross-shore distribution of water Level, waves, currents and sediment transport at one instance in time.	57
Figure 7-19: Time series of waves (at the offshore end of the profile), instantaneous sand transport (integrated across the profile) and accumulated net sand transport at Point B (-10 m MSL) on Profile 8 over the 31-year period.	58
Figure 7-20: Cross-shore distribution of the accumulated net and gross sand transport at Profile 8 over the 31-year period.	59
Figure 7-21: Horizontal profile movement due to longshore transport at Profile 8 over the 31-year period.	60
Figure 7-22: Comparison of predicted horizontal variability due to longshore transport with observed dry beach variability.	60
Figure 7-23: Normal distribution fit of the deviation of horizontal profile position from long-term trend.	61
Figure 7-24: Storm duration analysis based on 84 storms at Point A. The predicted storms are shown in shades of blue and purple. The synthetic tide for a 475-year event in 2026 (including storm surge and sea level rise) is shown for reference.	64
Figure 7-25: Example of profile recession due to sea level rise (x_{slr}), long-term trends due to longshore sand supply (x_{trend}), and horizontal profile variability due to longshore transport ($x_{variability}$) for Profile 4. The profile adjustment sensitivity to $x_{variability}$ for a 10-year return period is presented in dotted lines and values in brackets.	66
Figure 7-26: Erosion results for the two wave steepness candidates and two joint return period combinations for the 475-year storms at Profile 4 in 2026.	67
Figure 7-27: Erosion results for the two wave steepness candidates and two joint return period combinations for the 475-year storms at Profile 4 in 2046.	68

Figure 7-28: Erosion results for the two wave steepness candidates and two joint return period combinations for the 475-year storms at Profile 4 in 2076.....	69
Figure 7-29: Erosion results for the 1, 10, 100 and 475-year storms at Profile 4 in 2026 (top), 2046 (middle) and 2076 (bottom)	70
Figure 7-30: Location of existing seawall (blue) and proposed stepped revetment (red).....	72
Figure 8-1: Profile 4; Example 2DV mesh for 2076, 1 y SWL, 475 y waves ($s > 1/65$). The position of the structure is shown for visual purposes only.....	74
Figure 8-2: Schematic representation of modelled outputs extracted at the toe of the structure.....	75
Figure 8-3: Profile 4; Example results for a 2076 climate change scenario and a 475-year wave event ($s > 1/65$) combined with a 1-year still water level. Top: cross-section of instantaneous surface elevation (the structure is shown for visual purposes only). Bottom: Time-series of surface elevation, short waves and surf beat.	76
Figure 8-4: Comparison of H_{max} to $H_{1/3}$ for all profiles and cases modelled. The best estimate trendline (red) was fitted using least squares regression and the upper and lower envelopes (green) were visually fitted. ..	77
Figure 9-1: Local scour at the toe of a structure (van Rijn, L.C., 2018).	79
Figure 9-2: Comparison of methods for the 475-year return period in 2076.	81
Figure 9-3: Estimated local scour at structure toe for Profiles 2 to 5 for 1, 10, 100 and 475-year return period in 2026. Minimum and maximum levels reflect the range of estimates from empirical methods.....	83
Figure 9-4: Estimated local scour at structure toe for Profiles 2 to 5 for 1, 10, 100 and 475-year return period in 2046. Minimum and maximum levels reflect the range of estimates from empirical methods.....	83
Figure 9-5: Estimated local scour at structure toe for Profiles 2 to 5 for 1, 10, 100 and 475-year return period in 2076. Minimum and maximum levels reflect the range of estimates from empirical methods.....	84
Figure 10-1: Average profile (measured on 8 April 2008) compared to all measurements (2004 to 2022) along Profile B (refer to Section 7.1.4).....	85
Figure 10-2: Percentile plot of dry beach width in front of the existing seawall between 2002 and 2022.	86
Figure 10-3: Dry beach width variability for a SSP1-2.6 50 th climate change scenario. Note: the dry beach width is measured relative to the existing sea wall for 2022 and the new sea wall for 2026 onward.	87
Figure 10-4: Dry beach width variability for a SSP5-8.5 50 th climate change scenario. Note: the dry beach width is measured relative to the existing sea wall for 2022 and the new sea wall for 2026 onward.	88
Figure 10-5: Time-series of dry beach width variability due to climate change.	89

1. INTRODUCTION

1.1 Project background

The Muizenberg beachfront is a Coastal Destination Place, having the highest recreational beach use in Cape Town and it is also one of the top 20 international attractions in Cape Town, attracting an estimated 90 000 foreign visitors per year, and many more local visitors daily. However, the public coastal infrastructure and services at Muizenberg are in decline.

To protect the public amenity, the City of Cape Town (CCT) is undertaking a project to rehabilitate and upgrade the coastal public infrastructure and services along the Muizenberg Beachfront. Due to the potential diverse development objectives of the eastern and the western areas, the beachfront will be upgraded in two separate initiatives. Phase 1 extends from the St James walkway to the parking area just west of the pavilion, while Phase 2 is envisaged to extend from the Pavilion to the Zandvlei estuary mouth (Figure 1-1).



Figure 1-1: Muizenberg Beachfront location and aerial view.



The key project objectives are to:

- Retain and improve the recreational and amenity facilities along Muizenberg Beachfront to ensure a popular recreational and tourism destination is established over the long term;
- Construct a new coastal defense structure to protect the existing infrastructure and services, factoring in climate change and sea-level rise estimates;
- Ensure that such facilities are safe for public use and that such facilities optimise the use and enjoyment of the coastal environment by members of the public;
- Retreat infrastructure (excluding coastal defense infrastructure) to beyond the wave run up zone; and
- Ensure cost effective budget expenditure through ensuring the implementation of long-term sustainable coastal protection structures to protect infrastructure and services from present and future coastal hazards.

The City's Coastal Management Branch (CMB) have completed the feasibility design for Phase 1 (CCT, 2022a). The design framework for the Phase 1 development is shown in Figure 1-2, and includes the following key components:

- New stepped revetment coastal protection to replace the old wooden seawall and degraded stone steps. This is envisioned to provide continuous beach access, support and protect the promenade and other infrastructure, and preserve the sense of place and value of the beachfront;
- Refurbishment of hard and soft landscaping and amenities along the beachfront as well as an improved connection to the St James coastal walkway;
- Formalising and optimizing of the large informal parking area in the west of the site; and
- Reconfiguration of the parking area adjacent the Pavilion building (eastern boundary of the site).

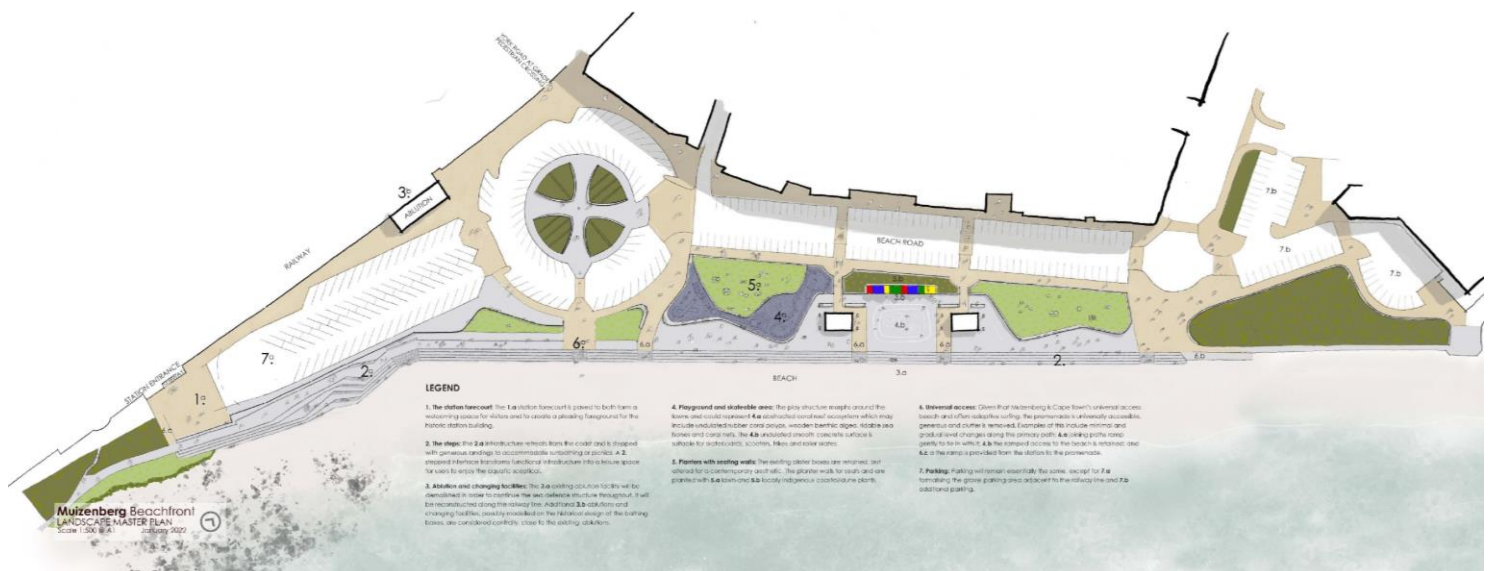


Figure 1-2: Muizenberg Beachfront design framework (CCT, 2022a).

1.2 Terms of reference

The CCT has appointed a panel of consultants for the Inception and Concept & Viability (preliminary design) stages of the Phase 1 project. PRDW has also been appointed directly by the CCT to provide coastal processes specialist studies required as input to the next design stage, which are the subject of this report.



The Terms of Reference for the specialist studies are:

- Bathymetric survey.
- Coastal hydrodynamics modelling study to determine design and construction water level and wave conditions, including climate change over the design life.
- Sediment dynamics study to determine minimum expected sediment levels in front of the seawall to design and optimise scour protection where required, and an assessment of the impact of the new seawall on the longshore and cross-shore sediment dynamics.
- Overtopping and flooding assessment and recommendations.

The overtopping and flooding assessment will be carried out in Financial Year (FY) 2023. This report covers the first three items in the Terms of Reference.

1.3 Scope of work

The Scope of Work includes the following:

- Bathymetric survey (combination of multi beam and single beam surveys as required);
 - Preparation of one Request for Quotation (RFQ) for the bathymetric survey scope;
 - Invitation of three service providers on PRDW's approved suppliers list to submit RFQs;
 - Evaluation of RFQs and preparation of brief recommendation on preferred service provider;
 - Award of business and preparation of sub-consultant agreement with service providers;
 - Review of deliverables and information provided by service provider; and
 - Sign-off on information for use on the project to inform the engineering design.
- Coastal hydrodynamics modelling study to determine design and construction water level and wave conditions:
 - Climate change assessment to determine projected climate change at the end of the design life of the proposed development. The assessment will be based on the projections provided in the 6th Assessment Report of the IPCC and other relevant literature. CMB input will be required to define the design lifetime and select the appropriate climate change scenario and projection uncertainty level. One present-day scenario and one future climate change horizon (e.g., end of design life) will be considered in this study.
 - Water level analysis of existing data to determine extreme storm surge, and analysis of joint probability between waves and storm surge.
 - Spectral wave modelling to determine the nearshore wave climate:
 - Operational wave climate (up to 10 years) as required for the sediment dynamics study (see below).
 - Extreme wave climate (1-, 10-, 100-, and 475-year return periods with and without climate change), as required to determine extreme conditions at the seawall for design.
 - The MIKE 3 Wave model will be used to determine extreme wave conditions at the toe of the seawall as required for design. The model will be used in profile mode to provide the conditions at representative locations.
- Sediment dynamics study:
 - Analysis of available data, including LiDAR, beach profiles, aerial images, satellite imagery, and maintenance procedures (annual beach lowering) to assess historical beach levels and potential trends.



- Longshore transport modelling to assess seasonal and interannual longshore transport, and potential changes due to climate change.
- Cross-shore storm erosion using SBEACH at up to 5 profiles to determine minimum beach levels following extreme storm events (1-, 10-, 100-, and 475-year). This will include one profile within the Phase 2 study area (Muizenberg Pavilion to Zandvlei mouth).
- Assessment of local scour against structures based on empirical equations.
- The above components will be used to provide minimum sand levels at the structure toe as required for the seawall scour protection design.
- Interpretation of the above model results to provide a qualitative assessment of possible changes in sediment dynamics due to the proposed new seawall. This will be complemented by an analysis of changes in wave reflection based on results from the MIKE 3 Wave model in Financial Year 2023.

1.4 Assessed return periods

In this study, a range of return periods has been considered to allow for the characterisation of extreme conditions at the site during construction and for design.

The recommendation of the specific return periods to be used for design will be defined in the Design Basis, which will be developed in the Concept Design phase. The approach in this study was to provide results within the range of return periods expected to be required for design, which was anticipated to range from the 100-year return period to the 475-year return period (10% encounter probability over a 50-year design life, see Table 1-1). The 1-year and 10-year return periods were also assessed as typical return periods considered for temporary works during construction.

Table 1-1: Return period and encounter probability.

Lifetime [years]	Return period [years]			
	1	10	100	475
1	63%	10%	1%	0%
10	100%	63%	10%	2%
20	100%	86%	18%	4%
50	100%	99%	39%	10%

1.5 Report structure

The bathymetric survey undertaken by Tritan is presented Section 2. Section 3 describes the climate change considerations for the increase in sea level, extreme wave height and storm surge from the baseline date. Section 4 contains the tide and storm surge analysis on measured water levels at Simon’s Town and the model used to derive storm surge at Muizenberg. The model descriptions, setup, calibration and results from the nearshore wave modelling are described in Section 5. Section 6 presents the joint probability of wave height and storm surge and the summary of the nearshore extreme conditions. The coastline stability is described in Section 7, including the analysis of historical data, beach adaption due to sea level rise, longshore transport modelling and storm erosion modelling. It also includes a qualitative assessment of the potential impact of the proposal wall on the sediment dynamics. Section 8 presents modelling of the extreme wave and water levels at the toe of the revetment. Section 9 presents the local scour estimations. An assessment of the impact of climate change on the beach width is presented in Section 10. A summary of the outcomes is presented in Section 11 and a list of references is provided in Section 12.



2. BATHYMETRIC SURVEY

2.1 Survey scope

The purpose of the survey was to provide adequate coverage of the nearshore and beach area for use in the coastal processes numerical models described in this report. The scope included a hydrographic survey of the nearshore area and a beach profile survey, covering both the Phase 1 and Phase 2 project areas, as shown in Figure 2-1.

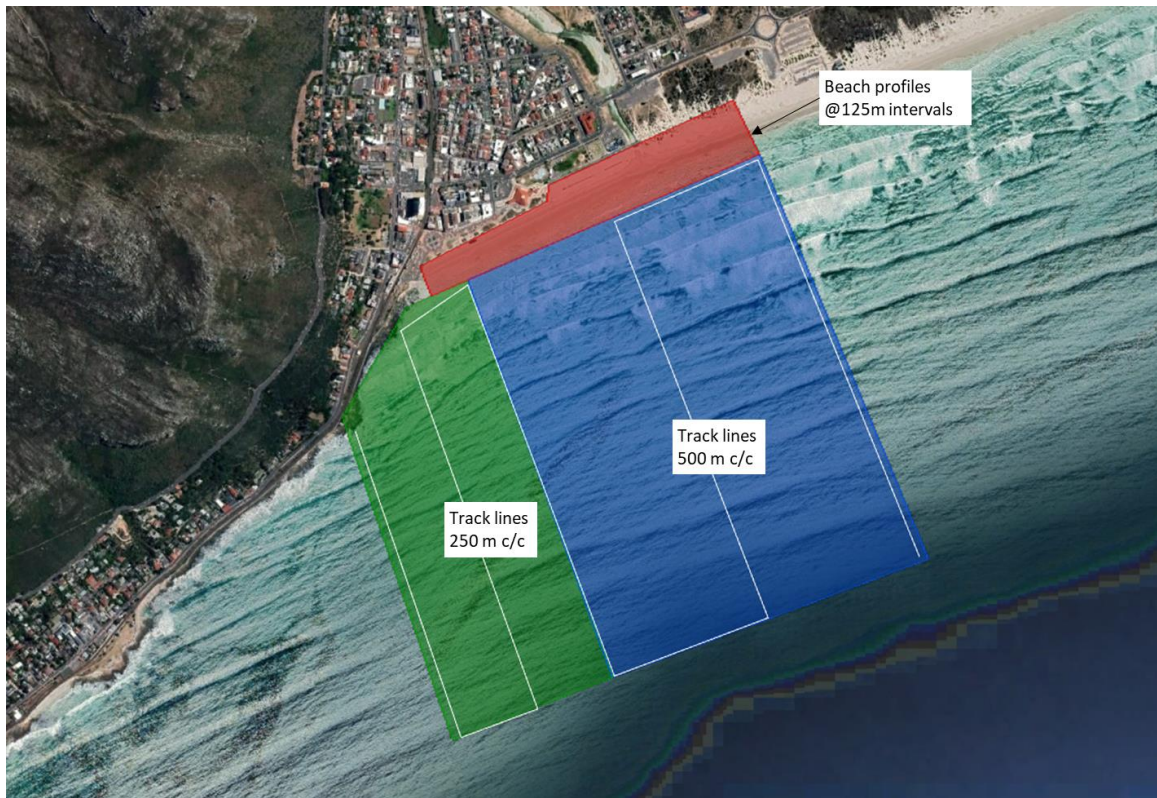


Figure 2-1: Hydrographic and beach profile scope.

Considering the flat beach profile and expected alongshore uniformity of the beach, it was not considered necessary to achieve full coverage of the nearshore bathymetry. The minimum specified coverage was cross-shore track lines at intervals of 250 m c/c in the green area where some curvature of the bathymetric contours was expected, and 500 m c/c in the blue area. Both areas extend from at least -11 m MSL to the shallowest depths possible. Based on the submissions from the service providers, profiles could be surveyed at up to 125 m intervals over both the blue and green areas within a single day of surveying, providing the best value for money in terms of survey coverage.

The beach profiles coverage was 125 m c/c from the top of the profile (or start of vegetation) to the deepest depth possible.

2.2 Survey results

The surveys were undertaken by Tritan Survey (Pty) Ltd. Full descriptions of the survey methodology, datum information and control, and survey results are provided in the survey report (Tritan Survey, 2022) included as Annexure A to this report. The survey results are presented in Figure 2-2.

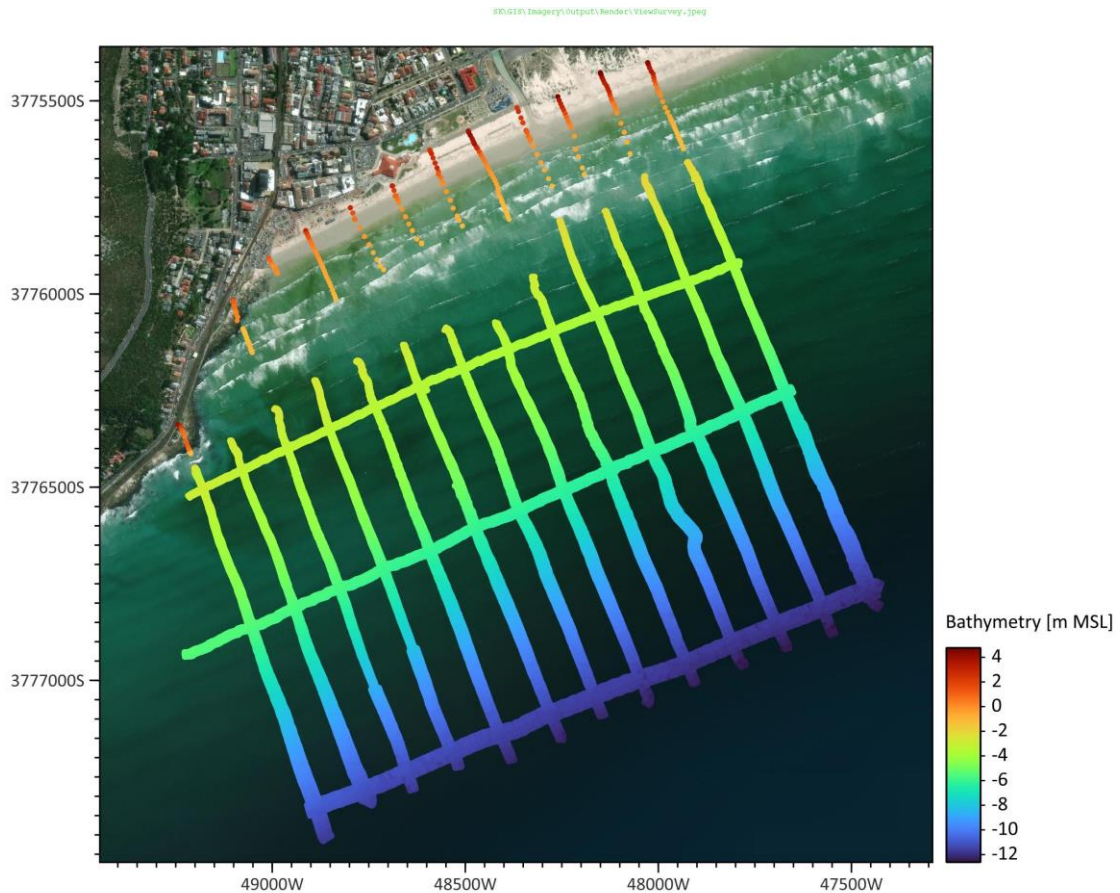


Figure 2-2: Survey results.

The hydrographic survey was carried out using a survey vessel equipped with a Multi-Beam Echo Sounder. The surveyors indicated that good coverage in the shallow areas at this site is more dependent on calm wave conditions than surveying at spring high tide. The hydrographic survey was initially carried out on 12 April 2022, when the water was calm but very murky closer to shore. After initial testing and calibration, the survey vessel hit the rocky reef off Bailey’s Cottage on the first survey line. This affected the instrument calibration, and the remainder of the survey was not salvageable. The survey was redone on the 5th of May 2022 and all lines were completed at approximately 125 m intervals. The profiles started at a depth of at least -12 m MSL and the shallowest profiles extended to -2.3 m MSL.

The beach profile surveys were originally carried out on 19 April 2022 during spring low tide. However, not all profiles were surveyed, and an additional survey was carried out during low tide on 10 May 2022. Beach profiles were provided at 125 m intervals. The deepest profiles extend to approximately -1.6 m MSL.

The above surveys together provide an adequate description of the nearshore bathymetry for use in the numerical modelling studies. In the centre of the survey area where the separation between the two surveys is greatest (approximately -1.4 m MSL to -3.2 m MSL), the bathymetry can be inferred from adjacent profiles using engineering judgement.



3. CLIMATE CHANGE

3.1 Introduction

This specialist study requires the assessment of low beach levels and the development of design wave and water level conditions for the proposed coastal defence structures, including accounting for the effects of climate change. This is achieved by conducting the assessment for present-day conditions and conditions at the end of the design life. This section sets out the basis for the climate change assessment, and the adjustments applied.

3.2 Basis

The estimated construction date of the upgrades is 2026 and the design life of the structures is 50 years (CCT, 2022a), resulting in a future end-of-life horizon of 2076. In addition to these dates, the cross-shore beach erosion in front of the proposed stepped revetment is also assessed for a 20-year horizon (2046) to allow an adaptive design to the scour protection, if required.

The projections are based on the latest information available from the 6th Assessment Report: Physical Science Basis (IPCC, In press) of the Intergovernmental Panel for Climate Change (IPCC) and supplemented with other relevant literature.

The AR6 presents projections for a range of emissions scenarios, referred to as Shared Socioeconomic Pathways (SSPs). This is an update of the Representative Concentration Pathways (RCPs) used in the 5th Assessment Report. In this study, median projections for the most conservative scenario (SSP5-8.5) have been used, in consultation with the CMB. Where projections are not yet available for SSP5-8.5, the nominally corresponding scenario from AR5 was used (RCP8.5).

3.3 Sea level rise

Projections for sea level rise (SLR) were based on the latest projections provided in AR6, which can be downloaded from the NASA Sea Level Change Portal (<https://sealevel.nasa.gov/>). Figure 3-1 presents the regional relative mean SLR at Cape Town for the median and upper end of the likely range for SSP1-2.6, SSP2-4.5, SSP3-7.0, and SSP5-8.5. While the IPCC projections are given relative to a baseline period of 1995-2014, the curves shown in the figure are presented relative to 2019, the baseline date for Mean Level at Cape Town (see Section 4.1).

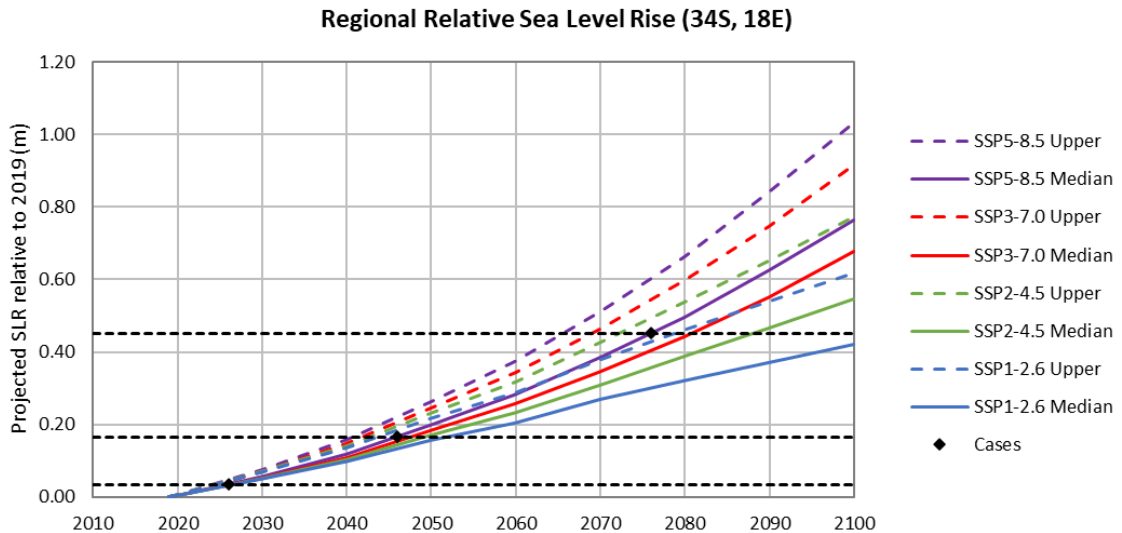


Figure 3-1: Regional relative sea level rise at Cape Town from AR6 (IPCC, In press), showing the median and upper end of the likely range for the SSP1-2.6, SSP2-4.5, SSP3-7.0 and SSP5-8.5 scenarios.

The median projections for SSP5-8.5 were used in this study and are presented in Table 3-1, and shown as the black dotted lines in Figure 3-1. The median projections for SSP1-2.6 are also shown as they are used for a sensitivity assessment in Section 10.

3.4 Storm surge

Storm surge is mainly composed of an atmospheric pressure component (low pressure for positive storm surge and high pressure for a negative storm surge) and a wind-induced component (wind set-up). The atmospheric pressure component of storm surge is proportional to the gradient in atmospheric pressure through the inverse barometer effect, while the wind set-up component of storm surge is proportional to the square of the wind speed.

Projections of wind speed and extreme sea level pressure were obtained from a 50 km resolution downscaled climate model ensemble run by the Council for Scientific and Industrial Research, as described in (Airshed, 2021). The data includes time-series of spatially averaged meteorological parameters over an area of 100 km by 100 km at Cape Town for a period of 1960-2099 and provides projections for RCP8.5. The data included the annual maximum hourly wind speed and annual mean sea level pressure. In the absence of data on extreme sea level pressure, the projections for extreme low pressure were assumed the same as the annual mean.

The projected increases in extreme wind speed were larger than the projected decreases in mean sea level pressure. In the absence of detailed projections available in literature, the projections for storm surge used here were based on the conservative assumption that the wind set-up component is dominant and were thus determined as the square of the projected extreme wind speed increase. The resulting projections applied in the study are presented in Table 3-1.

3.5 Extreme wave height

Projections for global changes in extreme wave heights have been determined from a seven-member wave model ensemble (Meucci, et al., 2020). For each of a present-day (1979-2005) and future time slice (2081-2100), extreme wave heights were determined by fitting an exponential distribution to the 1 000 highest



wave heights pooled from the seven models (after bias-correction). The projected changes for the 100-year return period significant wave height (H_{m0}) were linearly interpolated to the required dates, and converted to a baseline date of 2000, the mid-point of the dataset used to derive the nearshore extreme wave climate (see Section 5). The resulting projections applied in the study are presented in Table 3-1.

3.6 Summary

The climate change projections used in this study are summarised in Table 3-1.

Table 3-1: Climate change applied for each parameter and date.

Parameter	Description	Scenario	Units	Baseline date	2026	2046	2076
Sea level rise (SLR)	Regional relative mean sea level rise	SSP1-2.6 (median)	m	2019	0.03	0.13	0.30
		SSP5-8.5 (median)	m	2019	0.03	0.17	0.45
Wind speed	Annual maximum hourly averaged wind speed	RCP8.5 (mean)	%	1989.5	0.7%	1.2%	2.1%
Storm surge	Extreme positive	RCP8.5 (mean)	%	1989.5	1.4%	2.4%	4.3%
Wave height	Extreme wave height in deep water offshore	RCP8.5, no uncertainty ranges available	%	2000	1.0%	1.8%	2.9%



4. WATER LEVEL ANALYSIS

4.1 Measured water levels

Measured water level data was obtained from the University of Hawaii Sea Level Center (UHSLC) at the Simon's Town station for the period of 1959 to 2021 (UHSLC, 2022). The hourly measured data are plotted in Figure 4-1.

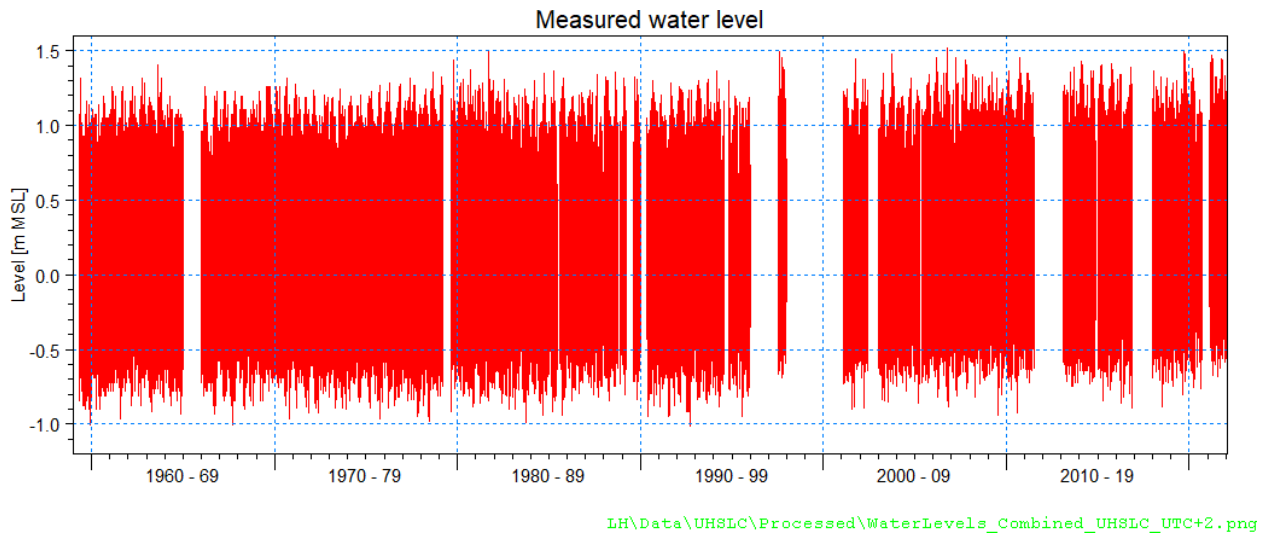


Figure 4-1: Measured hourly water levels at Simon's Town.

A linear regression fitted to the annual average water level over the measured period indicated a trend of +2.27 mm/year, which was removed prior to further analysis. A tidal harmonic analysis was carried out using the MIKE 21 tidal analysis and prediction toolbox (DHI, 2022a) to obtain the tidal constituents for the detrended Simon's Town dataset. The constituents were used to generate the predicted tide, using the Mean Level (ML) at Cape Town of +0.20 m MSL, representative of a baseline date of 2019 (PRDW, 2022). The predicted tide was used to calculate the 90th percentile of the high tides of +1.02 m mean sea level (MSL). This is defined as the level that is exceeded by 10 percent of the high tides over a continuous 19-year period. The 90th percentile of the low tides was calculated similarly as -0.59 m MSL.

4.2 Storm surge

The detrended measured water level at Simon's Town was subtracted from the predicted tide at Simon's Town to obtain the storm surge. The measured water level, predicted tide and storm surge are plotted in Figure 4-2.

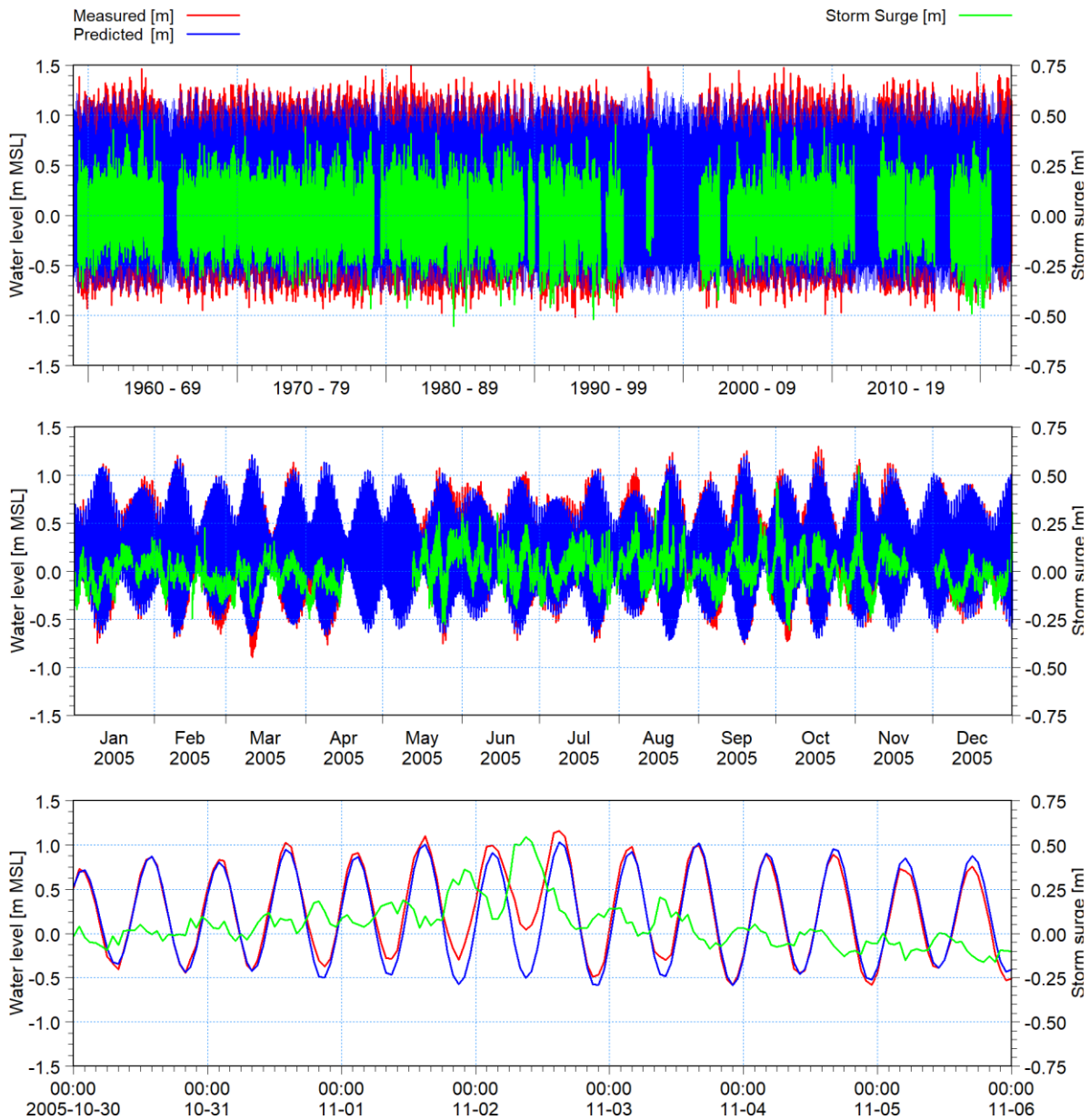


Figure 4-2: Measured water level, predicted tide and storm surge at Simon’s Town for the entire dataset (top), detail for 2005 (middle) and the November 2005 storm (bottom).

The storm surge measured in the Simon’s Town data does not account for the additional wind set-up between Simon’s Town and Muizenberg during southerly or south-easterly wind events. Similarly, the additional wind set-down during north-westerly events is also not accounted for. Therefore, a hydrodynamic model of False Bay was used to derive a wind set-up correction, as discussed in the next section.

4.3 False Bay wind set-up

4.3.1 Model description

The two-dimensional MIKE 21 Flow Flexible Mesh (HD) Model was used to model the wind set-up in False Bay. The application of the model is described in the User Manual (DHI, 2022b), while full details of the physical processes being simulated and the numerical solution techniques are described in the Scientific Documentation (DHI, 2022c). In the 2D formulation the model solves the non-linear, non-dispersive,



hydrostatic shallow water equations (NSWE), i.e., the depth-integrated incompressible Reynolds averaged Navier-Stokes equations. The time integration of the shallow water equations is performed using an explicit scheme. Horizontal eddy viscosity is modelled with the Smagorinsky formulation. An unstructured flexible mesh comprising triangles or quadrangles with variable sizes is utilised. The model includes the following physical phenomena:

- Water levels and currents due to wind stress on the water surface;
- Coriolis forcing;
- Bottom friction; and
- Flooding and drying.

The HD model was run using the instationary time formulation.

4.3.2 Mesh and bathymetry

The WG19 horizontal coordinate system was used for this study. All spatial plots include x and y axes showing the x and y coordinates in meters in the WG19 system. True north is always pointing upwards.

The vertical datum adopted in this study is mean sea level (MSL), which is 0.843 m above Chart Datum (CD).

The model mesh comprises quadrangular elements at the offshore boundaries with a resolution of 1 km and triangles with a resolution varying from about 1 km offshore to about 250 m nearshore.

The model bathymetry has been obtained from the MIKE by DHI CMAP Electronic Charts Database (DHI, 2022d). Figure 4-3 shows the model bathymetry and computational mesh.

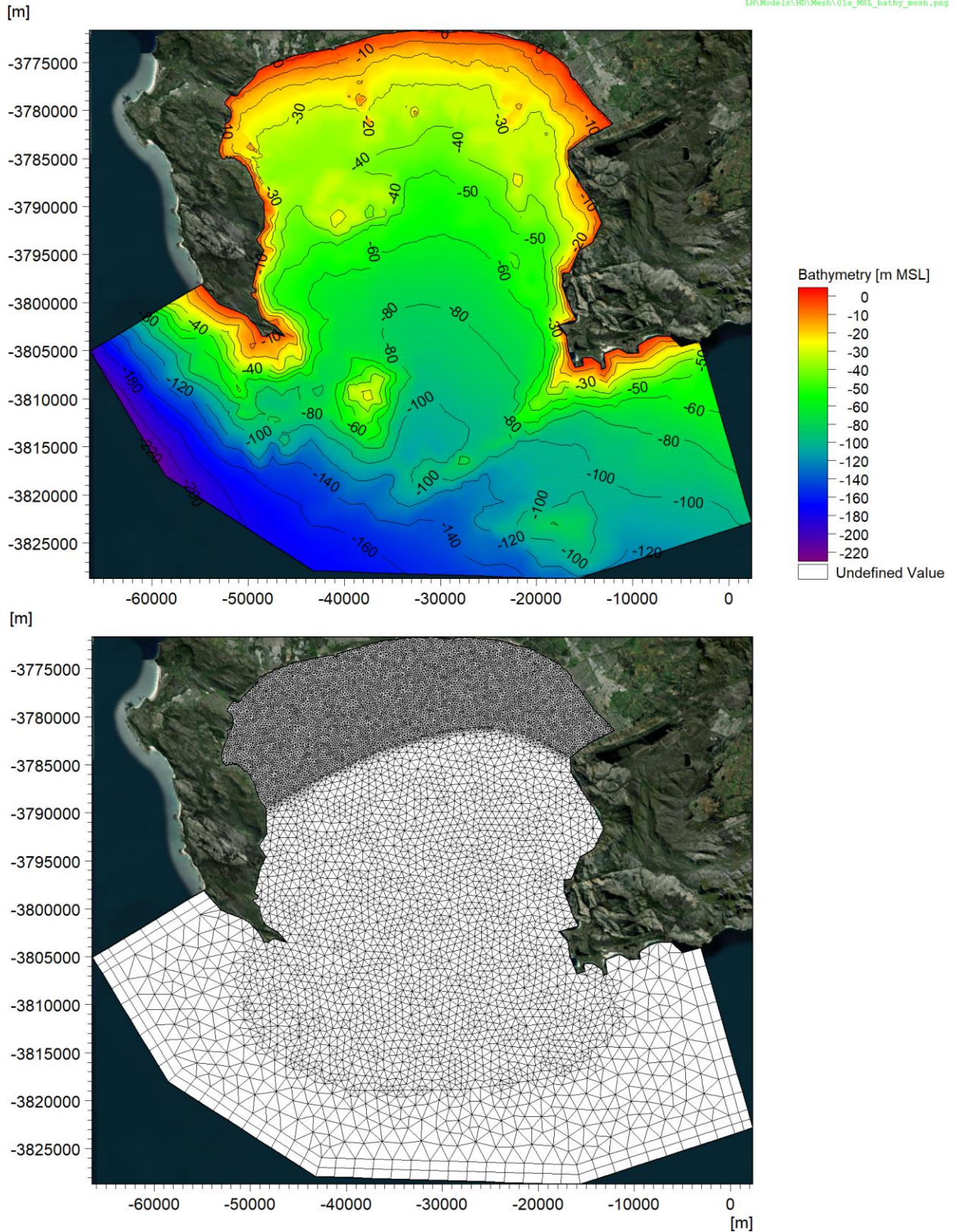


Figure 4-3: Bathymetry and computational mesh of the wind set-up model.



4.3.3 Boundary conditions

The offshore wind speeds were obtained as hindcast wind data from the NOAA/NCEP WAVEWATCH III CFSR Hindcast Dataset (NCEP, 2022). Three datasets are currently available, namely the Reanalysis (1979-2009), Production (2005-2019) and Forecast (2007-2021) datasets. The order of preference for the datasets was Reanalysis, Production, then Forecast with a combined dataset length of 42.2 years. The three datasets provide space and time varying 10 m wind fields at 3-hourly intervals on a 0.5 degree longitude/latitude grid. Time series of wind data was extracted at 34.5°S, 18.5°E for the period of 1979 to 2022. The maximum offshore wind speed for the dataset was 26.6 m/s.

The wind set-up was investigated for wind speeds from 5 m/s to 30 m/s at 5 m/s intervals for eight directions at 45 degree intervals to include the full range of wind speeds and directions, i.e., 48 cases. The wind forcing was applied as a constant wind speed and direction over the model domain. A constant water level of +0.157 m MSL (the published ML at Simon's Town (SANHO, 2018)) was applied as the initial water level condition over the whole model domain and along the offshore boundaries. Wind and Coriolis corrections were applied on the lateral boundaries. The wind drag coefficient used was $c_d = 0.0024$. Bottom friction was modelled using a Manning's $M = 32 \text{ m}^{1/3}/\text{s}$. The wind set-up model had a simulation time of 48 hours to reach a steady state throughout the model.

4.3.4 Results

Figure 4-4 shows the wind set-up relative to the initial water level for a southerly wind direction with a 25 m/s wind speed. The output locations at the Simon's Town Harbour and close to the Muizenberg shoreline at approximately -1 m MSL are also presented on Figure 4-4. Table 4-1 shows the wind set-up correction at Muizenberg to be applied to the Simon's Town data for the various wind speeds and directional sectors.

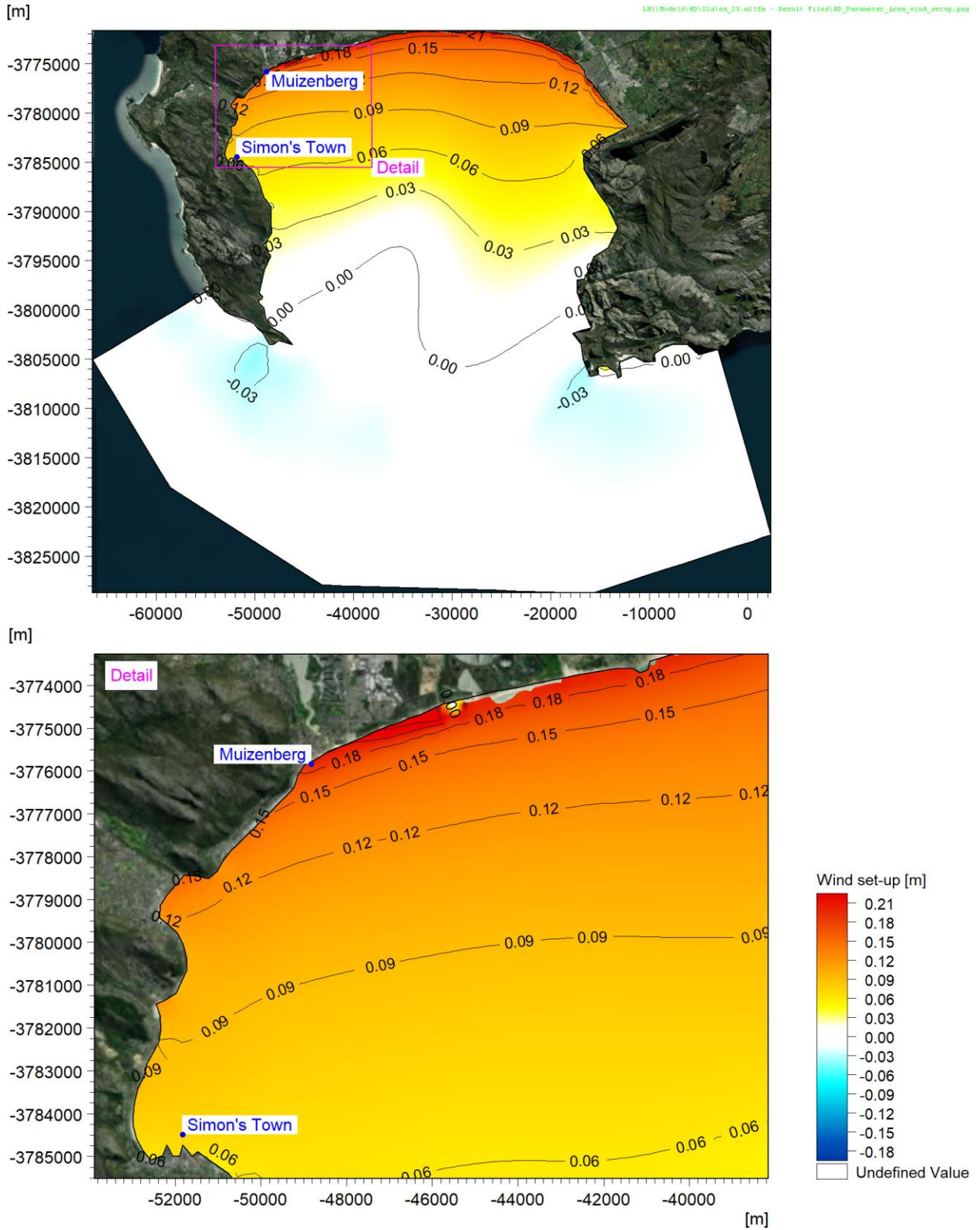


Figure 4-4: Modelled wind set-up for a southerly wind direction with a 25 m/s wind speed.



Table 4-1: Wind set-up correction at Muizenberg compared to Simon’s Town for all modelled wind speeds and directional sectors.

Direction [deg]	Wind set-up correction at Muizenberg compared to Simon’s Town [m]					
	Wind speed [m/s]					
	5	10	15	20	25	30
0	-0.005	-0.022	-0.050	-0.088	-0.138	-0.202
45	-0.004	-0.015	-0.033	-0.057	-0.088	-0.126
90	-0.001	0.000	0.002	0.004	0.008	0.013
135	0.004	0.014	0.034	0.060	0.095	0.135
180	0.006	0.023	0.049	0.083	0.127	0.180
225	0.005	0.017	0.036	0.063	0.096	0.136
270	0.001	0.002	0.003	0.004	0.006	0.006
315	-0.004	-0.014	-0.034	-0.062	-0.098	-0.145

A continuous time-series of wind set-up correction for the period of 1979 to 2022 was produced by interpolating the wind-setup results from Table 4-1 on the time-series of offshore wind speed and direction extracted at 34.5°S, 18.5°E. Where overlapping data was available the correction was added to the storm surge from Section 4.2 to obtain the corrected storm surge data for Muizenberg, as shown in Figure 4-5.

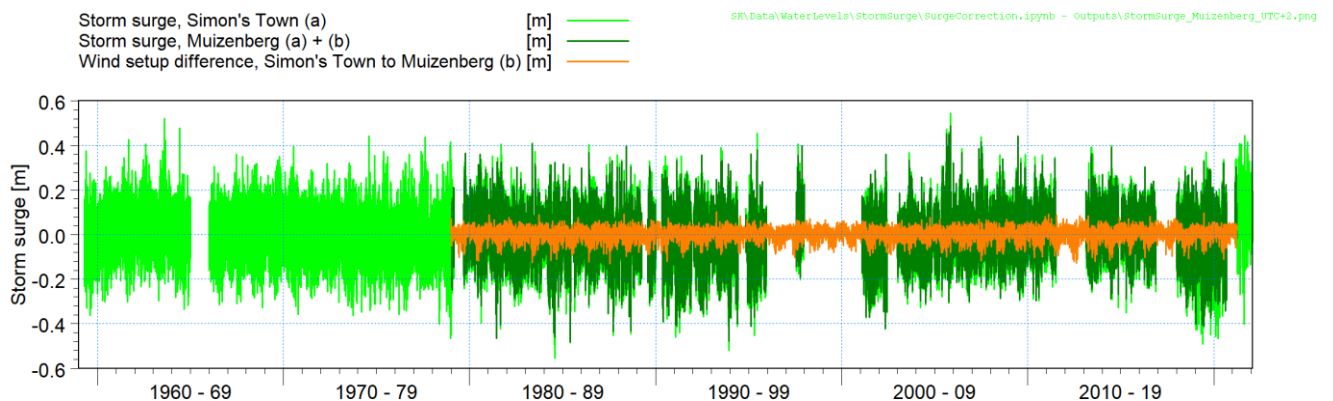


Figure 4-5: Storm surge at Muizenberg, obtained from measured storm surge at Simon’s Town offset with the difference in modelled wind setup between Simon’s Town and Muizenberg.

4.4 Extreme water levels

An extreme value analysis (EVA) was performed on the positive storm surge (measured water level higher than predicted tide) using the ‘MIKE by DHI’ EVA toolbox (DHI, 2022e). The analysis comprises fitting a three parameter Weibull distribution using the Method of Moments to an extreme value series extracted from the input time-series. The extreme value series was selected using the ‘peaks over threshold’ or ‘partial duration series’ method, with the threshold defined as the value that is exceeded two times per year on average. To ensure independence, two successive events were extracted only if the time between the events exceeded 48 hours. The uncertainty was calculated using Jackknife resampling to evaluate the mean and standard deviation of the estimate to obtain the 95% confidence (2.5th to 97.5th percentile) estimates. The extreme value analysis results for positive storm surge are plotted in Figure 4-6. The baseline date is 1989.5 which is the middle of the measurement period.

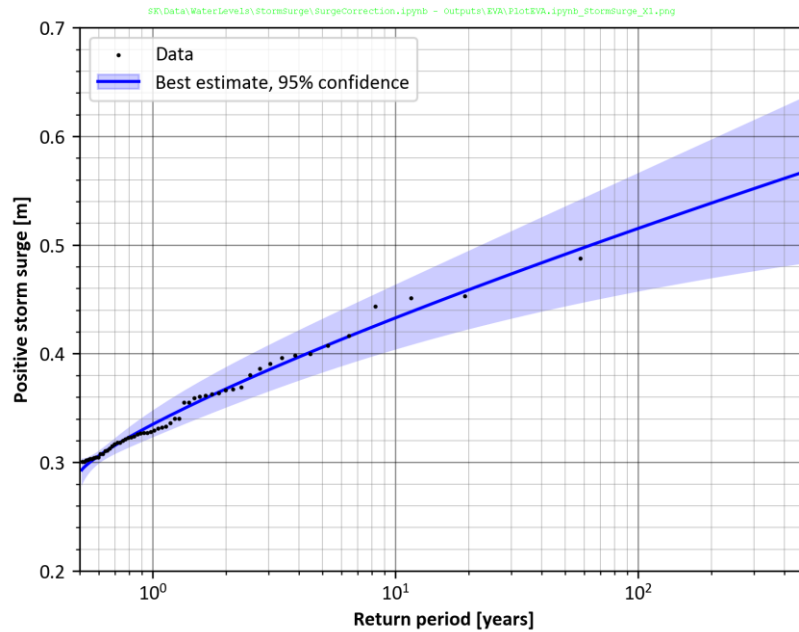


Figure 4-6: Extreme value analysis of positive storm surge at Muizenberg (baseline date is 1989.5).

The upper 95% confidence estimate positive storm surge was adjusted for climate change (refer to Table 3-1) and added to the 90th percentile high tide and the sea level rise to obtain the maximum still water level at the three dates of interest. Table 4-2 summarises the adjusted still water levels due to climate change.

Table 4-2: Extreme still water levels.

Return period	Tide ^(a) [m MSL]	Sea level rise ^(b) [m]			Positive storm surge ^(c) [m]			Still water level ^(d) [m MSL]		
		2026	2046	2076	2026	2046	2076	2026	2046	2076
		1	1.02	0.03	0.17	0.45	0.35	0.36	0.36	1.41
10	1.02	0.03	0.17	0.45	0.47	0.47	0.48	1.52	1.66	1.95
100	1.02	0.03	0.17	0.45	0.57	0.58	0.59	1.63	1.77	2.06
475	1.02	0.03	0.17	0.45	0.64	0.65	0.66	1.70	1.84	2.13

Notes:

- (a) 90th percentile high tide
- (b) Baseline date is 2019. Refer to Table 3-1 for climate change projections.
- (c) Upper 95% confidence storm surge, adjusted for climate change (baseline date is 1989.5)
- (d) Still water level is the sum of the tide, sea level rise and positive storm surge.



5. NEARSHORE WAVE CLIMATE

5.1 Introduction

The MIKE 21 Spectral Waves (SW) Flexible Mesh model was used for the wave refraction modelling to determine the nearshore extreme wave climate for the cross-shore storm erosion modelling and phase-resolving MIKE 3 Wave model, while long-term wave conditions were provided for the longshore sand transport modelling.

5.2 Model description

The application of the model is described in the User Manual (DHI, 2022f), while full details of the physical processes being simulated and the numerical solution techniques are described in the Scientific Documentation (DHI, 2022g). The model simulates the growth, decay and transformation of wind-generated waves and swells in offshore and coastal areas using unstructured meshes.

In this study the model was run in the fully spectral formulation. In the time domain, the regional model was run in the instationary formulation, while the nested model was run in the quasi-stationary formulation. The model included the following physical phenomena:

- Wind-wave generation;
- Non-linear wave-wave interaction;
- Dissipation due to whitecapping;
- Dissipation due to bottom friction;
- Dissipation due to depth-induced wave breaking;
- Refraction and shoaling due to depth variations; and
- The effect of time-varying water depth.

5.3 Regional wave model

The regional model bathymetry and mesh are presented in Figure 5-1 and Figure 5-2. The extent of the domain was chosen to coincide with the closest output nodes of the NCEP hindcast wave dataset, which was applied as a wave forcing on the model boundaries. The NCEP Production/Forecast and Reanalysis datasets are not available at the same hindcast nodes, therefore requiring two different regional model meshes. For brevity, only the mesh relating to the NCEP Production and Forecast dataset is shown here.

The flexible mesh comprises triangles with a resolution varying between approximately 8.0 km along the offshore boundaries and 2.5 km at the boundaries of the nested model.

The model bathymetry has been obtained from the following sources:

- MIKE by DHI CMAP Electronic Charts Database (DHI, 2022d); and
- Multi-beam echo sounder survey by Tritan Survey (2022).



SK\Model1\SW\01\01a_Bathy.png

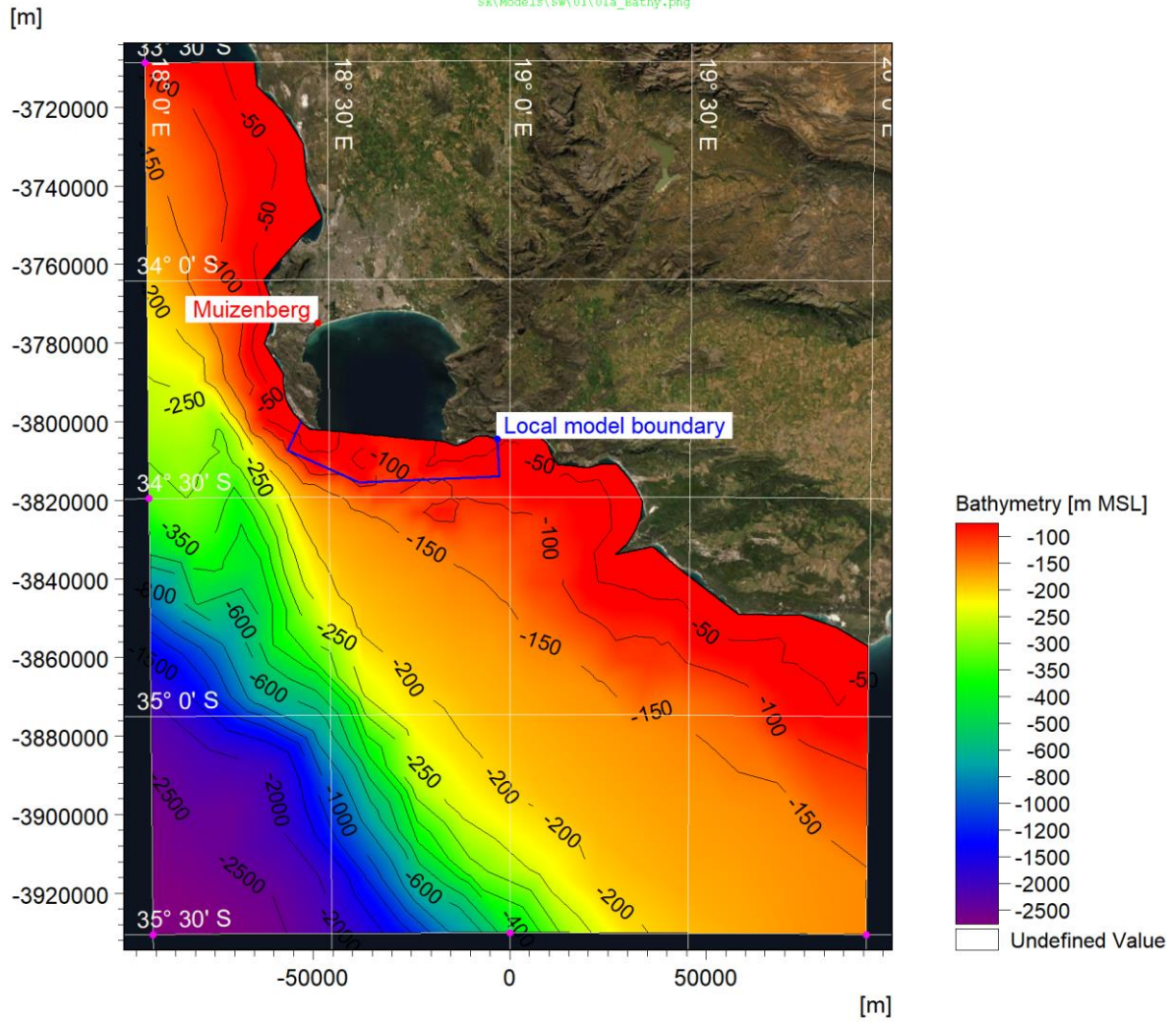


Figure 5-1: Regional model bathymetry. The magenta dots on the boundary indicate the nodes where hindcast NCEP data was available. Note the colour scale is non-linear.

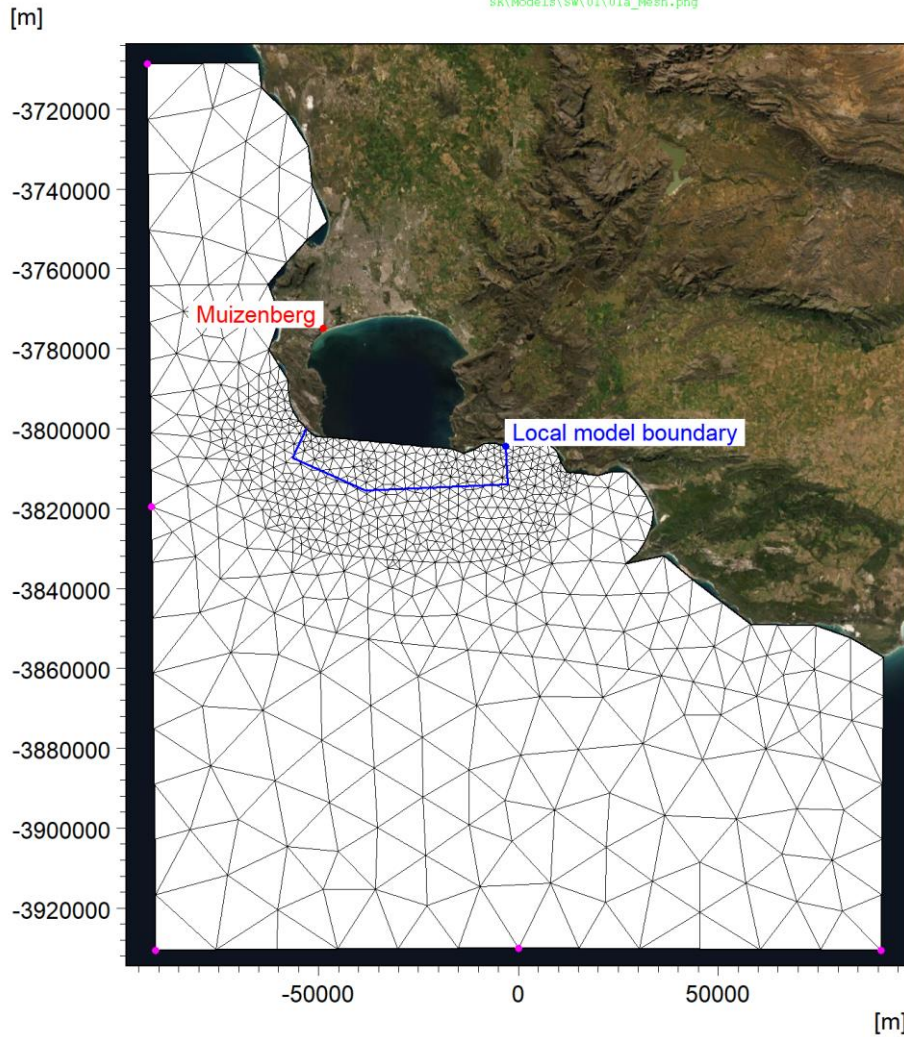


Figure 5-2: Regional model computational mesh. The magenta dots on the boundary indicate the nodes where hindcast NCEP data was available.

5.3.1 Water level

The predicted tidal levels at Simon's Town (Section 4.1) were applied as a time-varying, space constant water level.

5.3.2 Waves

Hindcast wave data was obtained from the NOAA/NCEP WAVEWATCH III CFSR Hindcast Dataset (NCEP, 2022). The wave partition data characterises the sea state by identifying wave parameters (significant wave height (H_{m0}), peak wave period (T_p), mean wave direction (D_m) and directional spreading (DSD)) for each of a variable number of peaks in the 2D wave spectrum. The wave partition data has been used to reconstitute the full 2D spectrum at each node and time step. The reconstituted spectra were applied as time and space-varying boundary conditions.

5.3.3 Wind

The NCEP hindcast wind data was applied as a space and time-varying wind field over the model domain. The uncoupled formulation of air-sea interaction was used for the wind-wave generation.



5.3.4 Model parameters

Bottom friction was modelled using a constant Nikuradse roughness of $k_N = 0.02$ m.

5.4 Nested wave model

5.4.1 Mesh and bathymetry

The local model bathymetry and mesh are presented in Figure 5-3 and Figure 5-4. The mesh extends approximately 40 km offshore of the project site and comprises triangles with a resolution varying between approximately 2.5 km at the offshore boundary and 135 m at the project site and surrounding area. Shallow areas, including the entrance to False Bay at Cape Point and Cape Hanglip, were refined to improve the accuracy of wave refraction into the bay.

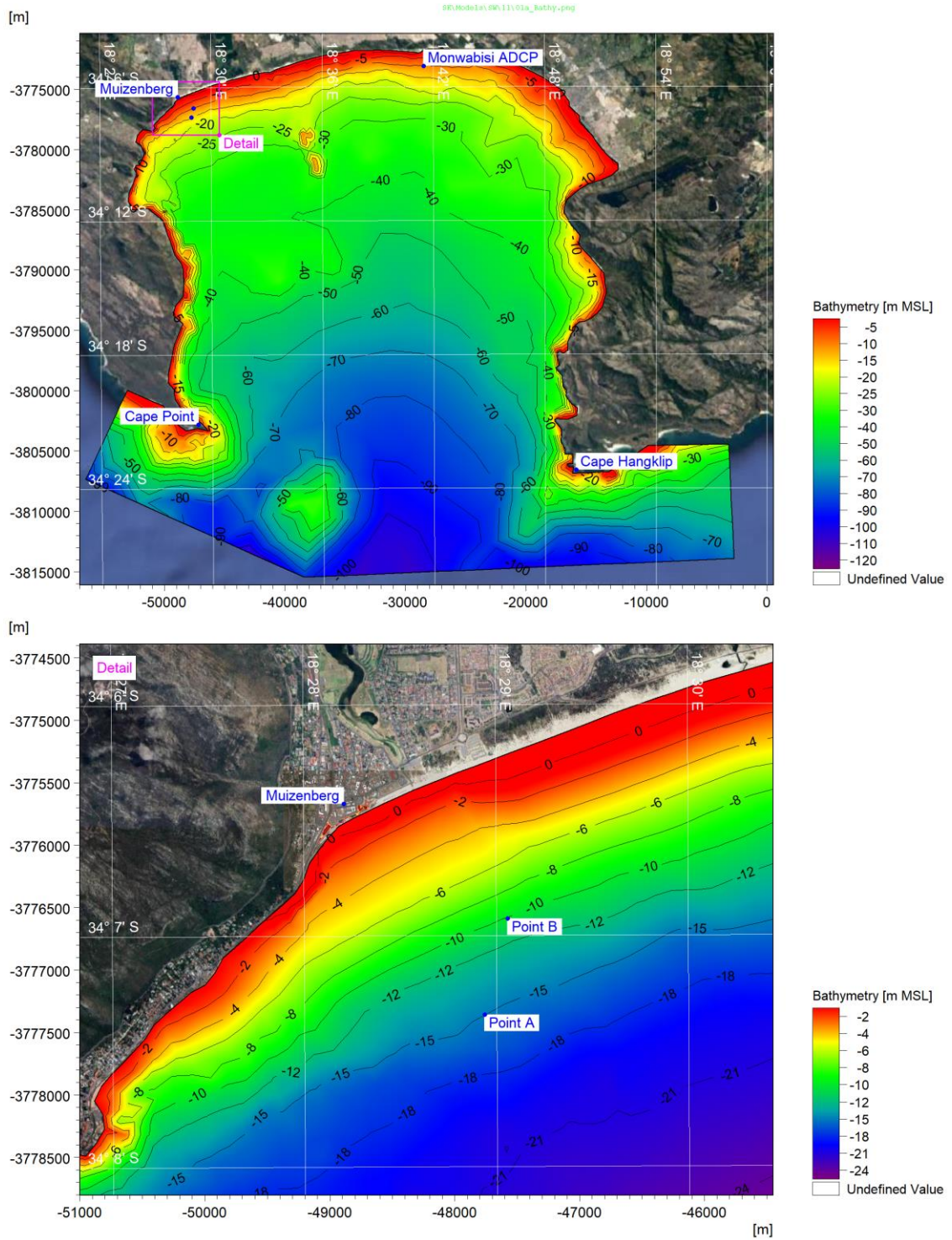


Figure 5-3: Nested model bathymetry. Note the top colour scale is non-linear.

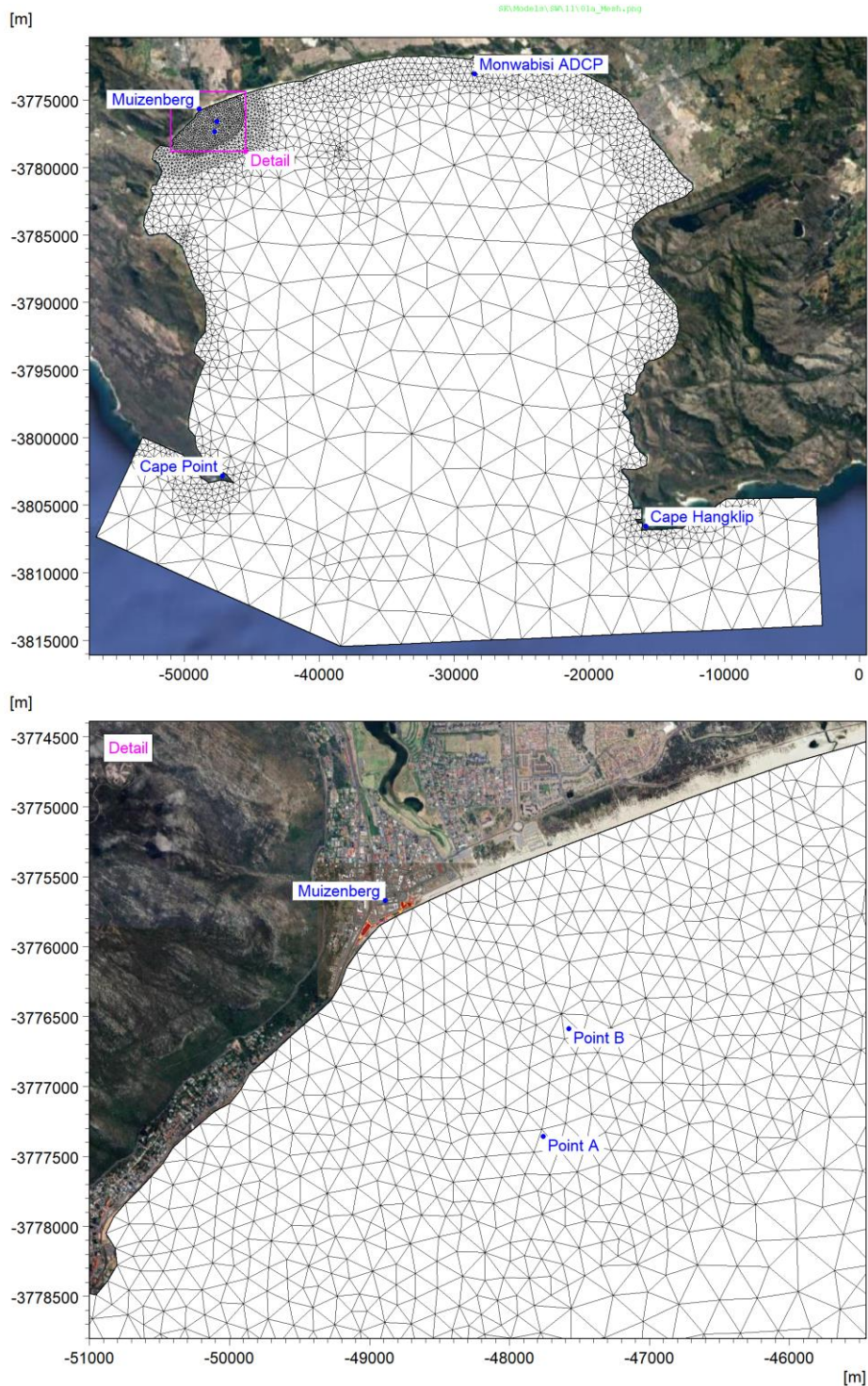


Figure 5-4: Nested model computational mesh.

5.4.2 Boundary conditions

The local wave model was forced using the same water levels, wind and model settings as the regional model. The wave boundary conditions for the local model were extracted from the regional wave model and were applied as time and space-varying wave spectra. The model was run in the quasi-stationary mode, which assumes fetch-limited wind-wave generation and sea states which are stationary in time.



5.5 Calibration

The model was calibrated to spectral wave data measured by Lwandle at Monwabisi (28 482 m E, 3 773 066 m S, approximately 12.5 km east of the site) between 4 January 2018 and 27 April 2018. The calibration model was run for the duration of the measurement period with a mesh refined in the area of the ADCP.

The coarse resolution (0.5°) of the NCEP wind hindcast model was unable to adequately resolve the local wind fields in False Bay and especially underpredicted storm events associated with south-easterly winds. A constant correction factor of 1.12 was applied to the wind speed to compensate for the underprediction, which resulted in an improved calibration of the modelled wave parameters.

Figure 5-5 presents a wave refraction plot of the regional model and the nested model. Figure 5-6 compares the time-series of measured and modelled wave parameters. A scatter plot showing the measured and modelled wave heights is shown in Figure 5-7 and wave roses are compared in Figure 5-8. Note that a discrepancy in the measured ADCP directions for three of the eight deployments was flagged and the directions were therefore adjusted to fit to the mean trend of the remaining measurements. By convention, wave direction is the direction from which the wave is coming, measured clockwise from true north.

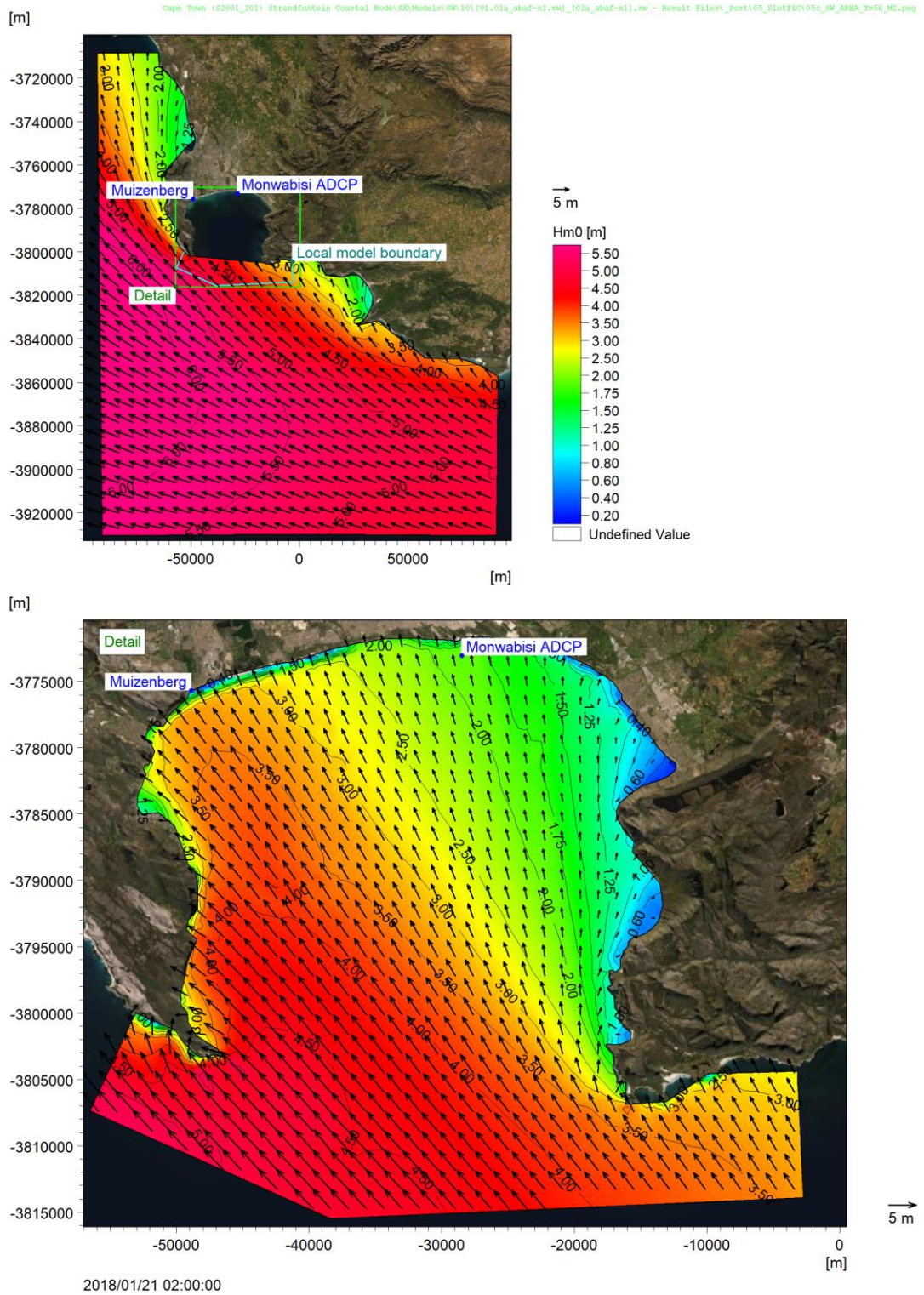


Figure 5-5: Wave refraction plot, demonstrating coupling between regional (top) and nested (bottom) model. Note the colour scale is non-linear.

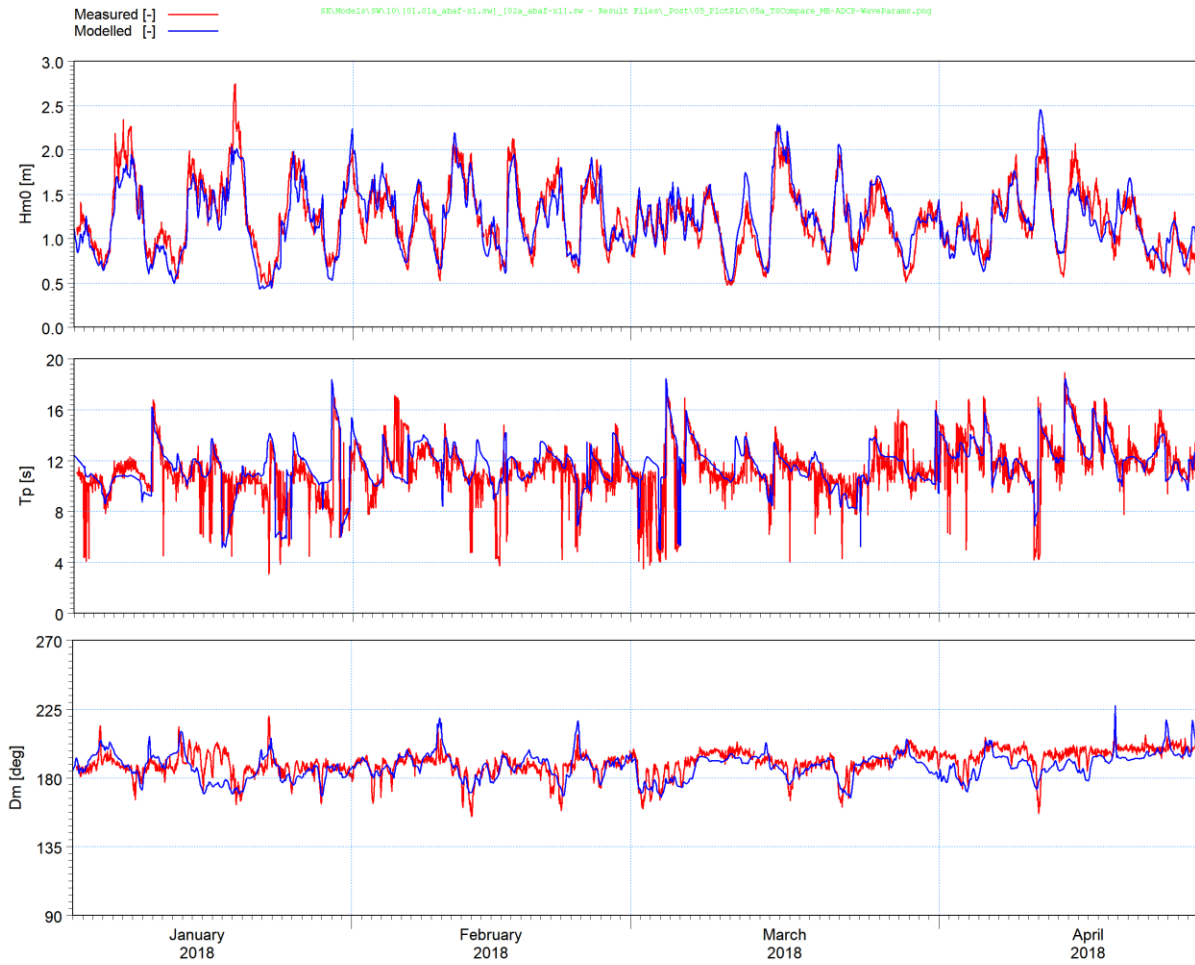


Figure 5-6: Time-series comparison of measured and modelled wave parameters at Monwabisi.

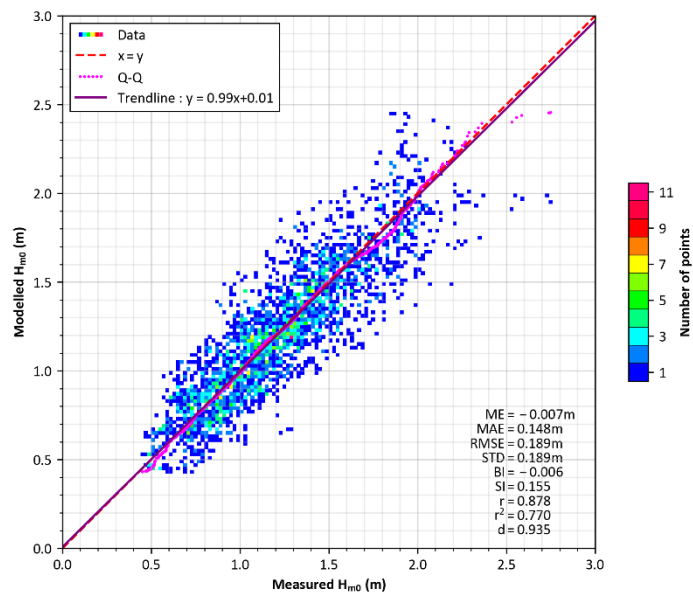


Figure 5-7: Scatter and quantile-quantile (Q-Q) comparison of measured and modelled wave parameters at Monwabisi.

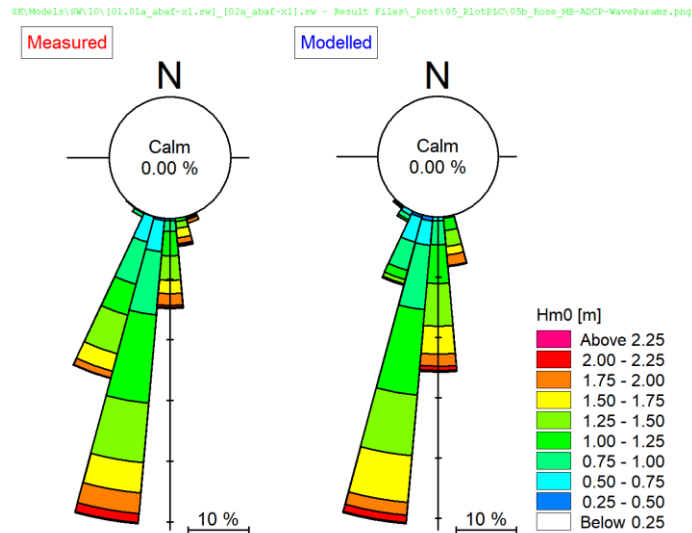


Figure 5-8: Comparison of measured and modelled wave roses at Monwabisi.

With the adjusted wind field the wave model accurately reproduced the spectral wave parameters with the exception of two underpredicted events in January and one overpredicted event in April. Considering the favourable comparison between the modelled and measured trendline shown in Figure 5-7, the model is considered to be sufficiently well-calibrated for the purpose of this study.

5.6 Modelling period

The model was run for the full duration of the three hindcast wind and wave datasets – namely the Reanalysis (1979-2009), Production (2005-2019) and Forecast (2007-2021) datasets. In the case of overlapping dates, the order of preference for the datasets was Reanalysis, Production, then Forecast with a combined dataset length of 42.2 years.

5.7 Results

5.7.1 Extreme waves

Figure 5-9 presents an example wave refraction plot for the 25 January 1981 storm event. Also shown are the output locations of Point A and Point B where the extreme and operational wave parameters were extracted. The coordinates of the locations are listed in Table 5-1.

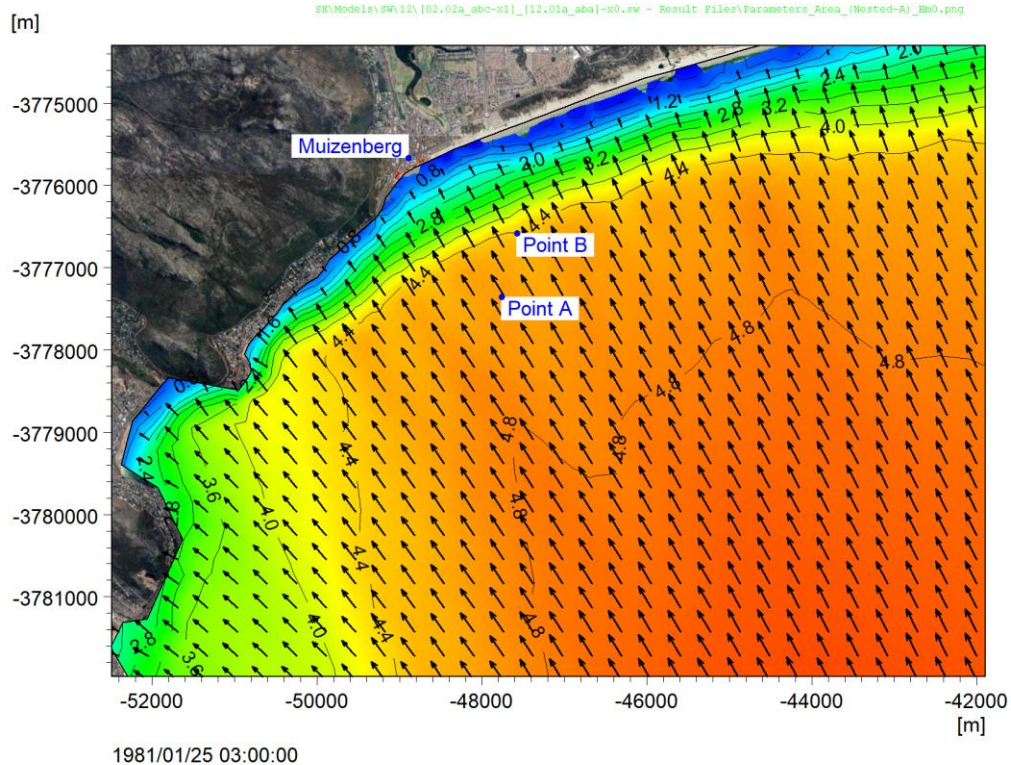
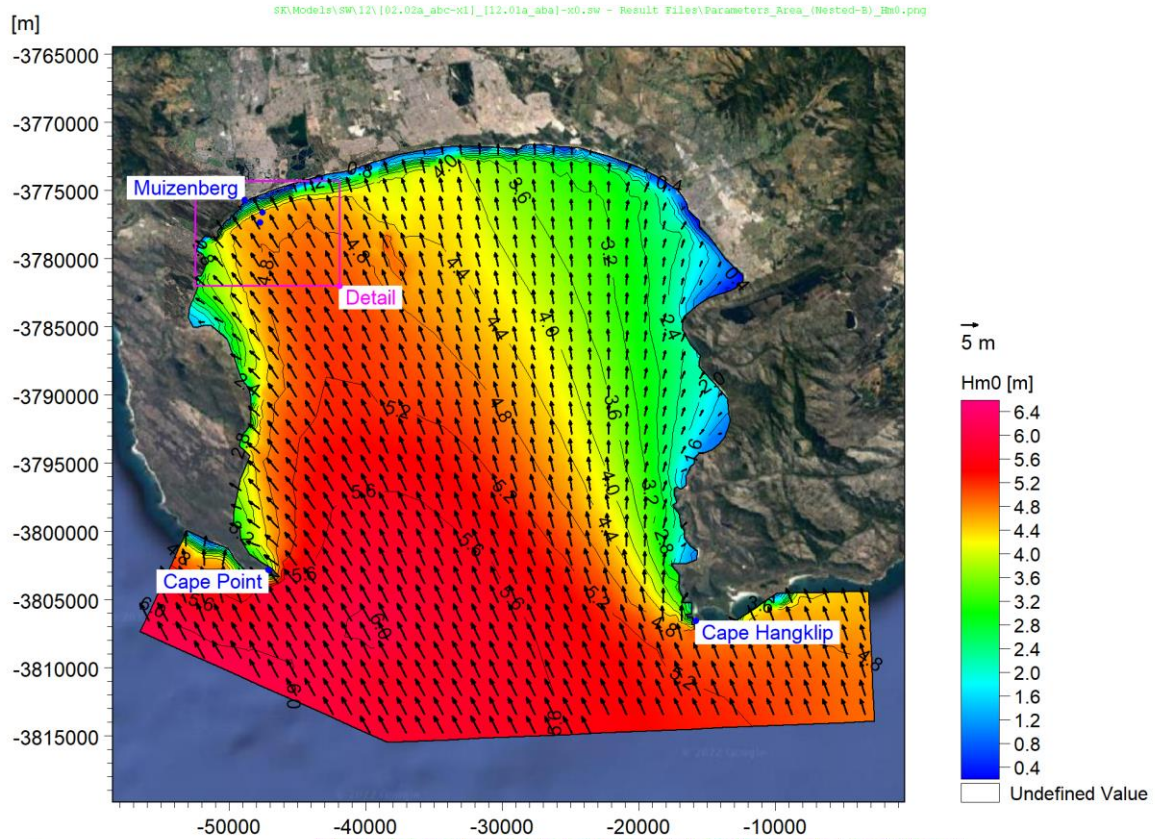


Figure 5-9: Wave refraction plot for the 25 January 1981 storm event.

Table 5-1: Output locations for the extreme and operational wave conditions.

Location	X [m WG19]	Y [m WG19]	Depth [m MSL]
Point A	-47 759	-3 777 356	-15
Point B	-47 577	-3 776 586	-10

The nearshore extreme wave climate was analysed from an extreme value series of storms selected using the ‘peaks over threshold’ or ‘partial duration series’ method, with the threshold defined as the value that is exceeded ten times per year on average, thus 422 events over 42.2 years. To ensure independence, two successive events were extracted only if the time between the events exceeded 48 hours. A time-window of 24 h before and after the storm peak was included in the selection. Figure 5-10 presents a scatter plot of H_{m0} and T_p extracted from 422 storm events at Point A.

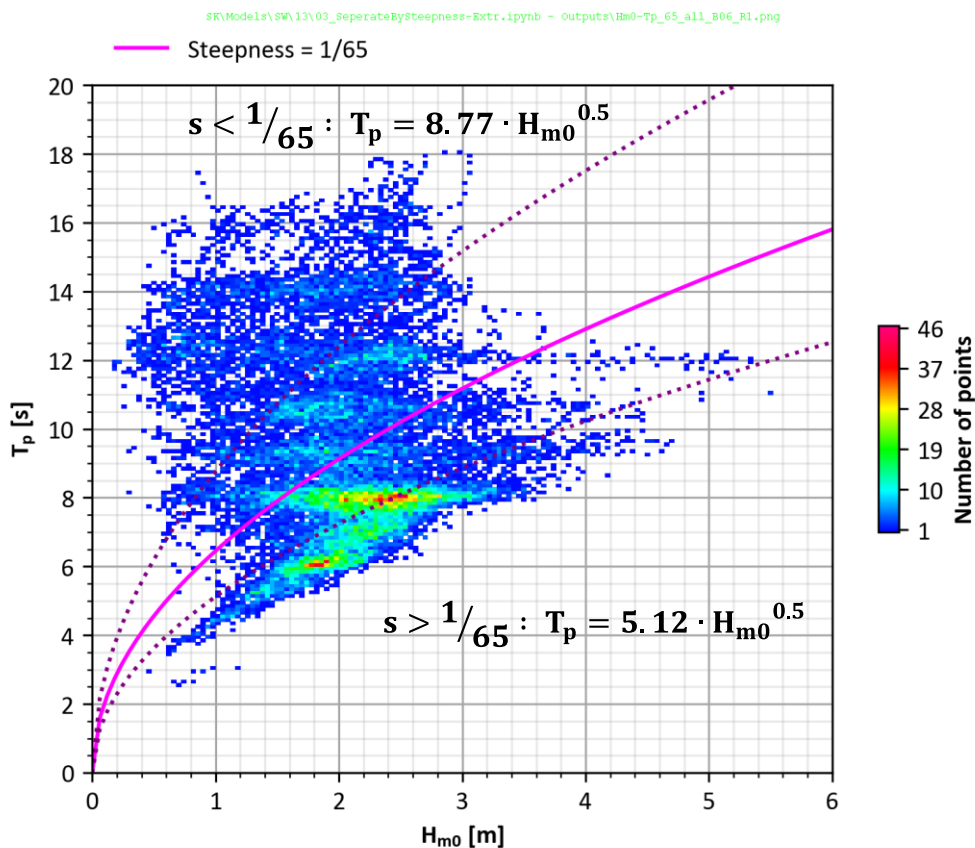


Figure 5-10: Scatter plot of H_{m0} and T_p at Point A from 422 storm events. Two partitions, separated at a wave steepness of $s = 1/65$ are shown. Also shown are the H_{m0} - T_p trendlines for each partition.

Two partitions of wave data can be observed:

- larger wave heights with shorter wave periods driven by strong south-easterly winds over a long, unobstructed fetch; and
- smaller wave heights with longer wave periods typically associated with south-westerly swells refracting around Cape Point.

The two partitions were separated for further analyses using the deep water spectral wave steepness equation:

$$s = \frac{H_{m0}}{L_0} = \frac{2\pi H_{m0}}{gT_p^2} \quad \text{Eq 5-1}$$

Where:

- s = deep water spectral wave steepness
- $g = 9.81 \text{ m/s}^2$ = gravitational acceleration
- L_0 = deep water wavelength

An extreme value analysis (EVA) of H_{m0} was performed on each partition using the ‘MIKE by DHI’ EVA toolbox (DHI, 2022e). The analysis comprises fitting a three parameter Weibull distribution using the Method of Moments to an extreme value series extracted from the input time-series. The extreme value series was selected using the peaks over threshold method, with the threshold defined as the value that is exceeded two times per year on average. To ensure independence, two successive events were extracted only if the time between the events exceeded 48 hours. The uncertainty was calculated using Jackknife resampling to evaluate the mean and standard deviation of the estimate to obtain the 95% confidence (2.5th to 97.5th percentile) estimates. An EVA plot is shown in Figure 5-11.

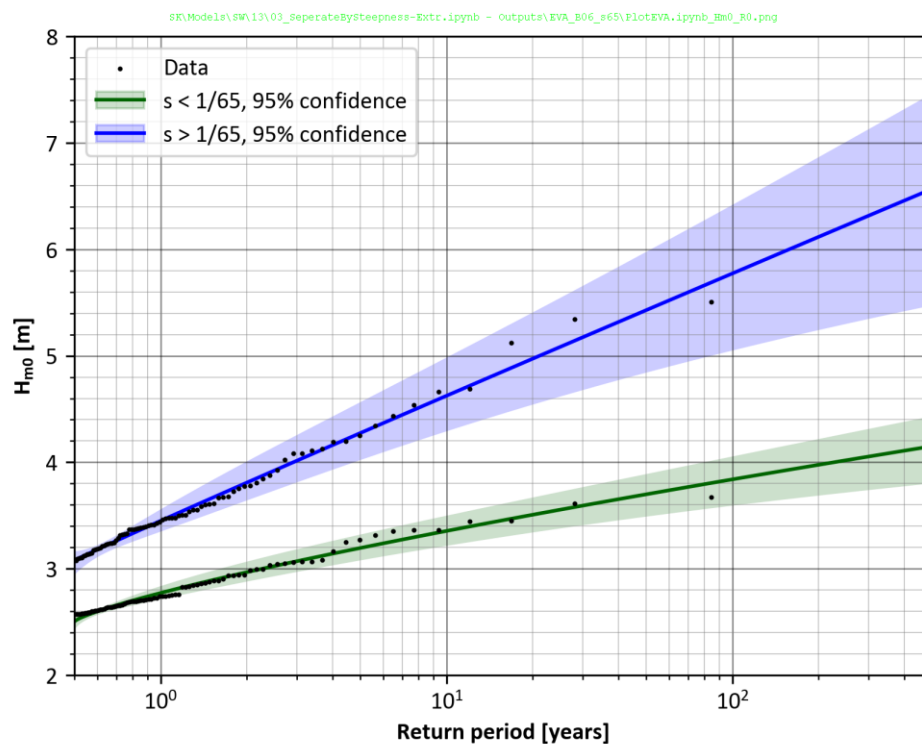


Figure 5-11: H_{m0} EVA plot for the extreme wave climate at -15 m MSL.

A summary of the extreme wave climate is provided in Table 5-2. The associated extreme peak wave periods were estimated by fitting a power curve ($T_p = a \cdot H_{m0}^{0.5}$; a = fitting coefficient) to each partition using the least squares method, as shown in Figure 5-10.



Table 5-2: Extreme nearshore wave climate.

Climate change horizon	Return period [y]	s > 1/65		s < 1/65	
		H _{m0} ^(a) [m]	T _p ^(b) [s]	H _{m0} ^(a) [m]	T _p ^(c) [s]
Present-day (baseline date 2000)	1	3.56	9.66	2.84	14.8
	10	4.98	11.43	3.50	16.4
	100	6.12	12.97	4.05	17.7
	475	7.43	14.0	4.42	18.4
2026 ^(d)	1	3.59	9.7	2.87	14.8
	10	5.03	11.5	3.53	16.5
	100	6.48	13.0	4.09	17.7
	475	7.51	14.0	4.46	18.5
2046 ^(d)	1	3.62	9.7	2.89	14.9
	10	5.07	11.5	3.56	16.5
	100	6.53	13.1	4.13	17.8
	475	7.56	14.1	4.50	18.6
2076 ^(d)	1	3.66	9.8	2.92	15.0
	10	5.13	11.6	3.60	16.6
	100	6.60	13.2	4.17	17.9
	475	7.65	14.2	4.55	18.7

Notes:

(a) Upper 95% confidence

(b) $T_p = 5.12 \times H_{m0}^{0.5}$

(c) $T_p = 8.77 \times H_{m0}^{0.5}$

(d) Refer to Table 3-1 for extreme wave height increase due to climate change

The complete set of extreme conditions considering the joint probabilities of storm surge and wave height are presented in Section 6.

5.7.2 Operational waves

Figure 5-12 shows the time-series of operational wave parameters (H_{m0}, T_p and D_m) for the 31 years of operational wave conditions extracted at Point B offshore of Muizenberg at -10 m MSL (location shown in Figure 5-9 and Table 5-1).

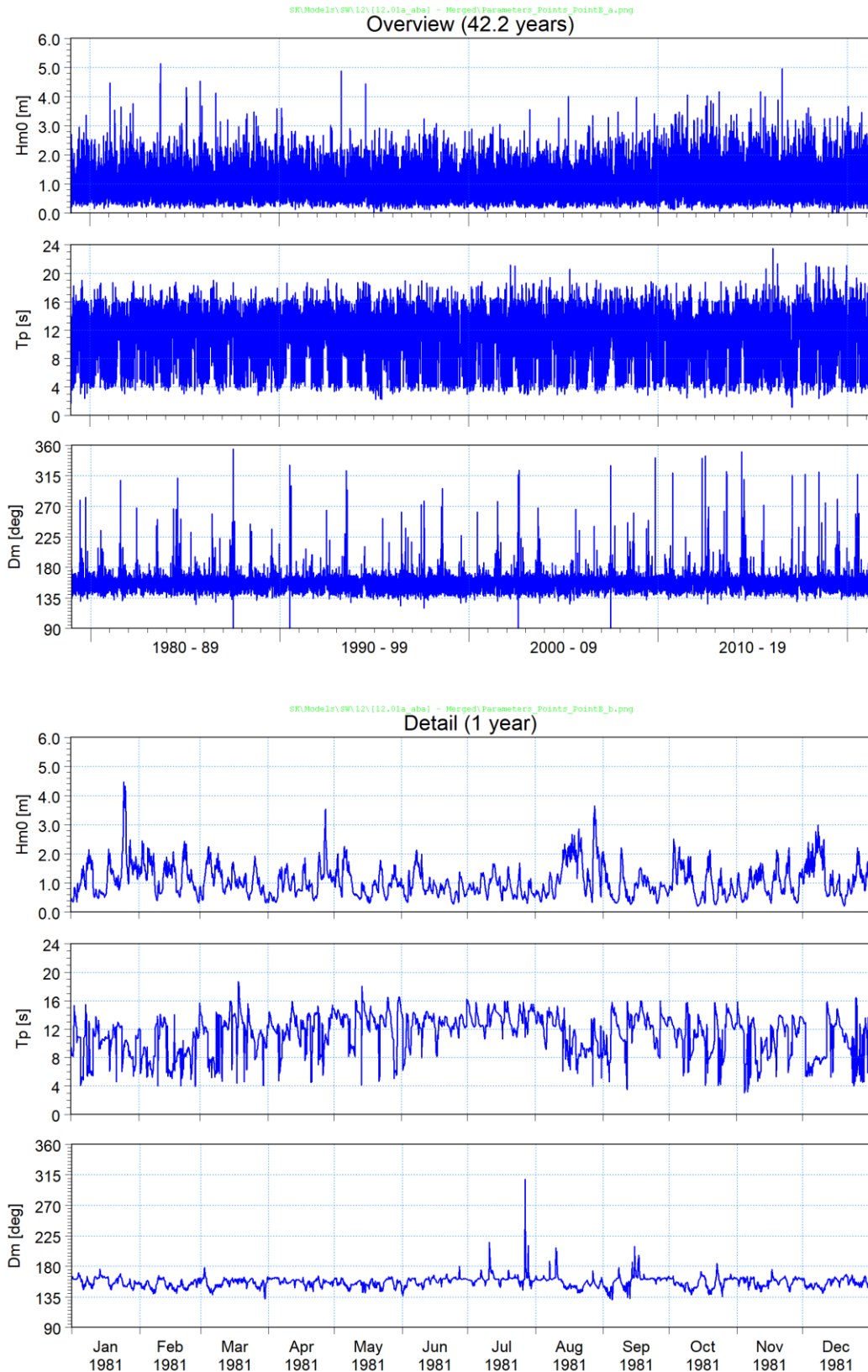


Figure 5-12: Time-series of operational wave parameters extracted at Point B.

The results will be used in the longshore sand transport modelling (Section 7.3).



6. NEARSHORE EXTREME WATER LEVELS AND WAVES

6.1 Joint probability of storm surge and wave height

A methodology for calculating the joint probability and resultant impact on coastal flooding of storm surge vs wave height, storm surge vs river discharge and wave height vs river discharge is described by Petroligkis, et al. (2016). This methodology has been applied in this section, based on the similarity of the application and the solid theoretical basis presented in Petroligkis, et al. (2016). The joint (combined) return period of two variables (e.g., storm surge and wave height) is given by:

$$T_{X,Y} = \sqrt{\frac{T_X \cdot T_Y}{\chi^2}} \quad \text{Eq 6-1}$$

where:

- $T_{X,Y}$ = joint return period of two variables occurring together
- T_X = exceedance probability of first variable
- T_Y = exceedance probability of second variable
- χ = dependence between the first and second variables ranging between 1 when fully dependent and 0 when independent.

The dependence parameter χ is calculated from a site-specific dataset containing simultaneous values of the first (X) and second (Y) variables. The methodology requires counting the number of events where both variables simultaneously exceed a common percentile threshold (x^* , y^*), which enables χ to be calculated for each percentile as shown in Eq 6-2:

$$\chi = 2 - \frac{\ln \left[\frac{\text{Number of (X,Y) such that } X \leq x^* \text{ and } Y \leq y^*}{\text{Total number of (X,Y)}} \right]}{\frac{1}{2} \ln \left[\frac{\text{Number of } X \leq x^*}{\text{Total number of } X} \cdot \frac{\text{Number of } Y \leq y^*}{\text{Total number of } Y} \right]} \quad \text{Eq 6-2}$$

The largest χ is then selected from the range of percentiles representing the more extreme events, e.g., events above the 85th percentile, since only the extreme events are of interest. The applicable formulas and the full details of the methodology are provided in Petroligkis, et al. (2016). The following categories of dependence are defined:

Table 6-1: Categories of dependence (Petroligkis, et al., 2016).

Dependence Parameter χ	Category
$\chi \leq -0.06$	Negative
$-0.05 \leq \chi \leq 0.05$	Zero
$0.06 \leq \chi \leq 0.14$	Low
$0.15 \leq \chi \leq 0.24$	Modest
$0.25 \leq \chi \leq 0.34$	Well
$0.35 \leq \chi \leq 0.44$	Strong
$\chi \geq 0.45$	Very Strong

The site-specific dataset used was the storm surge at Muizenberg (Section 4) and nearshore modelled wave heights extracted at Point A (Section 5.7). The intersection of the two datasets provides 28.9 years of storm



surge and wave height pairs. Figure 6-1 and Figure 6-2 show scatter plots of storm surge at Muizenberg and wave heights extracted at Point A for wave the partitions with $s < 1/65$ and $s > 1/65$ respectively, while Figure 6-3 and Figure 6-4 show the calculated dependence parameters of storm surge and wave height for both wave partitions.

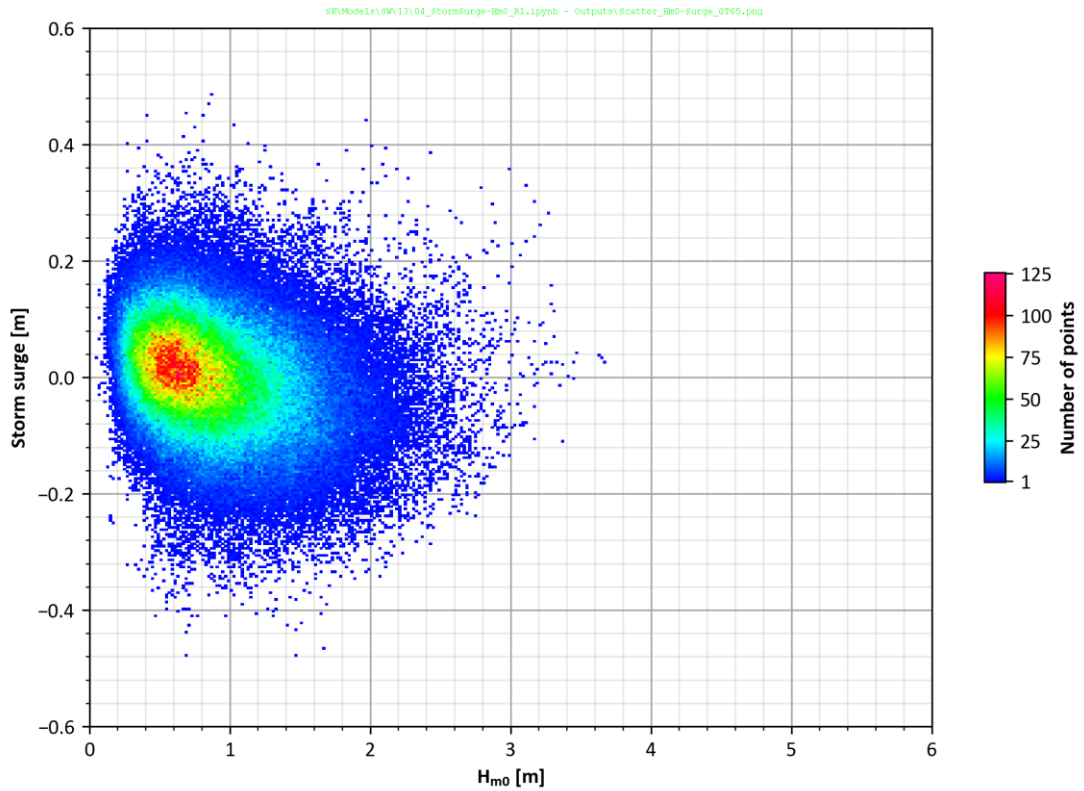


Figure 6-1: Scatter plot of 23.9 years of storm surge and wave height pairs at Muizenberg for waves with a steepness of $s < 1/65$.

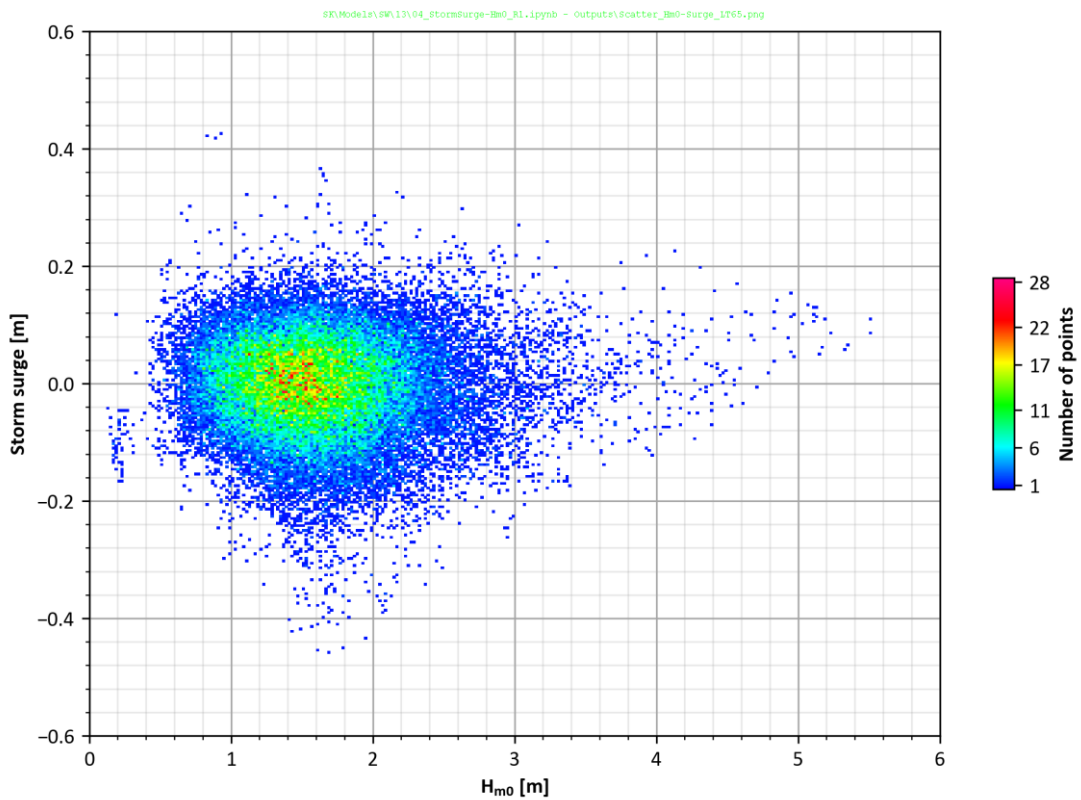


Figure 6-2: Scatter plot of 4.8 years of storm surge and wave height pairs at Muizenberg for waves with a steepness of $s > 1/65$.

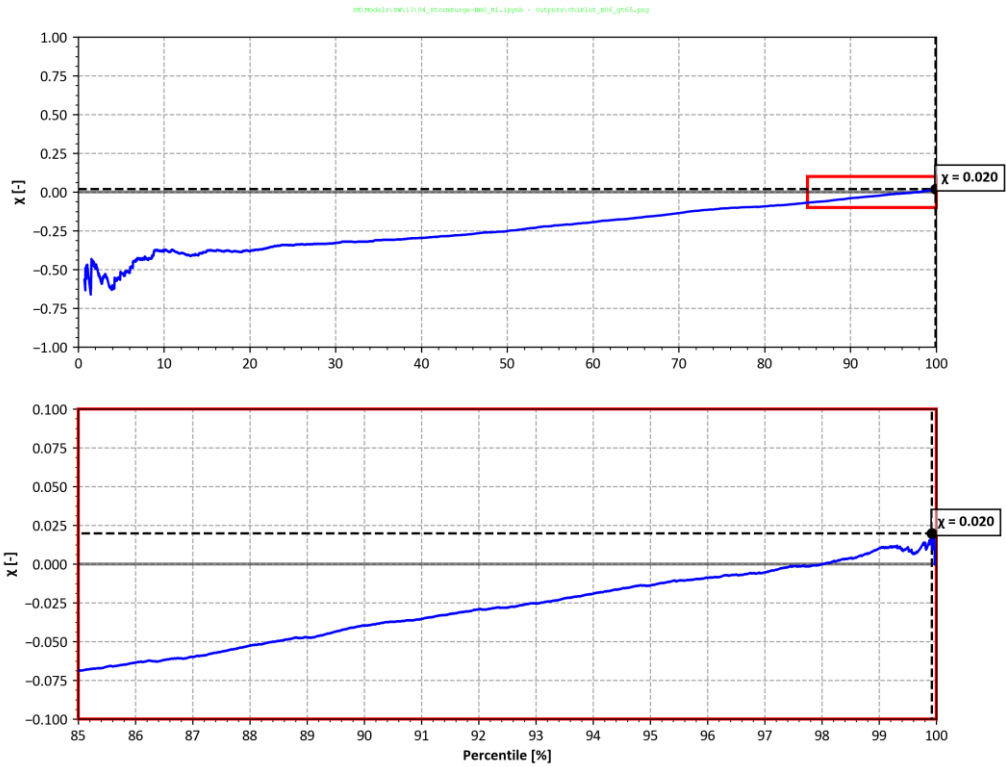


Figure 6-3: Dependence parameter χ of storm surge and wave height at Muizenberg for waves with a steepness of $H/L < 1/65$.

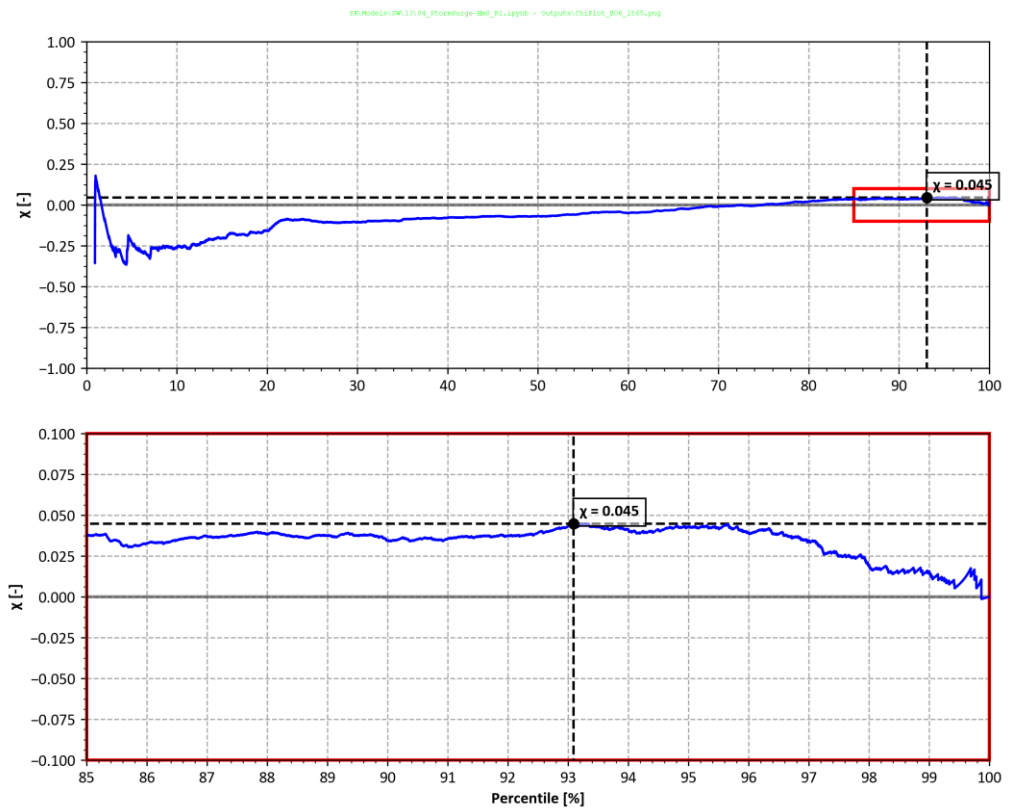


Figure 6-4: Dependence parameter χ of storm surge and wave height at Muizenberg for waves with a steepness of $s > 1/65$.



As shown in Figure 6-1 and Figure 6-2, storm surge and wave height exhibit little correlation at Muizenberg, since the low-pressure frontal weather systems generating the waves hundreds to thousands of kilometres offshore do not arrive at the same time as the waves. Furthermore, the south-easterly wind events which generate large waves and high wind set-up at Muizenberg are typically associated with high atmospheric pressure which counteracts the wind set-up through the inverse barometer effect.

The results show that χ has a maximum value of 0.020 for $s < 1/65$ and 0.045 for $s > 1/65$ which both are categorised in Table 6-1 as a “zero” dependence, i.e., independent. Since Eq 6-3 does not suited for χ values approaching zero, all return periods for variable 1 were combined with a return period of 1 year for variable 2, and vice versa – as shown in Table 6-2. This is a conservative approach considering that the storm surge and wave height are independent and the peak of the storm events have durations less than one day.

Table 6-2: Joint return period of storm surge and wave height for zero dependence.

Joint return period	Storm surge	Wave height
1	1	1
10	1	10
	10	1
100	1	100
	100	1
475	1	475
	475	1

6.2 Extreme conditions

The extreme conditions to be modelled were combined from the extreme wave climate in Table 5-2 and the extreme still water levels in Table 4-2 considering the joint probabilities of storm surge and wave height from Section 6.1. The total number of cases modelled was thus 4 return periods \times 2 joint probability combinations (excluding 1 year return period) \times 2 wave partitions = 14 cases for each of the 3 climate change dates. The extreme conditions are summarised in Table 6-3.



Table 6-3: Extreme conditions at -15 m MSL.

Extreme condition		Wave parameters ^(a)					Still water level ^(b)	
Climate change horizon	Return period	Return period	s > 1/65		s < 1/65		Return period	Water level
			H _{m0}	T _p	H _{m0}	T _p		
	[y]	[y]	[m]	[s]	[m]	[s]	[y]	[m MSL]
2026	1	1	3.59	9.7	2.87	14.8	1	1.41
	10	10	5.03	11.5	3.53	16.5	1	1.41
		1	3.59	9.7	2.87	14.8	10	1.52
	100	100	6.48	13.0	4.09	17.7	1	1.41
		1	3.59	9.7	2.87	14.8	100	1.63
	475	475	7.51	14.0	4.46	18.5	1	1.41
1		3.59	9.7	2.87	14.8	475	1.70	
2046	1	1	3.62	9.7	2.89	14.9	1	1.54
	10	10	5.07	11.5	3.56	16.5	1	1.54
		1	3.62	9.7	2.89	14.9	10	1.66
	100	100	6.53	13.1	4.13	17.8	1	1.54
		1	3.62	9.7	2.89	14.9	100	1.77
	475	475	7.56	14.1	4.50	18.6	1	1.54
1		3.62	9.7	2.89	14.9	475	1.84	
2076	1	1	3.66	9.8	2.92	15.0	1	1.83
	10	10	5.13	11.6	3.60	16.6	1	1.83
		1	3.66	9.8	2.92	15.0	10	1.95
	100	100	6.60	13.2	4.17	17.9	1	1.83
		1	3.66	9.8	2.92	15.0	100	2.06
	475	475	7.65	14.2	4.55	18.7	1	1.83
1		3.66	9.8	2.92	15.0	475	2.13	

Notes

(a) Refer to Table 5-2

(b) Refer to Table 4-2



7. COASTLINE STABILITY

7.1 Coastline trends from historical data

7.1.1 Historical aerial imagery

The coastline stability of the Muizenberg Beachfront was first investigated by comparing historical aerial and satellite imagery, which included using the following datasets:

- Historical aerial imagery between 1935 and 2022, kindly provided by the City of Cape Town.
- Historical satellite imagery available from online sources, including Esri World Imagery (Esri, 2022) and Google Earth.

The historical imagery was analysed chronologically to identify any significant changes in the coastline. To provide an overview of the historical changes, Figure 7-1 shows four aerial images from 1935, 1992, 2021 and 2022. The image from 1935 is the oldest available photograph, the image from 1992 was taken during the construction of the seawall and the images from 2021 and 2022 were taken after the construction of the seawall.

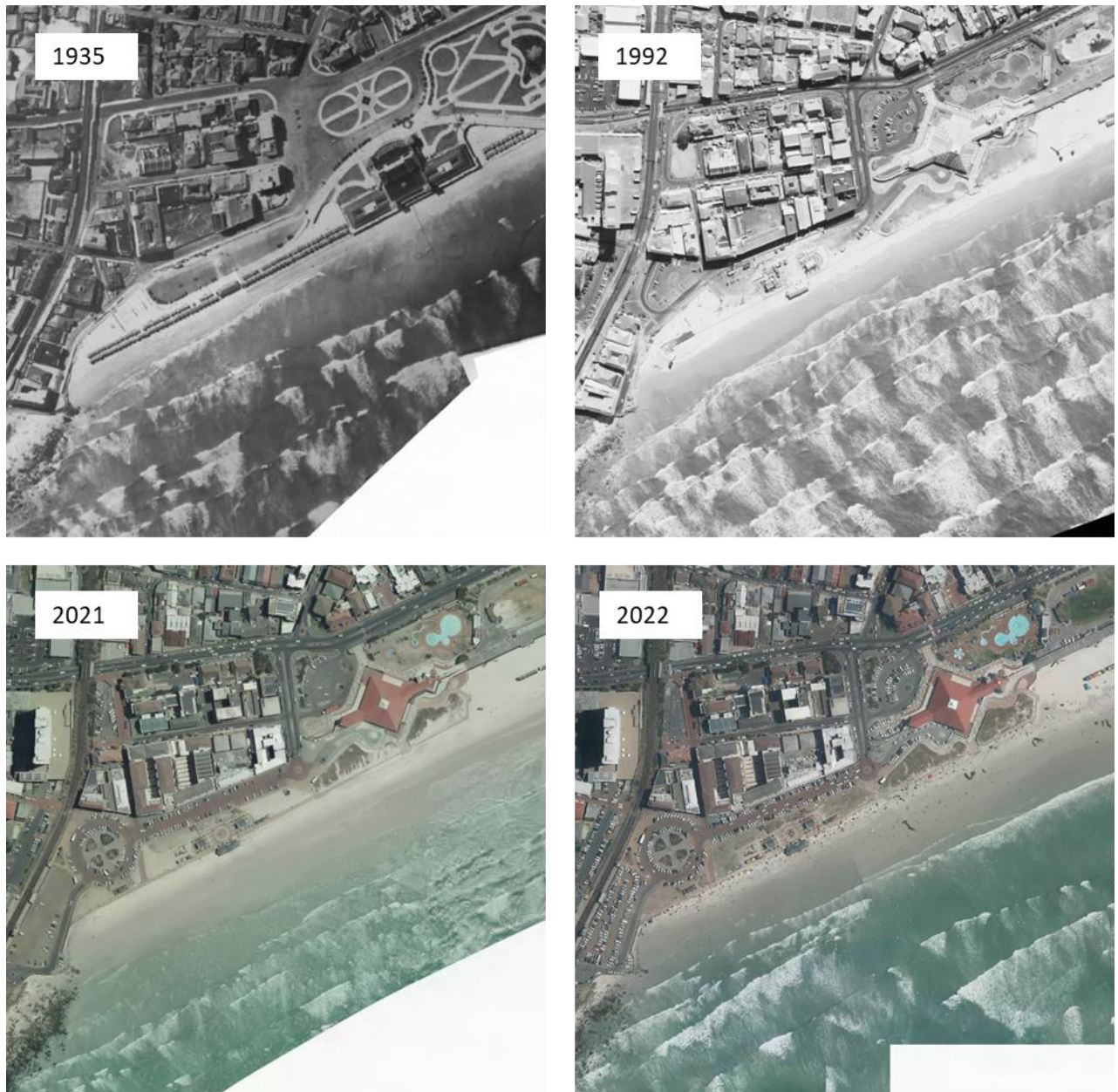


Figure 7-1: Historical aerial imagery of Muizenberg in 1935, 1992, 2021 and 2022.

The existing ablation block on the beach is visible in all four of the images. The changing rooms adjacent to the ablation block and the old pavilion visible in the 1935 image were demolished, and the present-day seawall was constructed landward of the ablation block. Throughout the images the wetted line is close to the seaward edge of the ablation block. Noting that the exact dates and times at which these images were taken are unknown and therefore the tidal level at the timestep is also unknown, the width of the dry beach is fairly consistent through all the images. The rocks at Surfer's Corner are most exposed in 1935, completely covered by sediment in 1992 and marginally exposed in 2021 and 2022. Therefore, the overview of the historical imagery does not provide an indication of an obvious accretive or erosive trend over the past 87 years.

7.1.2 Beach lowering

To manage windblown sand at Muizenberg, the CCT's Coastal Management Branch has undertaken mechanical beach lowering of the upper beach approximately since construction of the existing wooden seawall in 1992. As described in the Standard Operating Procedure (CCT, 2022b), the lowering occurs annually, typically between September and November before the strongest south-easterly winds occur. The crest of the beach is lowered from approximately +3 m MSL to approximately +2 m MSL. The sand removed at the crest of the beach is redistributed over the profile to the low water mark. Figure 7-2 illustrates the procedure, while Figure 7-3 shows a satellite image of the operation being undertaken.

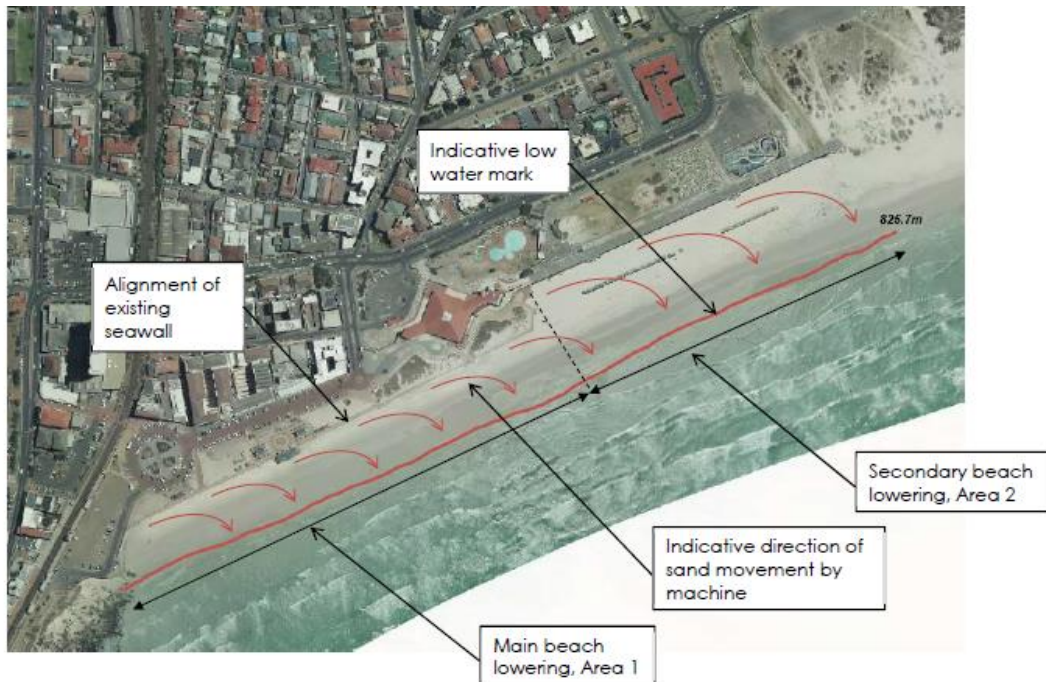


Figure 7-2: Illustration of beach lowering procedure (CCT, 2022b).

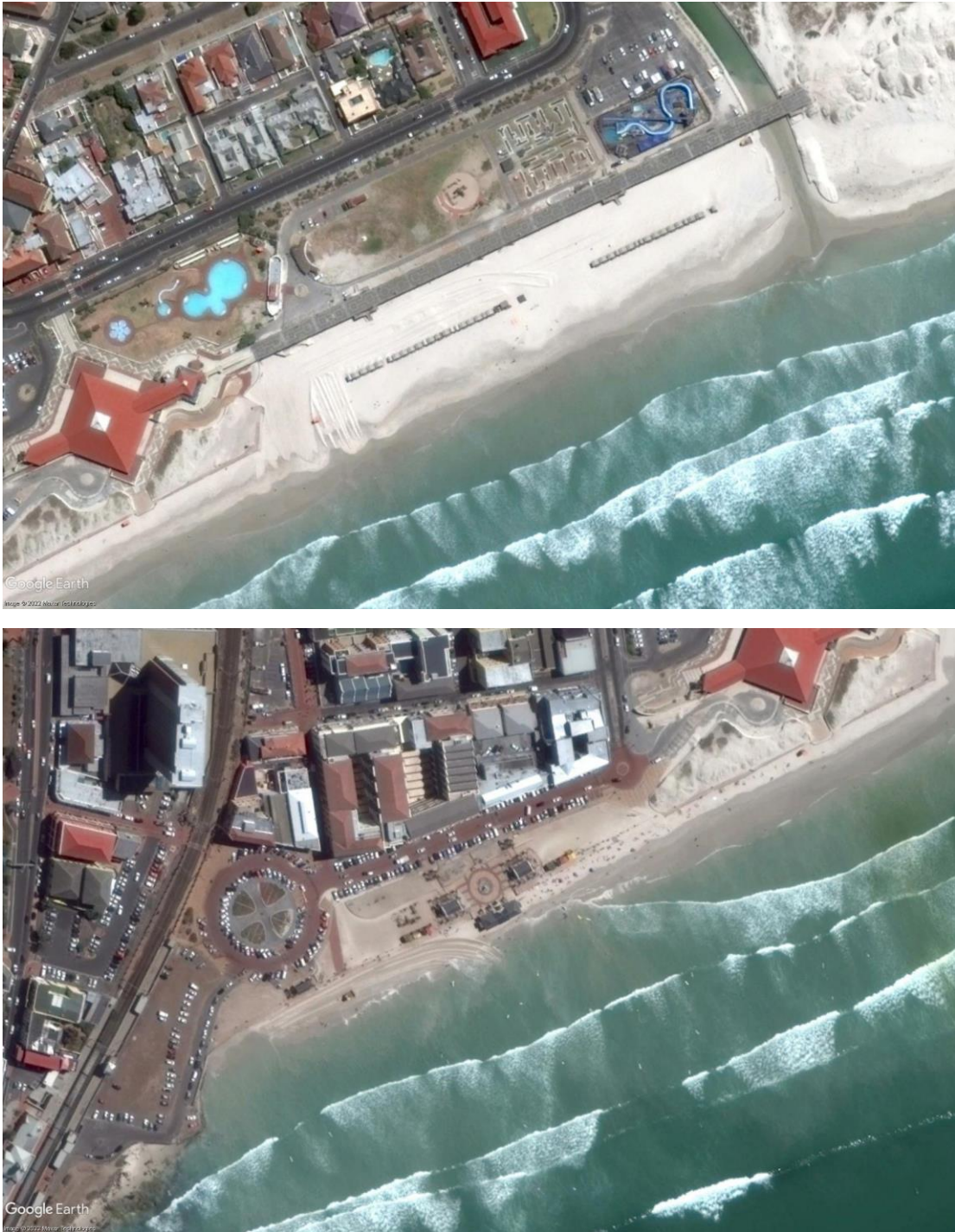


Figure 7-3: Satellite images showing the beach lowering in front of the promenade in February 2017 (top) and along the main beach in March 2017 (bottom).

The redistribution of sand from the top of the profile toward the low water mark does not impact the overall sand budget since no sand is removed from the beach. In fact, the lowering minimises the windblown sand losses which might otherwise occur. However, the redistribution does create a flatter beach profile above the low water mark. This contributes to variability in the upper beach profile, together with seasonal and storm cross-shore transport and wind-blown sand transport.

7.1.3 Wetted line analysis

A formal analysis of the long-term coastline trends was based on the estimation of the wetted line from historical aerial and satellite imagery. Figure 7-4 shows the five cross-shore lines along the Muizenberg Beachfront considered in the analysis. Lines 1 to 3 cross the main beach which is backed by the existing wooden seawall, whereas Lines 4 and 5 cross the promenade to the east of the main beach which is backed by an approximately horizontal berm.

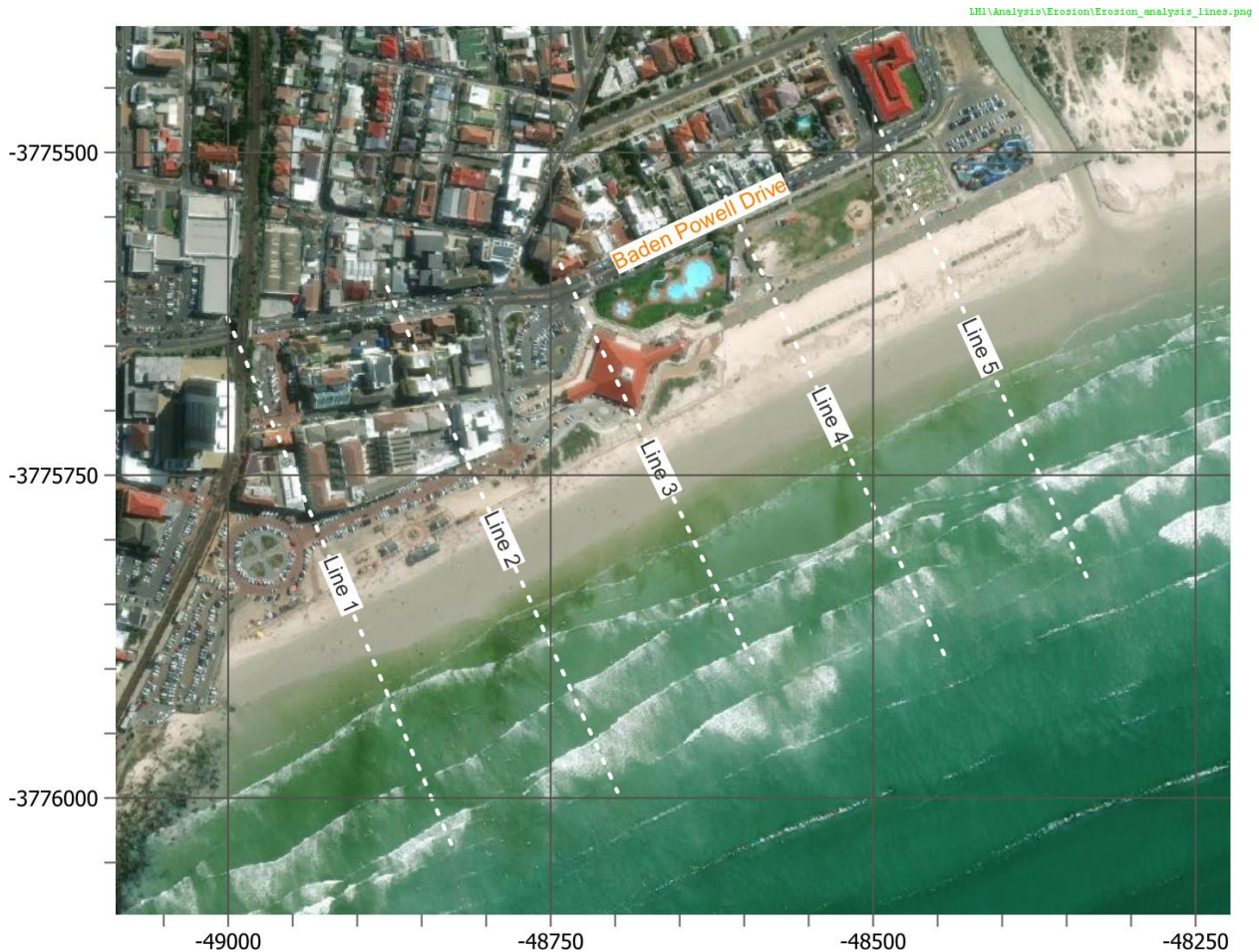


Figure 7-4: Cross-shore lines intercepting the wetted line.

Since the beach lowering does not affect the sand budget and the satellite images are sampled at all times of the year, the redistribution of sand is expected to add to the variability of a wetted line analysis, but not to affect the long-term trends. However, based on an initial analysis, the width of the dry beach at Lines 4 and 5 showed very high variability compared to Lines 1 to 3 due to the flat berm landward of the beach crest, which could be enhanced by the beach lowering. The very high variability makes the estimation of robust trends from these lines questionable. The subsequent analysis presented here was therefore focused on Lines 1 to 3 at the main beach.

For each line the interception with the wetted line was measured relative to a fixed base point which was the present-day sea wall. Besides being a convenient base point from which to estimate coastline trends, this also provides a direct measurement of the variability in the present-day dry beach width. Figure 7-5, Figure 7-6 and Figure 7-7 show the estimated long-term coastline trends at the respective cross-shore lines for the periods 1935 to 2022, 1968 to 2022 and 2002 to 2022, respectively.

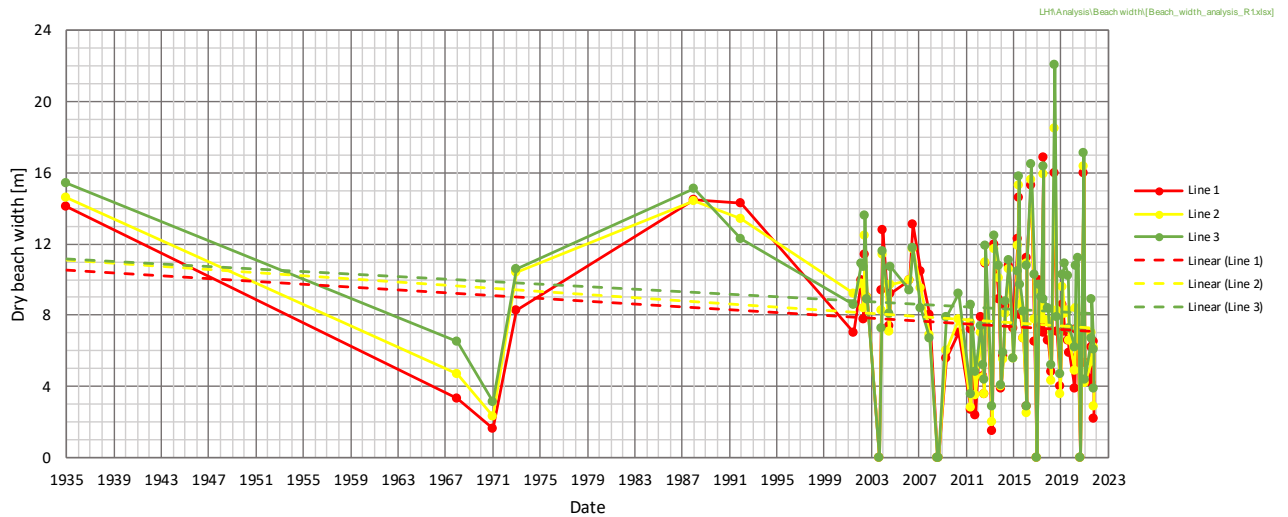


Figure 7-5: Estimated long-term wetted line trends for 1935 to 2022.

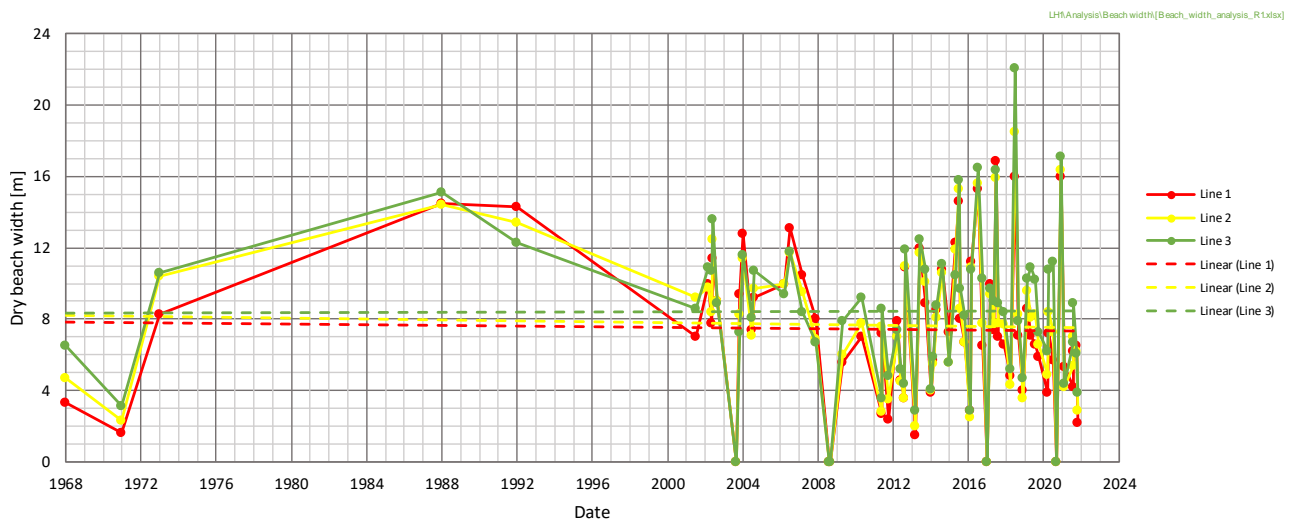


Figure 7-6: Estimated long-term wetted line trends for 1968 to 2022.

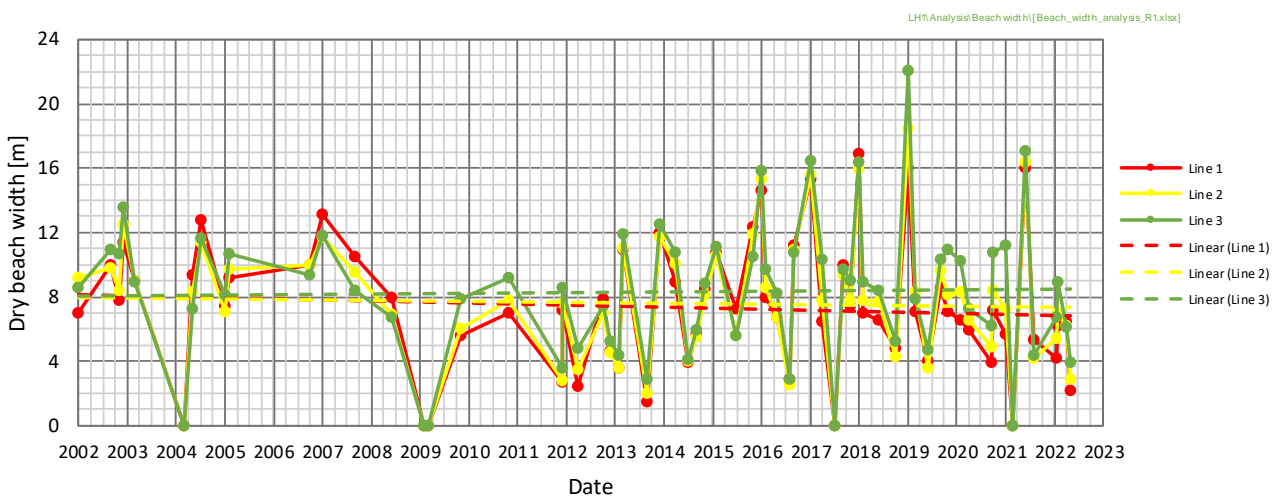


Figure 7-7: Estimated long-term coastline trends for 2002 to 2022.



There is significant scatter in the assessment, which arises from natural variability in the wetted line caused by varying water levels, wave conditions and seasonal changes in beach levels (including beach lowering), as well as limitations on image quality. The results for 1935 show an accreted beach state and the trendlines indicate slight erosion over the 87-year period. When the data points for 1935 are excluded, as shown in Figure 7-6, the trendlines show minimal change. The data points for 1935 are well within the range of variability of the rest of the data, but the point has a significant impact on the trendline results.

The analysis was also done for the period of 2002 to 2022 during which data was available more frequently. This period also showed minimal change. A notable feature visible in the results is the seasonal signal, typically showing a wider dry beach during the summer months and narrower dry beach in the winter months. This is likely due to a combination of increased longshore sand supply and increased onshore windblown sand during summer. While some influence of the beach lowering is possible, this would be expected to result in a narrower beach during summer than in winter. This is not clearly visible in the results.

The long-term trends for each line and the average of the individual trends are summarised in Table 7-1.

Table 7-1: Long-term coastline trends based on wetted line analysis.

Location	Historical trends [m/y]		
	1935 to 2022	1968 to 2022	2002 to 2022
Line 1	-0.04	-0.01	-0.06
Line 2	-0.04	-0.01	-0.03
Line 3	-0.04	0.00	0.02
Average	-0.04	-0.01	-0.02

Note: Positive is accretion, negative is erosion

Overall, the results do not support any significant trend, which suggests that the coastline has historically been approximately stable. Given historical sea level rise, the apparent stability implies a supply of sand to the beach, which otherwise would have shown an erosive trend.

7.1.4 Historical beach profile analysis

Beach profiles have been kindly provided by CCT from measurements between 2004 and 2010 over eighteen campaigns along three cross-shore transects: Profile A, B and C (locations shown in Figure 7-8). The CCT has also provided LiDAR data from four surveys (between 2013 and 2021) which was used to synthesise profiles by interpolating the data onto the coordinates of Profiles A to C. Similarly, spot height measurements taken for the Transport and Urban Development Authority (TDA) in 2018 were interpolated onto the profile coordinates. Due to the proximity of the 2022 Tritan beach survey (Section 2.2) the profiles were also included the historical beach profile analysis.

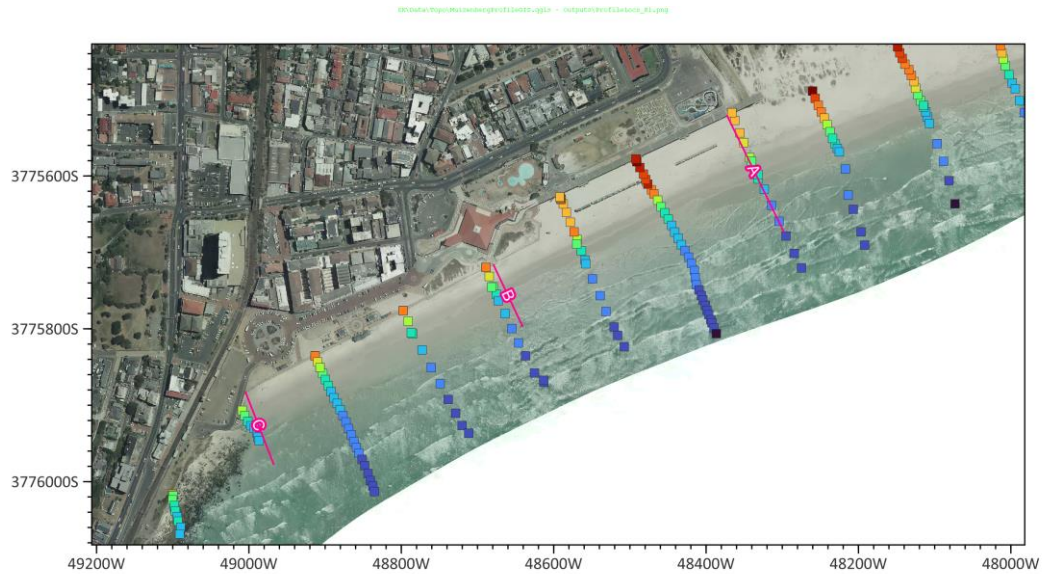


Figure 7-8: Locations of Profiles A, B and C used in the historical erosion/accretion analysis. Also shown is the proximity of the Tritan beach survey (coloured squares) relative to the profile locations.

To analyse the trends, the horizontal distance from the start of the beach profile to the 0, 0.5, 1.0, 1.5, 2.0 and 2.5 m MSL levels on the profiles have been extracted for each of the profiles. A trend line has been fitted to the relevant data and the slopes of the trend lines have been used to estimate erosion/accretion rates for each profile based on the horizontal changes at these elevations. The trend analyses for Profiles A, B and C are shown in Figure 7-9, Figure 7-10 and Figure 7-11 respectively.



SRK\Data\Topo\MuizenbergProfile11e010.ipynb - Outputs\Plots\Hybrid_Profile_a.png

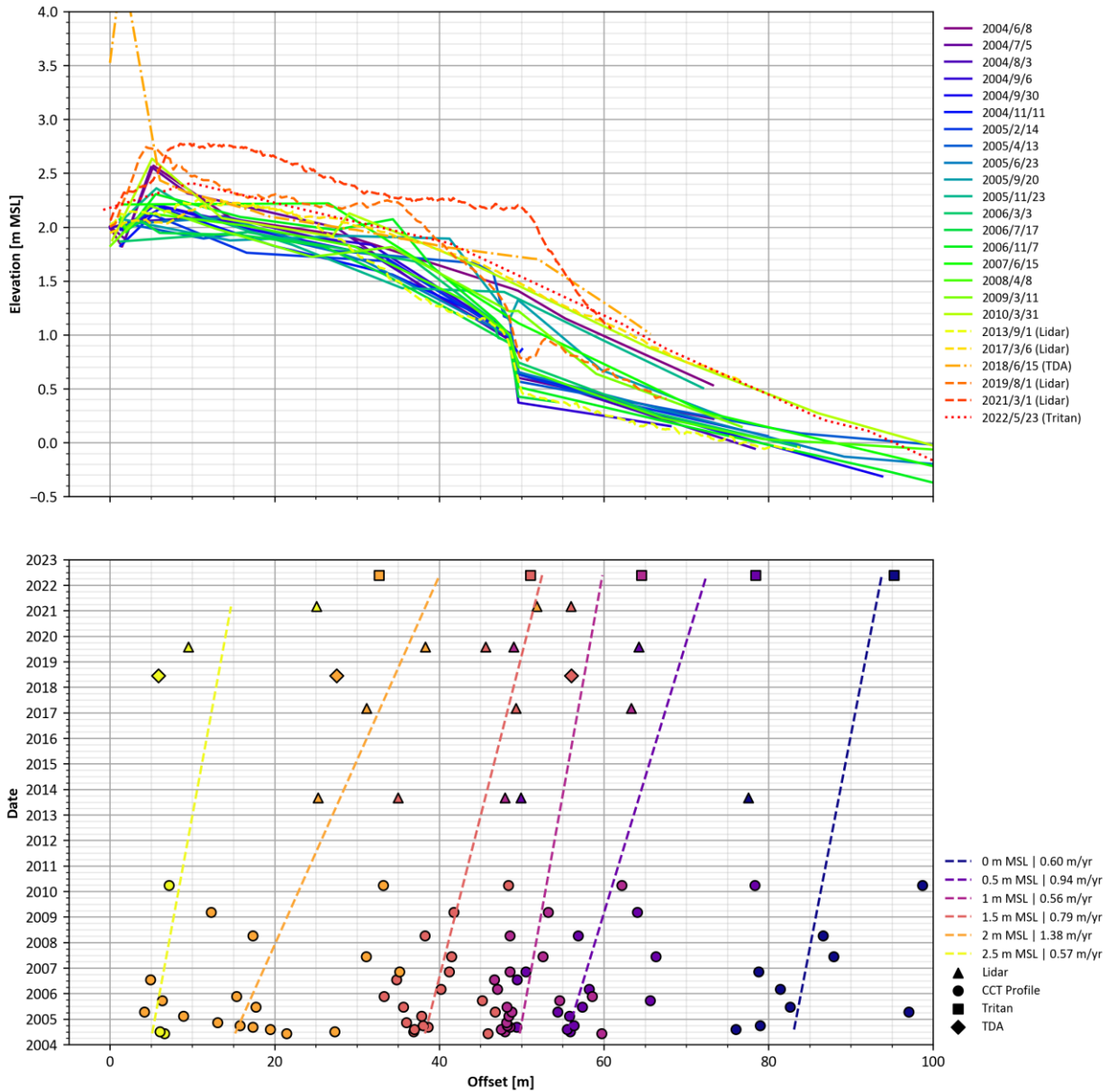


Figure 7-9: Profile A historical erosion/accretion analysis. Top: profile evolution over time. Bottom: horizontal movement of profile for the 0, 0.5, 1.0, 1.5, 2.0 and 2.5 m MSL levels.

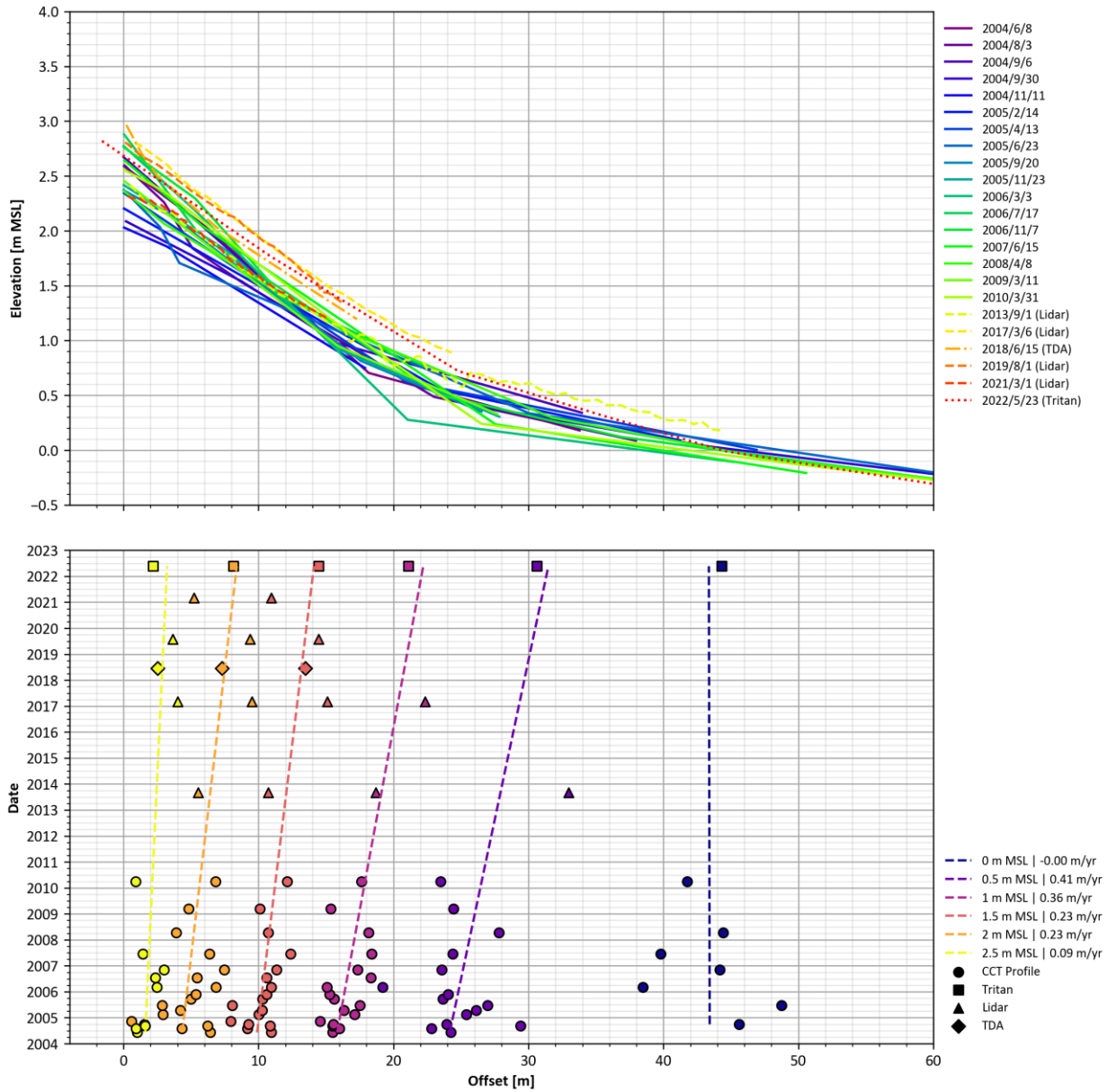


Figure 7-10: Profile B historical erosion/accretion analysis. Top: profile evolution over time. Bottom: horizontal movement of profile for the 0, 0.5, 1.0, 1.5, 2.0 and 2.5 m MSL levels.

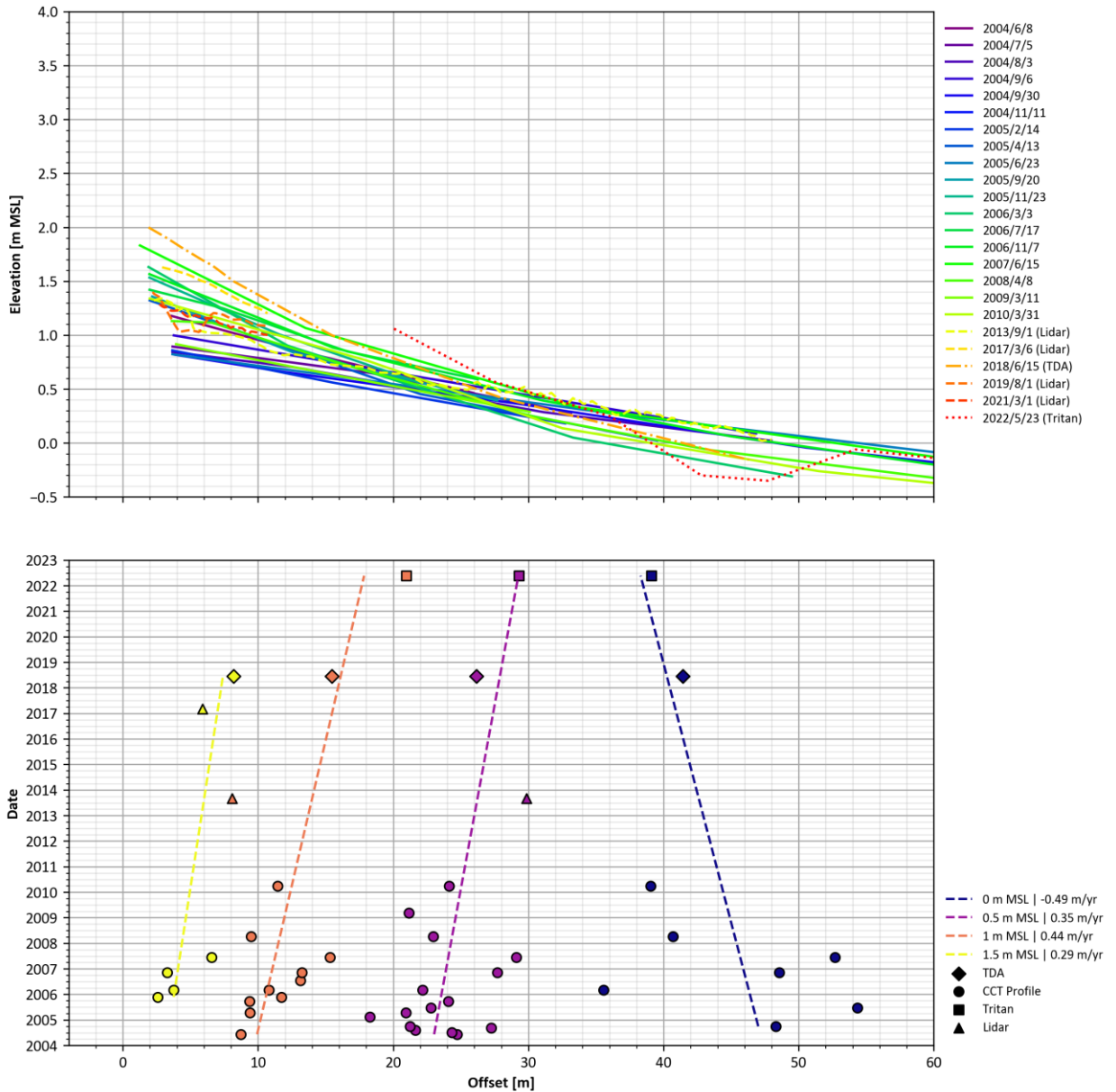


Figure 7-11: Profile C historical erosion/accretion analysis. Top: profile evolution over time. Bottom: horizontal movement of profile for the 0, 0.5, 1.0 and 1.5 m MSL levels.

The average trend from Profiles B and C was calculated between 0.5 and 2.0 m MSL levels, where sufficient data was available. Profile A was excluded from the analysis due to its proximity to the estuary mouth which influences the beach profile, and which is also actively managed to control the mouth conditions of the Zandvlei estuary. Note that Profile C has insufficient historical data above 1.5 m MSL. The horizontal trends are summarised in Table 7-2 below.



Table 7-2: Horizontal trends 2004 to 2022 based on beach profile analysis.

Elevation [m MSL]	Rate [m/y]	
	Profile B	Profile C
0.5	0.41	0.35
1.0	0.36	0.44
1.5	0.23	0.29
2.0	0.23	
Average	0.33	

Note: Positive is accretion, negative is erosion

The available measurements suggest a positive trend of approximately 0.3 m/year (accretion) over the period of the available beach profile data.

As for the wetted line analysis, since the beach lowering does not affect the sand budget, the redistribution of sand is not expected to affect the overall trends. Since the redistribution of sand occurs mostly within the upper part of the profile, any residual effect is likely removed by taking the average over the levels between +0.5 m and +2.0 m MSL.

7.1.5 Summary

The analysis of wetted lines over the period of historical data showed Muizenberg Beach to have remained approximately stable since 1935, with no clear erosive or accretive trend. This is supported by visual inspection of the historical imagery, which shows no clear signs of erosion or accretion. The beach has therefore remained approximately stable over the long-term, even under the influence of historical sea level rise, which implies a sand supply to the beach. The analysis of beach profile data suggested recent accretion at a rate of approximately 0.3 m/year. If such a trend were consistent over time, this would mean that in 1935 and 1970, the beach would have been 29 m and 17 m landward of its present position, respectively. Such changes would be clearly visible in the images from 1935 and around 1970, even considering the variability in wetted line positions, which is not the case. This trend is therefore inconsistent with the observed long-term trends and could be due to a shorter-term cycle.

7.2 Coastline recession due to sea level rise

The shore response model proposed by Bruun (1962) has been applied to estimate coastline recession due to long-term sea level rise at the site. The basic assumption behind the Bruun Rule is that with a rise in sea level, the equilibrium profile of the beach and the nearshore moves upward and landward conserving both mass and the original profile according to the following assumptions:

- The upper beach erodes because of a landward translation of the profile.
- Sediment eroded from the upper beach is deposited immediately offshore, with the eroded and deposited volumes being equal.
- The rise in the nearshore seafloor is equal to the rise in sea level.

Bruun's Rule has been applied in the following form (USACE, 2002) and (Hands, 1983) (refer to Figure 7-12):

$$x = \frac{zX}{Z}$$

Eq 7-1

where:

- x = horizontal profile recession due to sea level rise
- z = sea level rise
- Z = vertical distance from the depth of closure (the depth at which no significant changes in seabed level occurs) to the upper point of profile adjustment (the maximum wave run-up level)
- X = the corresponding horizontal distance from the depth of closure to the upper point of profile adjustment

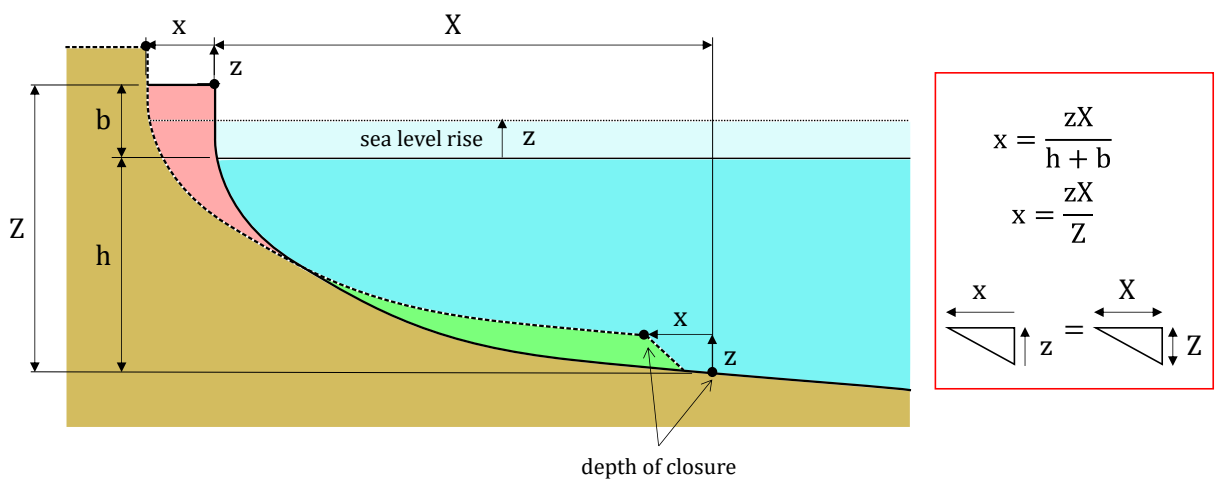


Figure 7-12: Schematic representation of the Bruun Rule, modified after Hands (1983).

The depth of closure was approximated using the inner Hallermeier analytical equation (USACE, 2002):

$$d_{\ell} = 2.28H_e - 68.5 \left(\frac{H_e^2}{gT_e^2} \right)$$

Eq 7-2

where:

- d_{ℓ} = is the annual depth of closure below the mean water level
- H_e = the non-breaking significant wave height that is exceeded 12 hours per year (0.137% exceedance probability)
- T_e = the wave period associated with H_e
- g = gravitational acceleration (9.81 m/s^2)

The Bruun Rule assumes that the sand accretion at the bottom of the profile is balanced by the erosion from the landward berm. Therefore, the standard Bruun Rule cannot be applied where the active zone is truncated by a seawall. For this study it is assumed the beach profile response to sea level rise will be similar along the local coastline due to the alongshore uniformity of the beach, and the slow erosive process of recession due to sea level rise in comparison to longshore sediment transport processes. The parameters from Eq 7-1 were therefore calculated from a single representative profile, Profile 8 (see Figure 7-13), where no seawall or hard

structure was present. The parameters were then applied to the remaining profiles with structures, assuming the conservation of mass (i.e., lack of sand source from the berm) is maintained by the longshore sand supply from the east.

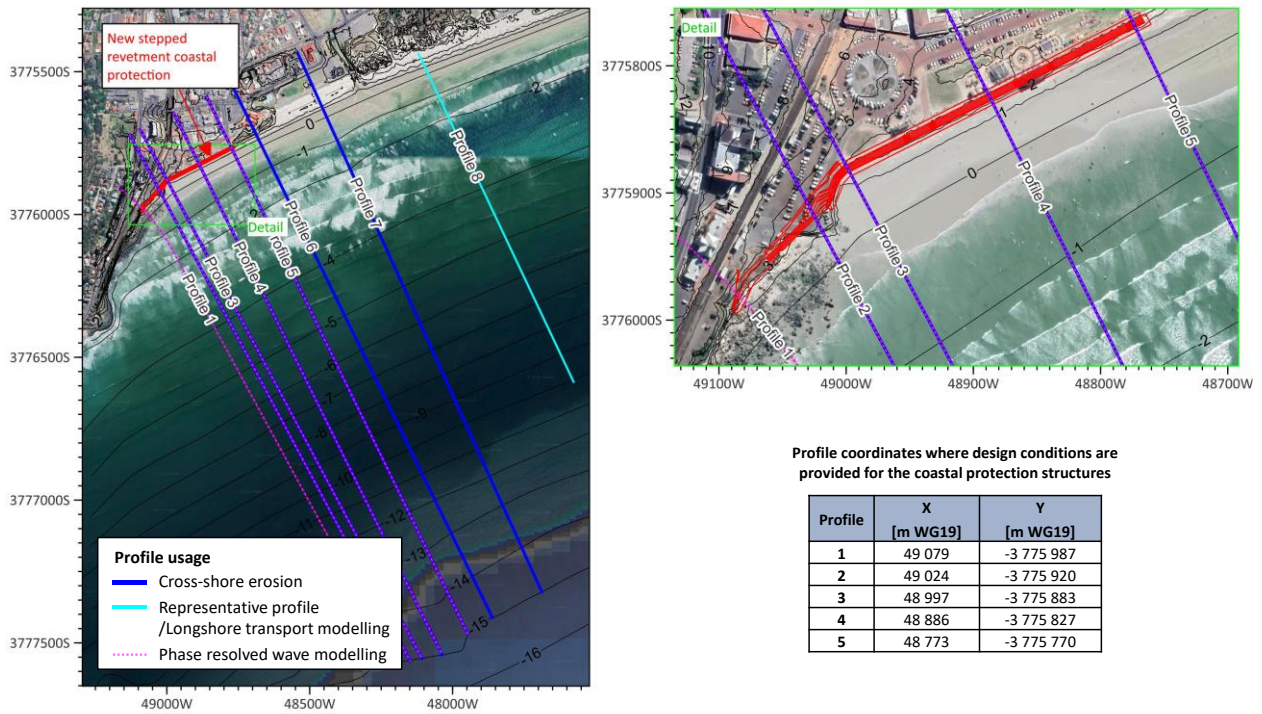


Figure 7-13: Left: overview of profiles used in coastline stability and phase resolved wave modelling. Right: detail of profiles used for the design conditions of the coastal protection structures.

The depth of closure was calculated from 42.2 years of modelled wave data along Profile 8 with $H_e = 2.94$ m and $T_e = 11.2$ s, which yielded $d_c = 6.21$ m. The upper point of profile adjustment is at the foredune crest which at 5.67 m MSL and located 899.8 m from the depth of closure. Thus, from Eq 7-1 the recession due to sea level rise is:

$$x = 75.8z \quad \text{Eq 7-3}$$

The application of coastline recession due to sea level rise is further discussed in the cross-shore profile adjustments in Section 7.4.3.

7.3 Longshore transport modelling

7.3.1 Model description

The MIKE Littoral Processes Flexible Mesh model was used to calculate the longshore sediment transport potential along the coastline at the site. The application of the model is described in the User Manual (DHI, 2022h), while the full details of the physical processes and numerical implementation are provided in the Scientific Documentation (DHI, 2022i). The calculation of littoral transport consists of three calculation parts:

- Wave transformation;
- Longshore current calculation; and
- Sediment transport calculation.

The cross-shore distributions of wave height and direction are found by solving the wave energy balance equation for an arbitrary coastal profile. The longshore current and set-up are found by solving the long and cross-shore momentum balance equations. The model includes a description for regular and irregular waves, the influence of tidal current and non-uniform bottom friction, as well as wave refraction, shoaling and breaking.

The non-cohesive sediment transport rates are found directly by calls to the quasi three-dimensional sediment transport model (STPQ3D). The transport rates are integrated based on the local wave, current and sediment conditions. As a result, the littoral drift calculation is able to give a deterministic description of the cross-shore distribution of longshore sediment transport for an arbitrary, non-uniform bathymetry and sediment profile. By applying a time varying wave climate, one can obtain a detailed description of the sand budget.

7.3.2 Model setup

Longshore transport was calculated at one cross-shore profile, labelled as Profile 8 in Figure 7-13. The profile was extracted from the bathymetry dataset described in Section 5.1, and extends from a depth of -10 m MSL to the foredune crest, at a constant 5 m horizontal resolution. The extracted cross-shore profile is shown in Figure 7-14.

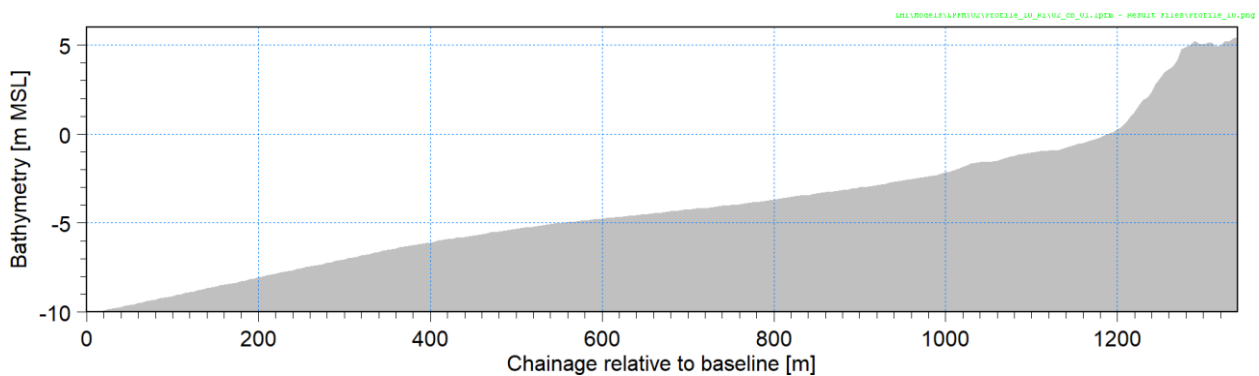


Figure 7-14: Cross-shore Profile 8.

The position of the profile was selected to provide an indication of the sediment entering or leaving the Muizenberg beachfront through longshore transport.

Analyses of sediment grain size from twelve samples at Muizenberg are available as part of the Marine Landside Site Investigations for the Muizenberg Beachfront Upgrade (Southern Oceanering, 2021). Samples were taken at high, mid and low points on the beach at four transects, as shown in Figure 7-15, which presents the median grain diameter (d_{50}) from each sample.

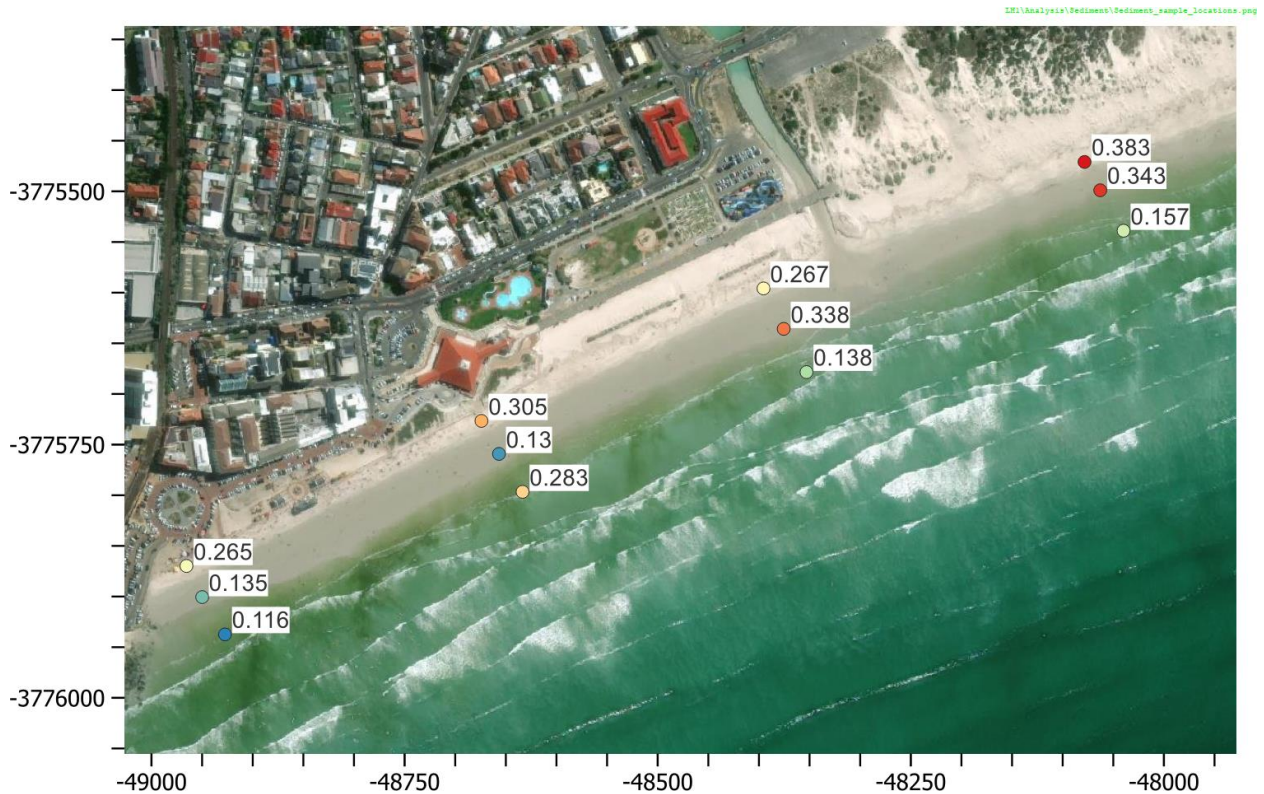


Figure 7-15: Median grain diameters of sediment samples taken at Muizenberg.

The average median diameter of the eight samples taken on the mid and low parts of the beach which are most representative of longshore sand transport was 0.21 mm. A constant median diameter of 0.21 mm with a typical grading of 1.6 were used in the littoral drift model.

The predicted tide at Simon’s Town described in Section 4.1 was applied as a time-varying boundary condition. Wave boundary conditions for the period of 1979-2009 were extracted from the operational wave model (see Section 5.7.2) at the offshore end of the profile (Point B), to be applied as time-varying boundary conditions. These include the Root-Mean-Square (RMS) wave height ($H_{rms} = H_{m0}/\sqrt{2}$), T_p and D_M . The period of 1979 to 2009 (31 years) was chosen as it is the longest available period covered by a single, homogenous hindcast wind and wave dataset (i.e., NCEP Reanalysis). This was chosen for robustness, since the assessment of trends in longshore sand transport is sensitive to small systematic changes in wave conditions, which may be present when applying different underlying hindcast datasets. A wave height (H_{rms}) and period (T_p) rose of the input wave conditions is shown in Figure 7-16, which also shows the modelled shoreline normal for reference.

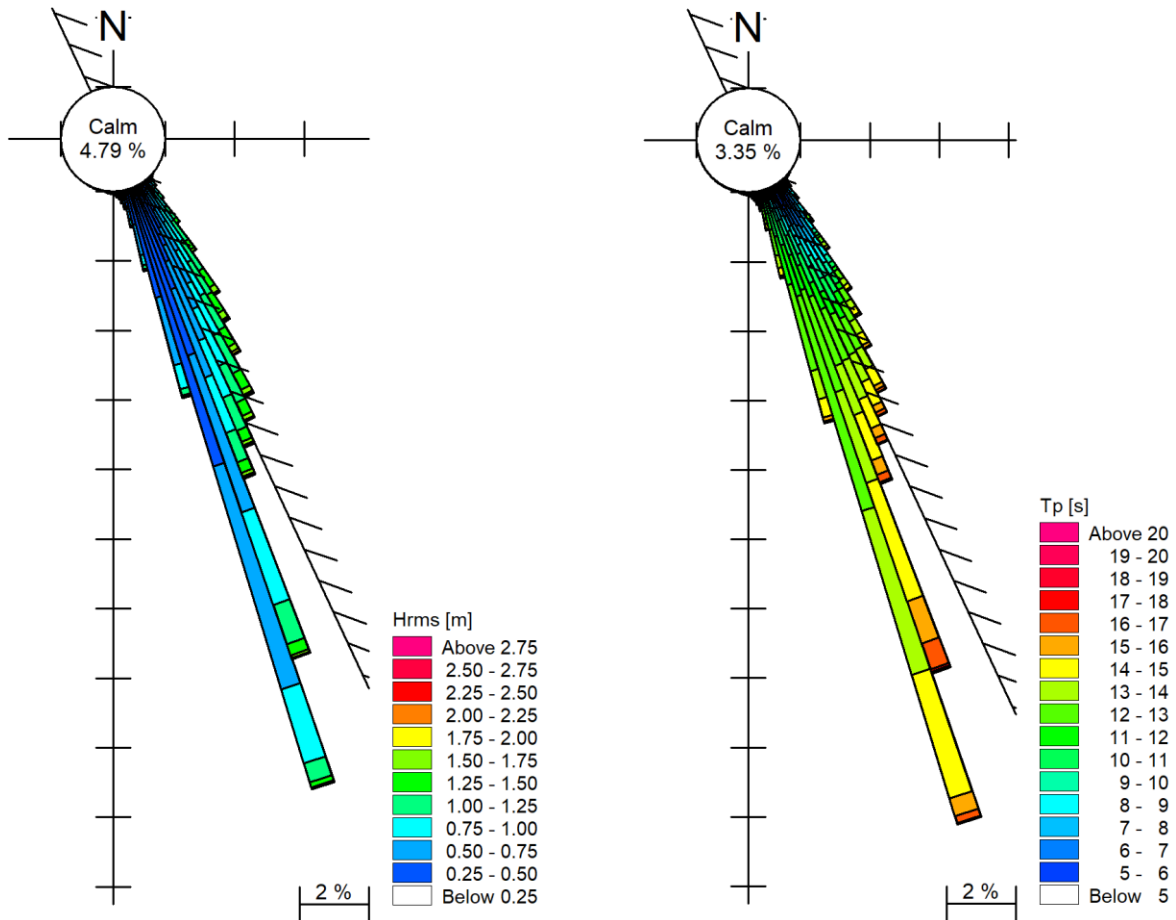


Figure 7-16: Wave roses of H_{rms} and T_p at Point B with modelled shoreline normal shown for reference.

The model settings were as follows: the critical Shields parameter was set to 0.045, ripples were excluded, the deterministic formulation for bed concentration was used, the wave theory was Stokes' 1st Order, the wave breaker index was 0.8, the roughness height for bed resistance was 0.004 m, the reduction factor for wave spreading was 0.81 and the water temperature was 16.5°C.

Thirty-one years (1979-2009) of operational conditions were modelled for the present-day cross-shore profile.

7.3.3 Model calibration

The coastline trends from historical data (refer to Section 7.1) showed that the coastline is approximately stable over the long term, even under the influence of historical SLR, which implies a sand supply to the beach.

The historical global mean SLR over the period of 1979 to 2009 was calculated as 2.79 mm/year based on the observed rates presented in AR6 (IPCC, In press). The projected regional relative mean SLR at Cape Town is 8.0% higher than the global mean for the SSP5-8.5 scenario in 2020. Using this adjustment, the historical regional relative SLR at Cape Town was estimated as 3.01 mm/year for 1979 to 2009. Using Eq 7-3 with $z = 3.01$ mm/year the shoreline recession rate for Profile 8 due to SLR is 0.23 m/year.

The observed rates of sea level rise from satellite altimetry and the tide gauge at Simon's Town over the period of 1993 to 2018 is summarised in Figure 7-17. For the same period, the reported global mean SLR rate



from AR6 is 3.25 mm/y, which if increased by 8%, results in a local rate of 3.51 mm/y. The approach followed is therefore well within the range of rates reported in literature.

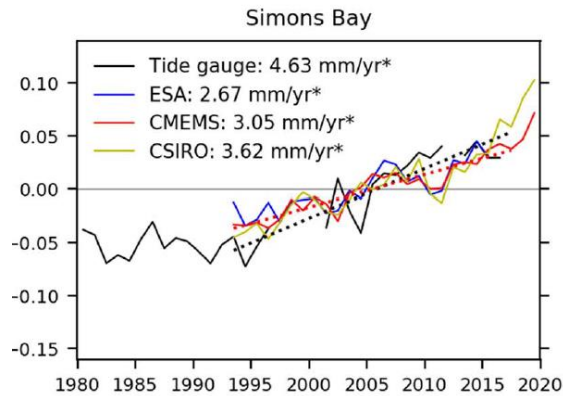
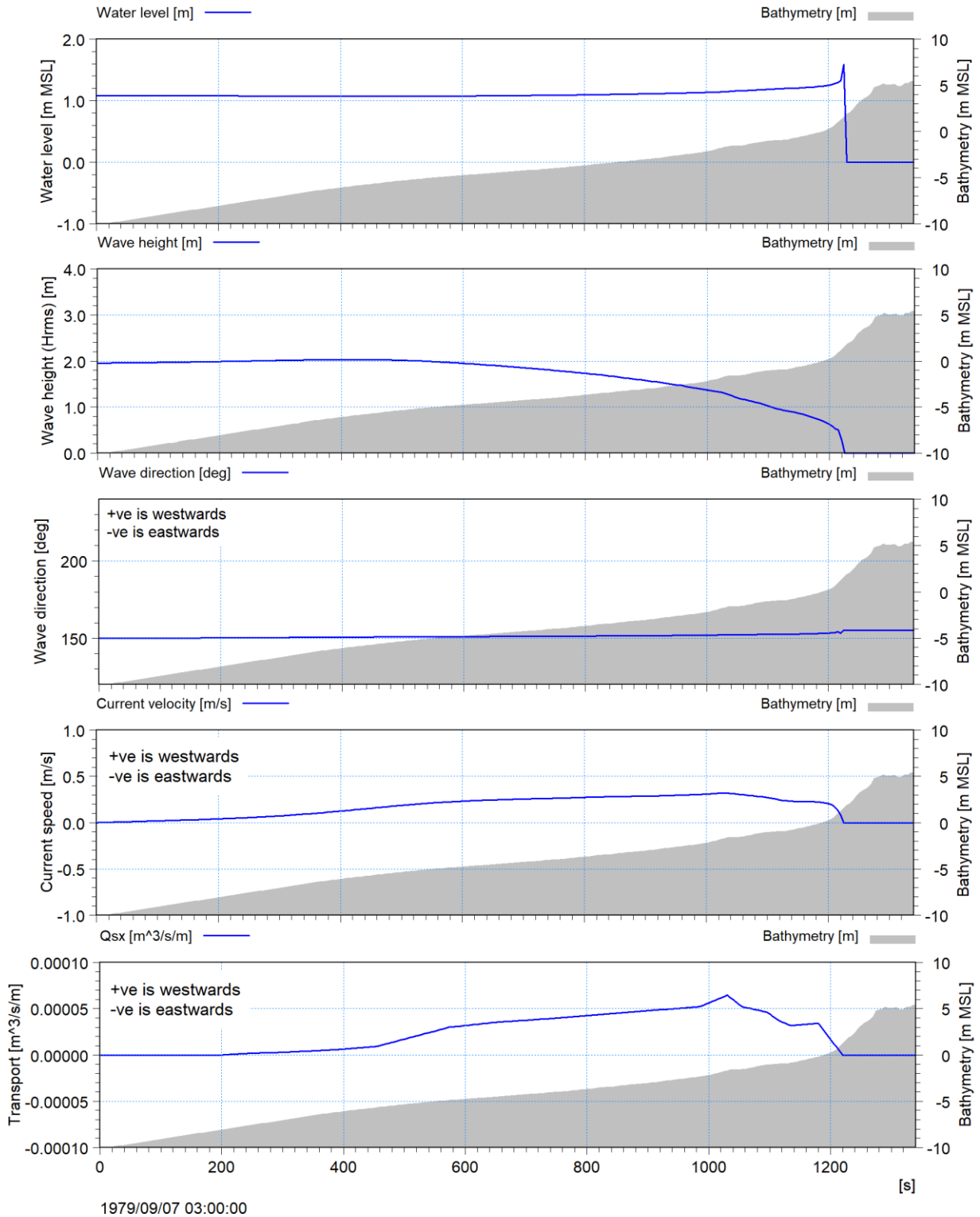


Figure 7-17: Observed rates of sea level rise at Simon’s Town over the period of 1993-2018 (Allison, et al., 2022). ESA, CMEMS, and CSIRO are three different satellite altimetry products.

The calibration of the model was based on balancing the erosion expected from historical SLR over the modelled period (1979-2009) with a sediment supply. Thus the results of the littoral drift modelling should produce an average accretion rate of 0.23 m/year due to longshore transport. The horizontal accretion rate is converted to a volume of sand supply by multiplying the rate by the length of the coastline from Profile 8 to the western end of the beach at Surfer’s Corner (1 375 m) and by the active height for longshore sand transport. The active height was estimated as the difference between the height of the first dune crest, taken as 3 m MSL, and the depth above which 99% of the gross longshore transport occurs, -6.17 m MSL. The bottom of the active height was determined from the littoral drift results and is shown in Table 7-3. The implied net transport volume was calculated as a westward transport of 2 880 m³/year. The model was calibrated to produce this transport rate over the 31-year period.

7.3.4 Results

The cross-shore distribution of the water level, waves, currents, and sediment transport is shown at an instance in time in Figure 7-18.



1979/09/07 03:00:00

Figure 7-18: Cross-shore distribution of water Level, waves, currents and sediment transport at one instance in time.

The figure shows a south-easterly wave condition, which drives a westward longshore current and westward sediment transport across the profile.



Time series of the wave conditions at the offshore end of the profile, instantaneous sediment transport (integrated across the profile), and accumulated sediment transport are shown in Figure 7-19 for the full 31-year period.

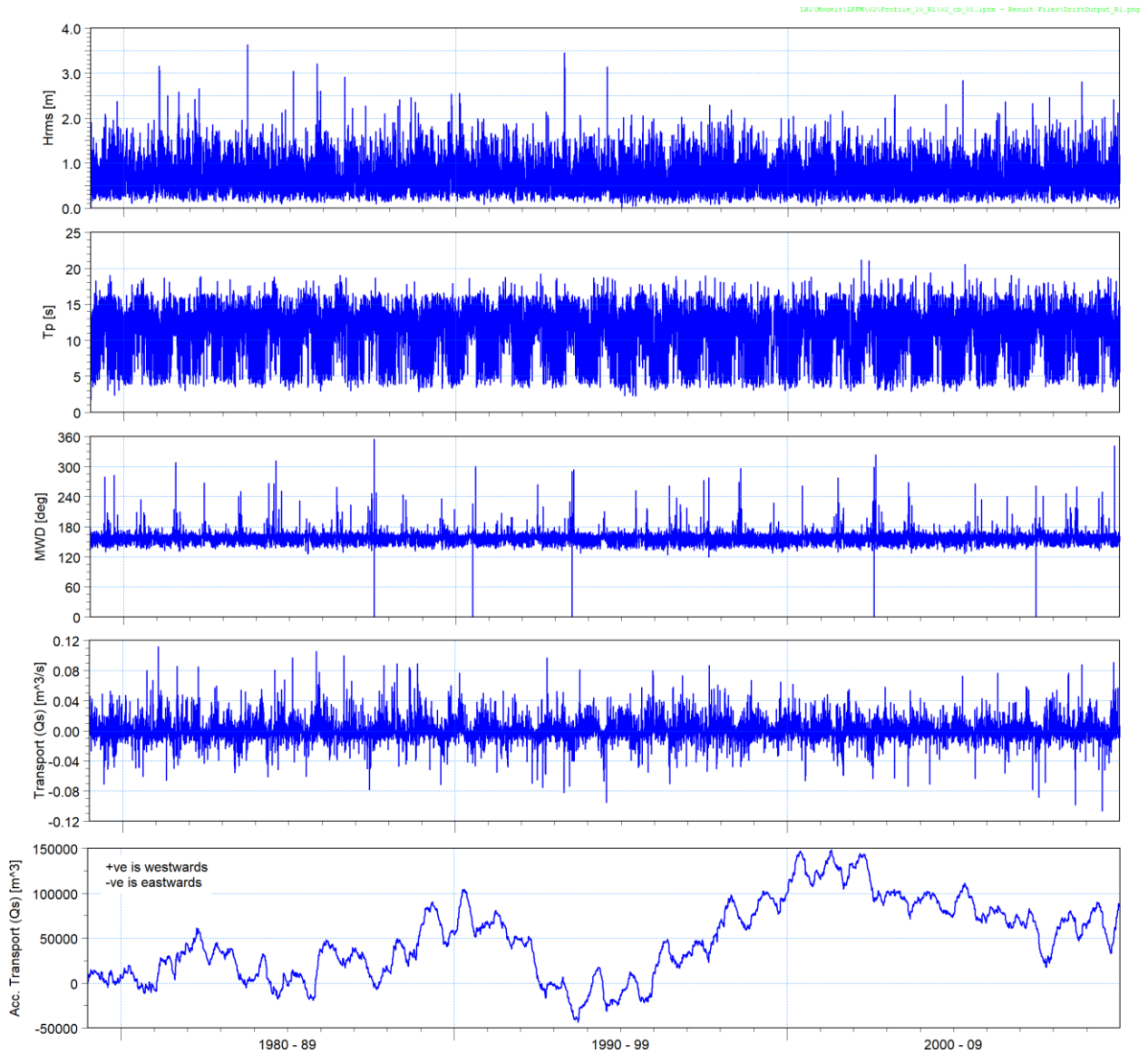


Figure 7-19: Time series of waves (at the offshore end of the profile), instantaneous sand transport (integrated across the profile) and accumulated net sand transport at Point B (-10 m MSL) on Profile 8 over the 31-year period.

The cross-shore distribution of the accumulated net and gross sand transport over the 31-years are shown in Figure 7-20. The modelled longshore sediment transport rates are summarised in Table 7-3.

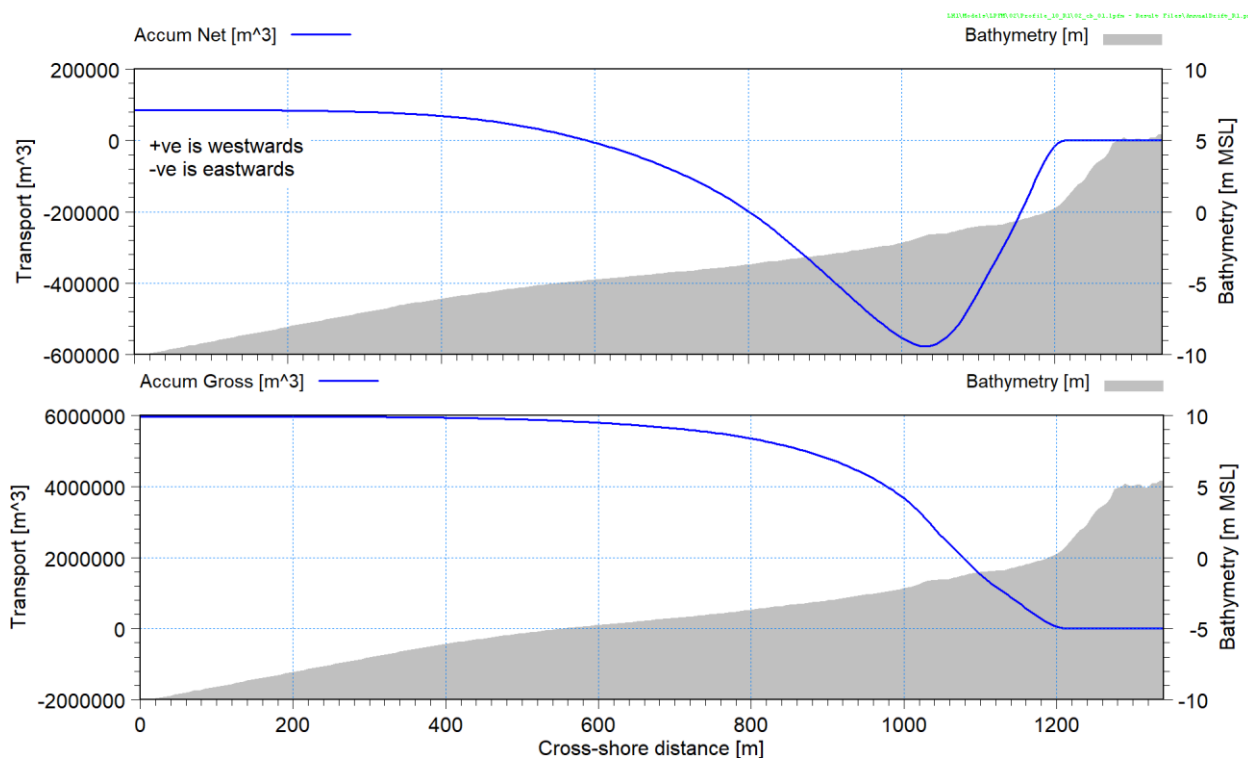


Figure 7-20: Cross-shore distribution of the accumulated net and gross sand transport at Profile 8 over the 31-year period.

Table 7-3: Longshore sediment transport results for Profile 8.

Parameter	Unit	Value
Net transport	[m ³ /y]	2 750
Gross transport	[m ³ /y]	192 600
Eastward transport	[m ³ /y]	94 900
Westward transport	[m ³ /y]	97 700
Depth above which 99% of the gross transport occurs	[m MSL]	-6.17

From Figure 7-20, the depth of closure (taken as the depth above which 99% of the gross transport occurs) is at -6.17 m MSL. The net westward transport of 2 750 m³/year agrees with the estimated supply of 2 880 m³/year discussed in Section 7.3.3, supporting the calibration of the model for the purposes of this study.

7.3.5 Horizontal profile variability

The time series of the accumulated longshore sediment transport volume within the Muizenberg beach area (i.e. the transport through Profile 8) was converted to a horizontal profile movement by dividing the volume by the length of the coastline and the active height. Figure 7-21 shows the time series of the calculated horizontal profile movement at Profile 8 over the 31-year period.

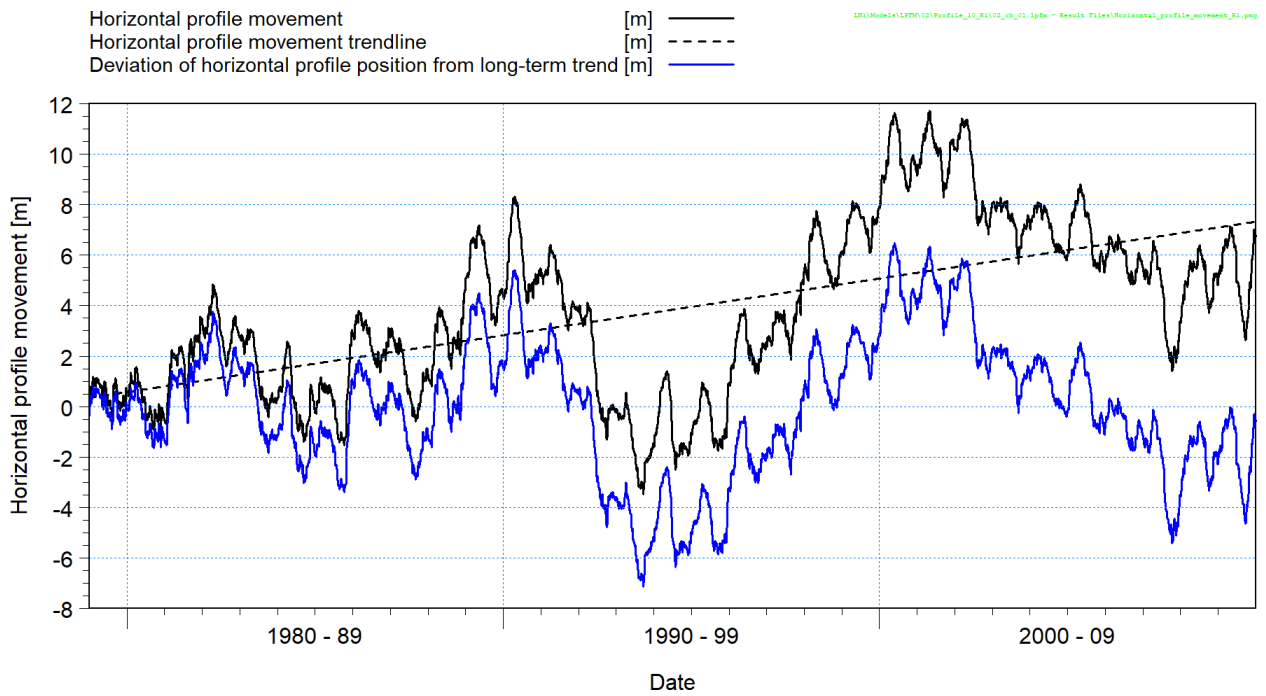


Figure 7-21: Horizontal profile movement due to longshore transport at Profile 8 over the 31-year period.

A linear regression fitted to the horizontal profile movement indicated a long-term trend of +0.22 m/year, which approximately balances the expected recession due to historical SLR.

The horizontal profile variability due to variations in longshore supply was investigated by calculating the deviation of the horizontal profile position from the long-term trend, as presented in Figure 7-21. To compare the predicted variability against observations, the horizontal profile variability is overlaid on the wetted line analysis in Figure 7-22.

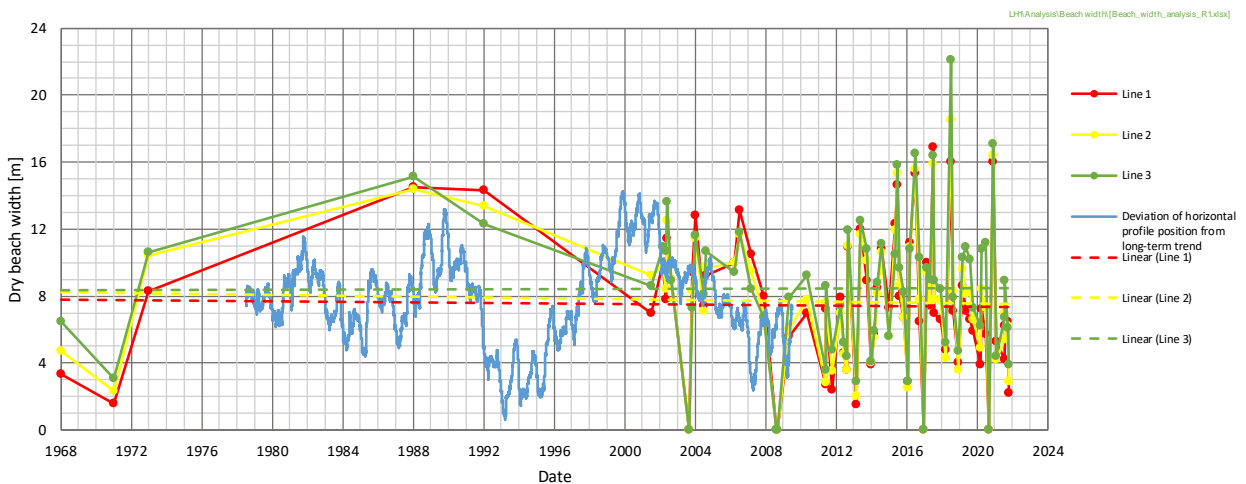


Figure 7-22: Comparison of predicted horizontal variability due to longshore transport with observed dry beach variability.

The wetted line data is generally supportive of the model, where the erosive trend in 2002-2009 and to some extent the accreted state in 1988-1992 agree with the predicted variability. The wetted line data is more

variable than the model, which can be expected since the wetted line experiences additional variability due to water levels, wave runup and profile changes.

The trend deviation data was plotted as a histogram line graph with a bin width of 1.0 m, as shown in Figure 7-23. The theoretical normal distribution was plotted using the mean and standard deviation of the data calculated as 0.0 m and 2.68 m, respectively. The data was found to adequately fit a normal distribution.

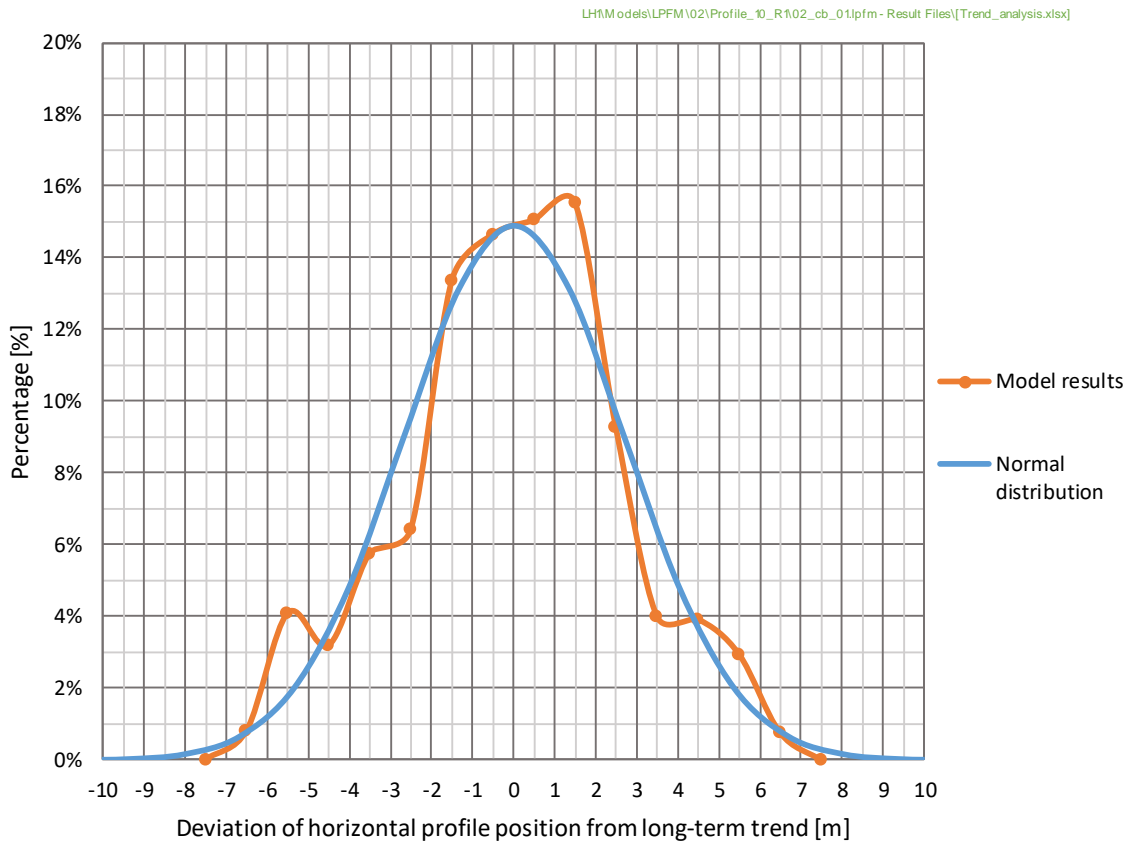


Figure 7-23: Normal distribution fit of the deviation of horizontal profile position from long-term trend.

The probability of exceeding a value in a normal distribution can be related to an annual return period as shown in Eq 7- .

$$P = \frac{n}{T} \tag{Eq 7-4}$$

where:

- P = probability of exceedance
- n = number of sampling intervals per year
- T = return period (years)

The return period refers to the average interval at which the value will be exceeded for a duration corresponding to the sampling interval. For a normal distribution, the expected horizontal profile movement



at a given exceedance probability can be expressed as a number of standard deviations from the mean, as shown in Eq 7-5.

$$x_T = \mu + Z \cdot \sigma \quad \text{Eq 7-5}$$

where:

- x_T = expected horizontal profile movement
- μ = mean of the trend deviation dataset
- σ = standard deviation of the trend deviation dataset
- Z = number of standard deviations from the mean

Horizontal profile variability due to longshore transport is typically slowly varying, on the scale of months or seasons. If assuming a typical event duration of one month, then the expected horizontal profile movement for the range of return periods under consideration is given in Table 7-4.

Table 7-4: Extreme horizontal profile movement.

Return period ^(a) [y]	Horizontal profile movement [m]	Number of standard deviations from mean
1	3.73	1.39
10	6.43	2.40
100	8.44	3.15
475	9.59	3.58

Notes:

(a) Using a sampling interval of 30 days

Extreme profile variability occurs not due to single storm events, but due to several sequential years with small shifts in wave conditions (e.g., wave direction). These events are therefore independent of individual storms. However, considering that these events last for long periods of time, there remains a risk that they can co-occur with large storms. Although not quantified, a pragmatic approach is used in this study where the 100-year horizontal profile variability is used for all cases. This results in a landward horizontal profile movement of 8.44 m.

It is noted that the sensitivity to this assumption is shown in Figure 7-25 which presents the profile adjustment for both a 100-year and a 10-year profile variability. If the 10-year estimate is applied instead, this would result in a vertical difference at the structure toe of <0.2 m in 2026, <0.1 m in 2046, and <0.05 m in 2076. The approach is therefore fairly insensitive to the chosen return period.

7.4 Cross-shore erosion

7.4.1 Model description

The SBEACH (Storm-induced BEACH CHange) storm erosion model was used to simulate the cross-shore erosion of the beach along the Muizenberg Beachfront during storm events, to inform the low beach levels for design of the scour protection of the proposed stepped revetment.



The SBEACH model developed by the US Army Corps of Engineers (Larson & Kraus, 1989) consists of a wave model and a beach response model. The wave model calculates the transformation of wave height and direction at user specified grid points along the beach profile, taking into account the effects of wave refraction, shoaling and dissipation due to depth-induced breaking. Water level variations due to wave- and wind-induced set-up are also included in the wave model. The formulation of the wave model is based on the solution of best practice deterministic equations.

The beach response model is empirically based, with the underlying assumptions and relationships derived from observations made from prototype-scale laboratory experiments. The model assumes the conservation of sediment across the profile (longshore processes are uniform and neglected in calculating profile change). The direction and rate of cross-shore transport is determined from the local wave, water level, beach profile and sediment properties, and the equation describing the conservation of beach material is solved to compute profile change as a function of time.

7.4.2 Model setup

Six cross-shore profiles (Profiles 2 to 7 presented in Figure 7-13) were selected along the Muizenberg Beachfront between Surfer's Corner and the Zandvlei estuary mouth. Profile 1 at the St. James walkway was not included, since the coastline in this area is rocky. The profiles reached a water depth of -15 m MSL. Where the profiles intersected the stepped revetment, seawall (in the Phase 2 area) or the bedrock at Surfer's Corner, these structures were modelled as a non-erodible bed.

The grid spacing applied to the cross-shore profiles ranged from 1 m to 10 m. Analyses of sediment grain size are available from the Marine Landside Site Investigations for the Muizenberg Beachfront Upgrade (Southern Oceanering, 2021). The average median grain size of all the sediment samples, 0.24 mm, was applied in the model. It is noted that from experience the model results are fairly insensitive to median grain sizes in the range of 0.17 to 0.30 mm. The profile setup parameters are listed in Table 7-5.

Table 7-5: SBEACH model setup parameters.

Setup parameter	Input
Land surf zone depth	0.1 m
Median grain size	0.24 mm
Maximum slope prior to avalanching	30°
Transport rate coefficient	2E-6 m ⁴ /N
Overwash transport parameter	0.005
Coefficient for slope-dependent term	0.003 m ² /s
Transport rate decay coefficient	0.5
Scour attenuation coefficient	1.0 m ⁻¹
Seawater temperature	16.5°C

The model was run for all the extreme wave and water level conditions with a joint return period of 1, 10, 100 and 475 years for the 2026 and 2076 climate change horizons, as presented in Table 6-3. The interim horizon of 2046 was also modelled for Profiles 2 to 5. In total, 14 joint return period combinations were modelled per profile per climate change horizon.



The storm duration was predicted by fitting a two-part gaussian time-series to the 84 largest storms modelled over the 42-year period at Point A, as shown in Figure 7-24. Since no correlation was observed between the wave height peak and duration of the storm a constant duration of 100 hours was used for all storms.

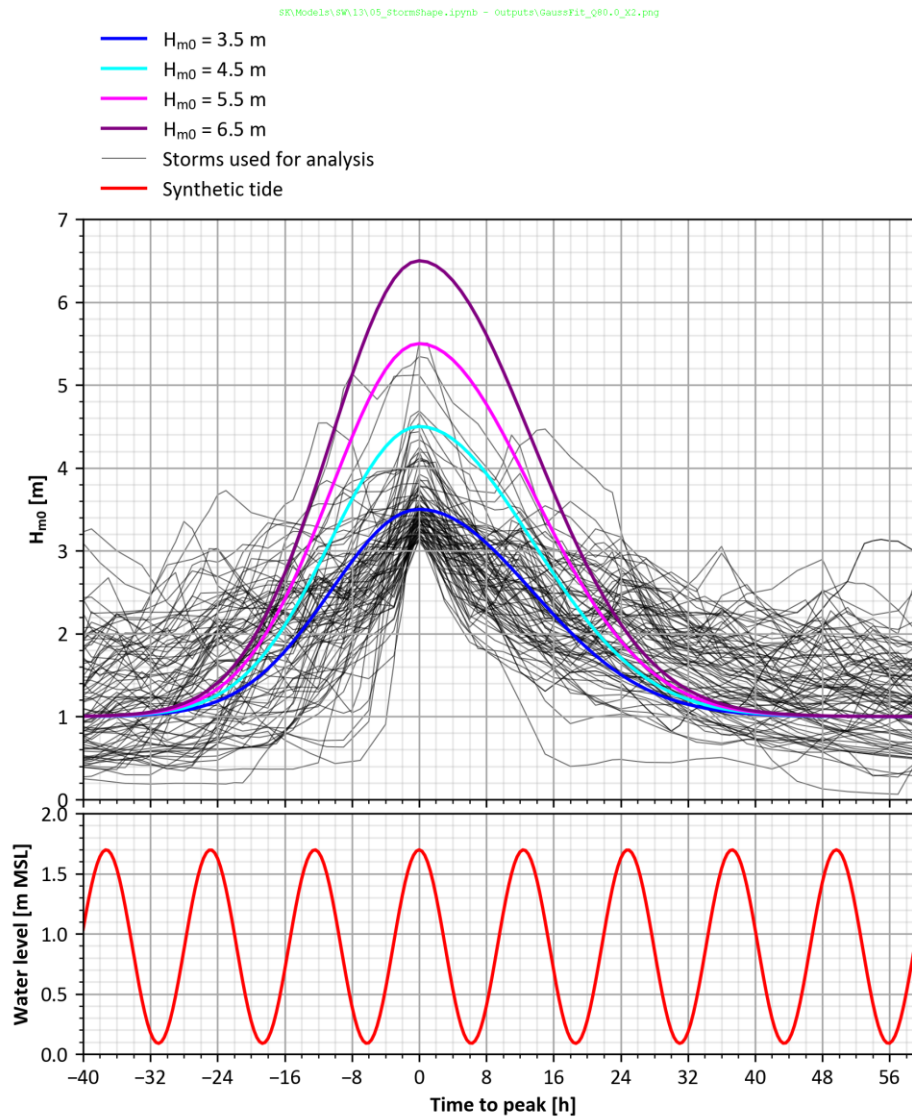


Figure 7-24: Storm duration analysis based on 84 storms at Point A. The predicted storms are shown in shades of blue and purple. The synthetic tide for a 475-year event in 2026 (including storm surge and sea level rise) is shown for reference.

The extreme wave heights and wave periods (see Table 5-2) were used to obtain the peak of the time series. A 20 min interval was used for the storm time series. The wave conditions were applied at a water depth of -15 m MSL. The wave direction was perpendicular to the cross-shore profile for all timesteps and profiles. No wind was applied in the model.

The time series of the water level for each case was set up using a tidal height of 1.61 m, which is the difference between the 90th percentile high tide (+1.02 m MSL) and the 90th percentile low tide (-0.59 m MSL, see Section 4.1). A semi-diurnal tide was simulated using the extreme water level conditions from Table 6-3 as the peak of the tidal sequence. The peak of the water level and wave time series coincided. The output time steps were every minute for 100 hours.



7.4.3 Profile adjustment

The cross-shore profiles were adjusted for the long-term trend due to longshore sand supply (+0.22 m/year, see Section 7.3.5), the horizontal profile variability due to longshore transport (-8.44 m, see Section 7.3.5) and sea level rise for 2026, 2046 and 2076 (see Section 7.2), prior to the SBEACH analysis. For each profile the landward extent of the profile adjustment was where the profile intersected the existing or proposed structure.

Bedrock levels at the toe of the structure of Profiles 3 to 7 were interpreted from the geotechnical survey cross-section by HHO (2022), which included waterjet probes, boreholes, trial pits, test pits, electrical resistivity surveys and seismic refraction surveys. The rock level at the toe of the stepped revetment of Profile 2 was estimated from three surrounding waterjet probe refusal depths, ranging between -1.5 and 0.6 m MSL, to be -0.5 m MSL. The bedrock levels determine the minimum level of the profile adjustment prior to the cross-shore erosion modelling and was included as a hard-bottom (non-erodible surface) in the SBEACH model, where relevant.

Table 7-6: Bedrock levels interpreted from geotechnical survey.

Profile	Level [m MSL]
Profile 2	-0.5
Profile 3	-0.75
Profile 4	-1.3
Profile 5	<-10
Profile 6	<-10
Profile 7	<-10

An example of the profile recession due to sea level rise, long-term trends, and horizontal profile variability is shown in Figure 7-25 for Profile 4.

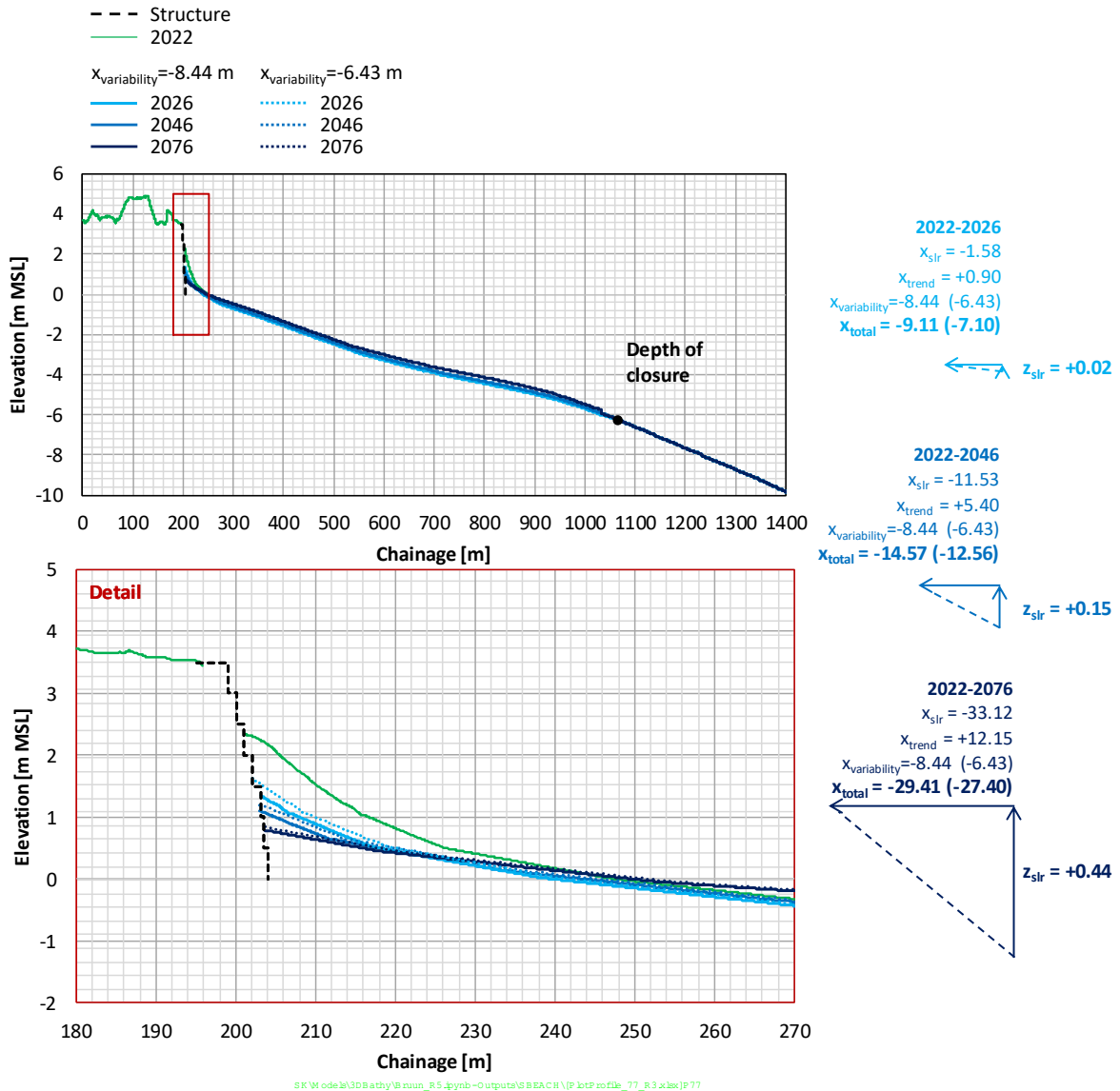


Figure 7-25: Example of profile recession due to sea level rise (x_{slr}), long-term trends due to longshore sand supply (x_{trend}), and horizontal profile variability due to longshore transport ($x_{\text{variability}}$) for Profile 4. The profile adjustment sensitivity to $x_{\text{variability}}$ for a 10-year return period is presented in dotted lines and values in brackets.

Although the longshore sand supply was found to have historically balanced the expected erosion due to SLR, the accelerating rate of SLR outweighs the sand supply for the future horizons. This results in a net recession of the profiles in the future, which lowers beach levels in front of the seawall.

7.4.4 Results

For each modelled case the minimum profile elevation at each grid point throughout the 100-hour simulation was used to assess the low beach level. Figure 7-27, Figure 7-28 and Figure 7-29 present the initial and eroded profiles for Profile 4 for the 475-year return period cases in 2026, 2046, and 2076. The two wave steepness candidates and two joint return period combination cases are shown in each figure. The proposed stepped revetment is indicated by the hard structure.

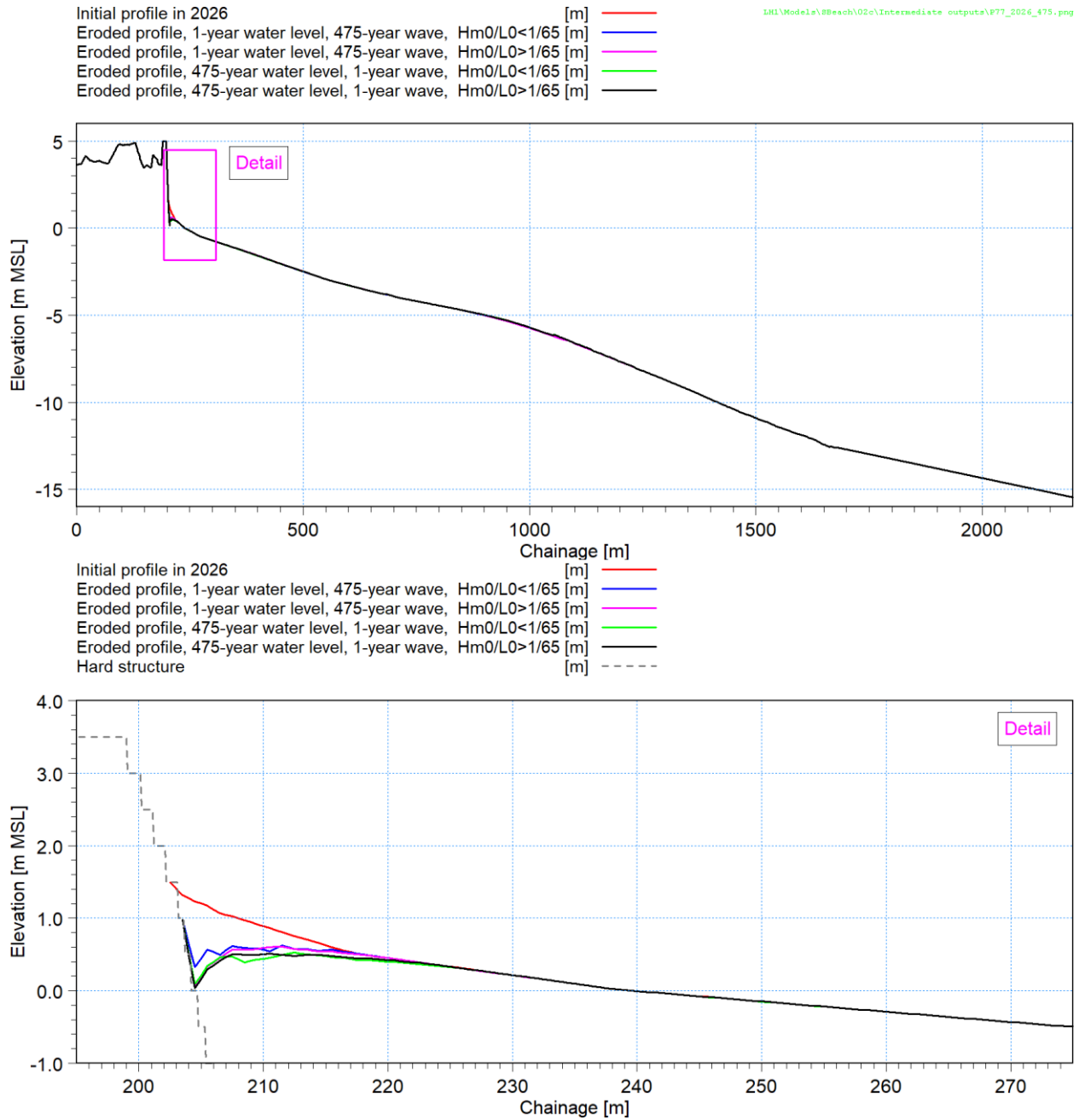


Figure 7-26: Erosion results for the two wave steepness candidates and two joint return period combinations for the 475-year storms at Profile 4 in 2026.

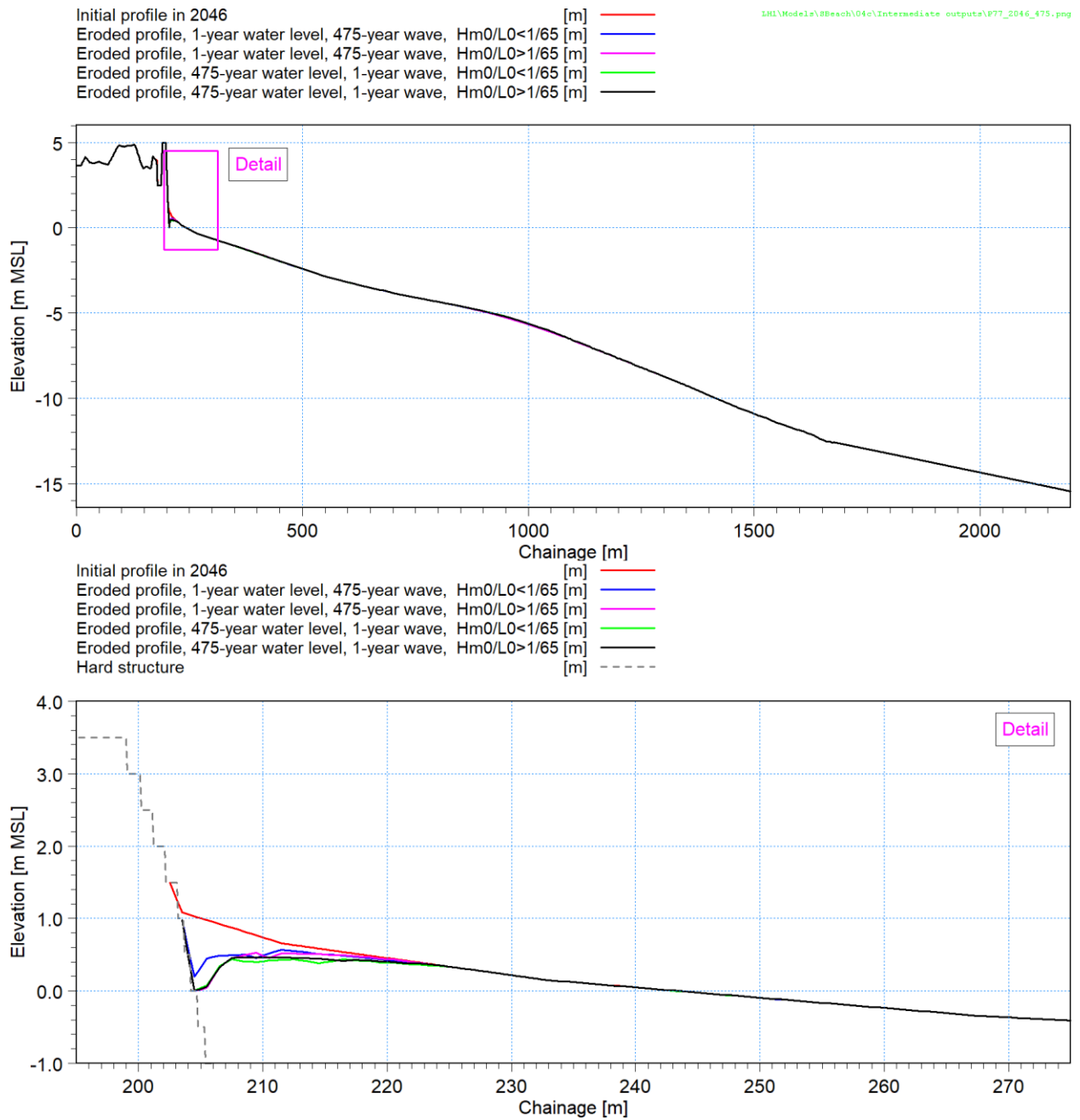
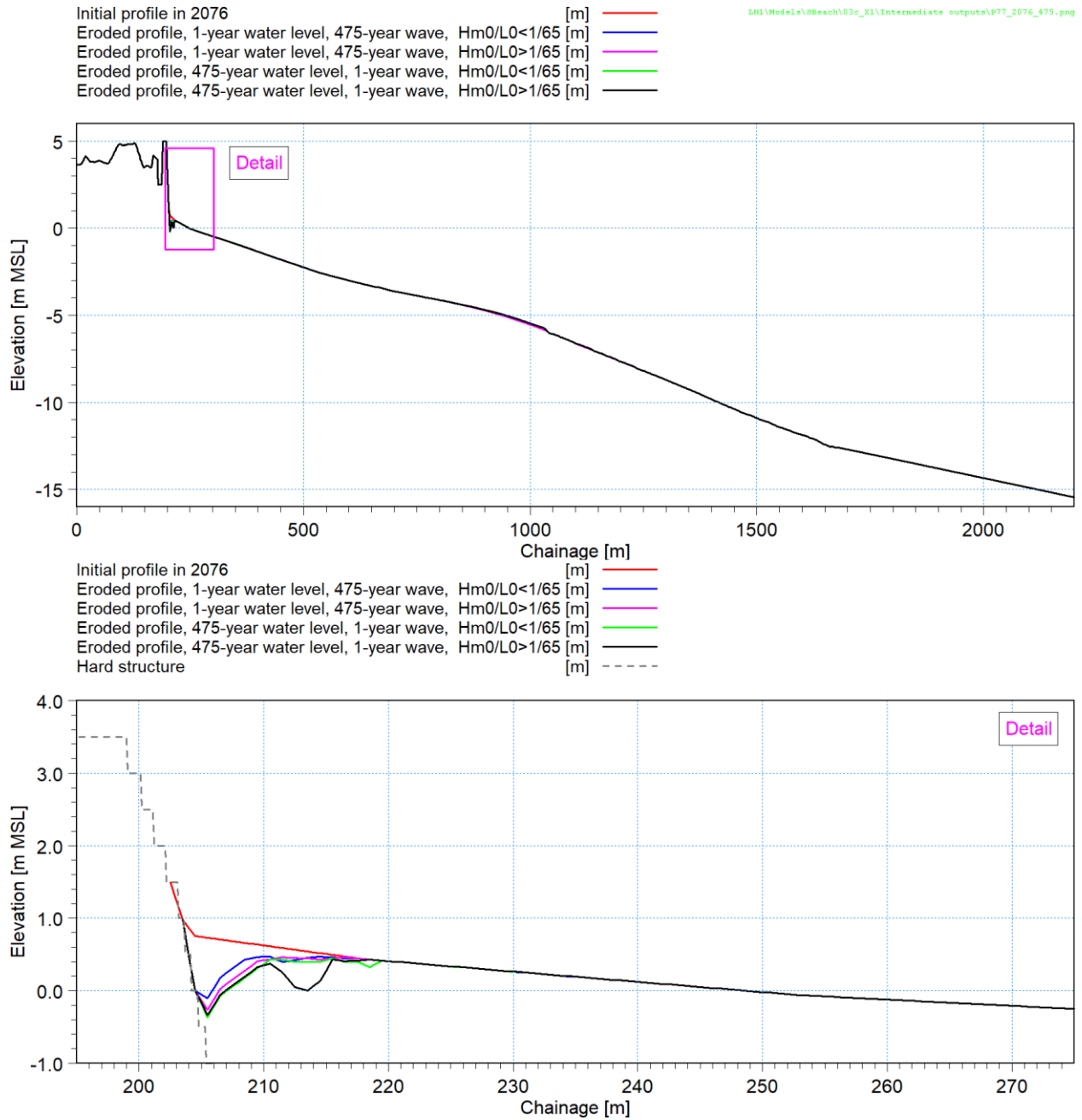


Figure 7-27: Erosion results for the two wave steepness candidates and two joint return period combinations for the 475-year storms at Profile 4 in 2046.



A comparison of the different cases per return period showed that generally the water level dominated cases caused worse erosion at the toe of the structure. It was not clear whether the flatter or steeper wave steepness candidates showed worse erosion results. To obtain the lowest eroded beach level for each return period, the minima of the minimum eroded profiles was calculated spatially, as shown in Figure 7-29 for Profile 4.

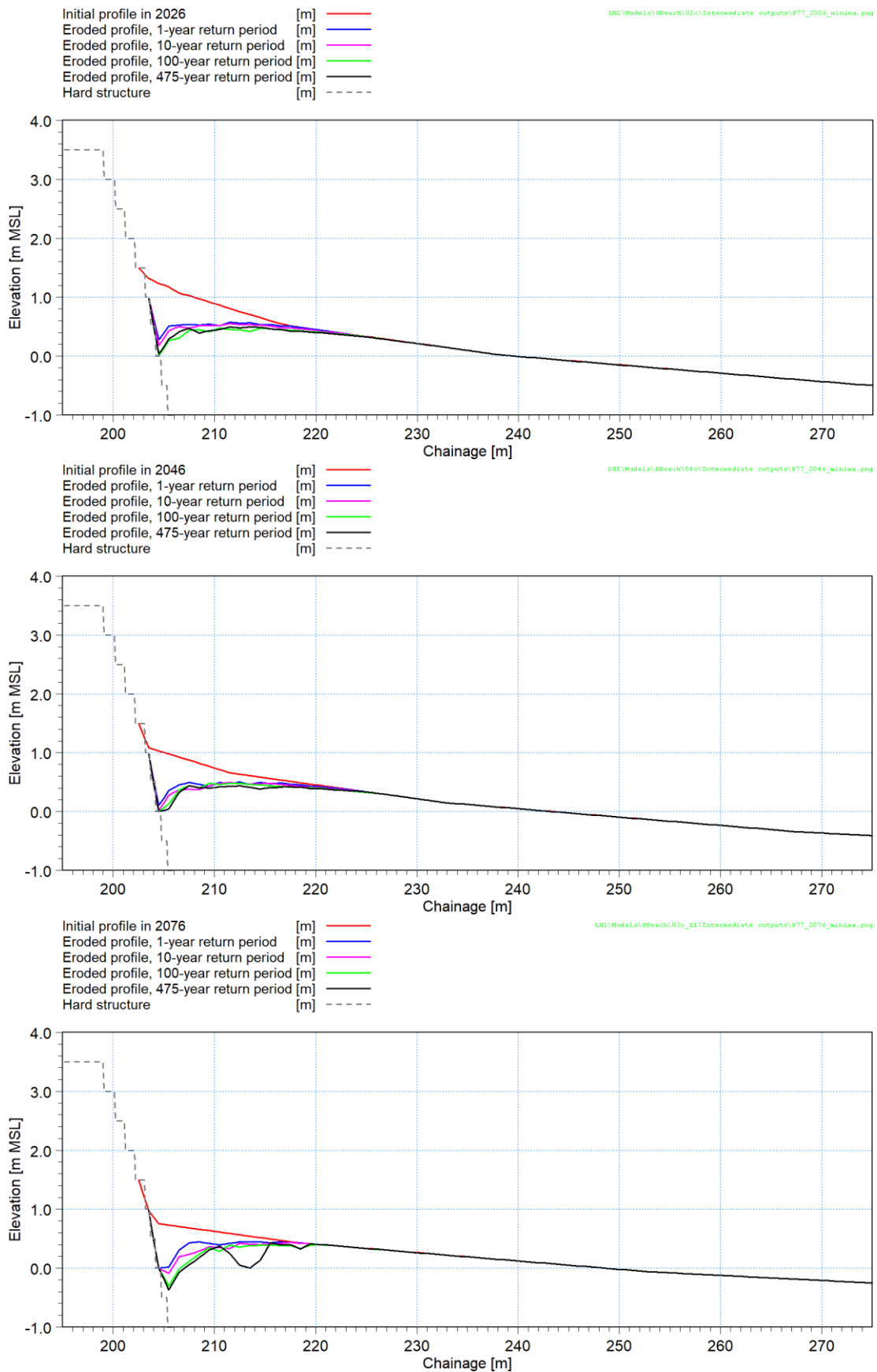


Figure 7-29: Erosion results for the 1, 10, 100 and 475-year storms at Profile 4 in 2026 (top), 2046 (middle) and 2076 (bottom).



Annexure B contains the full set of minimum eroded profiles for Profile 2 to 5 in 2026, 2046 and 2076 and for Profile 6 and Profile 7 in 2026 and 2076.

The results for Profile 2 to 5 in front of the proposed stepped revetment generally indicate the storms to remove the top steepest sloping portion of the beach. The resulting eroded beach crest levels typically vary between +0.3 m MSL and +0.7 m MSL depending on the profile, return period and climate change horizon. These eroded profiles for each of the individual 14 cases per profile for the 2026 and 2076 climate change scenarios were further used in the MIKE 3 Wave model to obtain the inshore design conditions, discussed in Section 8.

In addition to being used to obtain inshore design conditions, the results for Profile 2 to Profile 5 indicate the development of local scour in front of the stepped revetment. There is some uncertainty in the predicted scour since the model does not include local dynamic processes such as wave reflection and runup return flow, and the development of the scour hole is sensitive to the scour attenuation coefficient. One study comparing a version of SBEACH modified to include wave reflection found the reflection process to be less pronounced than expected (McDougal, et al., 1996). However, the modified model was able to predict the local scour level observed in one of the three physical model tests considered, while the standard version of SBEACH was not. Therefore, there remains some uncertainty in the scour level predicted by SBEACH. The results were compared to the local scour estimates from empirical methods discussed in Section 9.

The results for Profile 6 located in front of the pavilion indicate the storms to remove the top steepest sloping portion of the beach, with little variation between return periods. The dune in front of the promenade at Profile 7 is predicted to experience approximately 10 m of horizontal erosion during the 1 year return period storms, and up to 20 m of erosion for return periods of 10 years or greater.

7.5 Impact of proposed seawall on sediment dynamics

The layout of the proposed stepped revetment in relation to the existing seawall is shown in Figure 7-30. A qualitative assessment of the potential impact of the revised seawall on the sediment dynamics of the adjacent beaches is given here.



Figure 7-30: Location of existing seawall (blue) and proposed stepped revetment (red).

In general, the proposed stepped revetment is an upgrade of the existing seawall, and approximately follows the same footprint on the main beach area, where both the existing and proposed structures are shore-parallel and located at the back of the beach. Neither is expected to interrupt the longshore sand transport processes. An exception to this is the existing abutment facility which extends onto the beach seaward of the existing seawall. The proposed removal of this structure from the littoral active zone will reduce any existing impact on the longshore sand transport, although this is expected to be minimal since no significant effect can be observed on the present-day shoreline. Furthermore, since the proposed seawall approximately follows the footprint of the existing structure, it also does not pose any additional reduction in sand available for cross-shore transport processes.

The proposed layout of the stepped revetment presents a departure from the layout of the existing seawall in the Surfer's Corner area. The existing Surfer's Corner is a short abutment which extends to a depth of approximately 0 m MSL. The longshore transport modelling presented in Section 7.3.4 shows the longshore gross sediment transport to be mainly limited to depths deeper than 0 m MSL. This implies that the existing abutment does not present a significant interruption of longshore transport processes, and its removal is not expected to significantly alter the longshore transport sediment budget.

The existing abutment which has a near-vertical wall oblique to the main beach causes some wave reflection, which is expected to be responsible for the locally lower beach levels at the western end of the main beach. The proposed new coastal protection structure is a stepped revetment, which is expected to be less reflective than a vertical wall. Furthermore, the layout of the proposed stepped revetment is less oblique to the wave direction and is set back further landward than the existing wall. Considering these two factors, the wave reflections with the new proposed stepped revetment are expected to be lower than those of the existing Surfer's Corner. The reflections of the new stepped revetment can be investigated in more detail during the full 3D wave overtopping and flooding assessment.



8. DESIGN WATER LEVELS AND WAVES AT REVETMENT

8.1 Model description

The MIKE 3 Wave (M3W) Flexible Mesh model was used to determine the design wave and water level parameters at several locations in front of the proposed stepped revetment and at the proposed sleeping rock revetment at the St. James Walkway, for the 2026 and 2076 climate change horizons. The application of the model is described in the User Manual (DHI, 2022j), while full details of the physical processes being simulated and the numerical solution techniques are described in the Scientific Documentation (DHI, 2022k).

The M3W is a phase-resolving wave model based on the 3D Navier-Stokes equations. An unstructured (flexible) mesh is used in the horizontal dimension with sigma layers in the vertical. The model includes the following processes:

- Wave refraction;
- Wave diffraction;
- Wave reflection;
- Bottom friction;
- Non-linear wave transformation;
- Surf and swash zone hydrodynamics;
- Wave breaking and run-up;
- Wave overtopping; and
- Coastal flooding.

The model is based on the numerical solution of the three-dimensional incompressible Reynolds-averaged Navier-Stokes equations. Thus, the model consists of continuity and momentum equations, and it is closed by a $k-\epsilon$ turbulence closure scheme in the vertical and horizontal. The free surface is taken into account using a sigma coordinate transformation approach. The spatial discretization of the governing equations in conserved form is performed using a cell-centred finite volume method. The time integration is performed using a semi-implicit scheme. The vertical convective and diffusion terms are discretized using an implicit scheme to remove the stability limitations associated with the vertical resolution. The remaining terms are discretized using a second-order explicit Runge-Kutta scheme. The projection method is employed for the non-hydrostatic pressure. The interface convective fluxes are calculated using a HLLC approximate Riemann solver. This shock-capturing scheme enables robust and stable simulation of flows involving shocks or discontinuities such as bores and hydraulic jumps. This is essential for modelling of waves in the breaking zone. The numerical dissipation accounts for the dissipation in the breaking waves.

8.2 Model setup

Profiles 1 to 5 (Figure 7-13) were selected to provide a representative set of inshore design conditions for use in the structural design. The post-storm beach profiles at Profiles 2 to 5 for 2026 and 2076 were obtained from the cross-shore erosion modelling (Section 7.4.4). Profile 1 was adjusted for longshore profile variability (Section 7.3.5) and sea level rise (Section 7.2) but cross-shore erosion modelling was excluded due to the rocky coastline. Each profile was set up as a one element wide numerical flume, i.e., a 2DV model. The wave generation line was placed at the -15 m MSL contour, with the offshore boundary extending 250 m seaward to accommodate the wave relaxation zone for wave generation and absorption. A bathymetry cut-off of -15 m MSL was applied to aid in the stability of the wave generation. On the landward side the bathymetry was levelled to a constant height where the profile intersects the revetment, and an absorbing sponge layer

was applied to prevent reflective waves from confounding the incident wave conditions, since the structural design requires the incident wave height only.

The model mesh comprises quadrangular elements with a depth-varying resolution varying between approximately 4.2 m offshore and approximately 1.2 m nearshore. This resulted in a resolution of approximately 25 points per wavelength across the whole domain for the shortest T_p modelled (9.7 s). The vertical mesh comprises 10 sigma layers with variable layer thickness distribution. An example model computational mesh is shown in Figure 8-1.

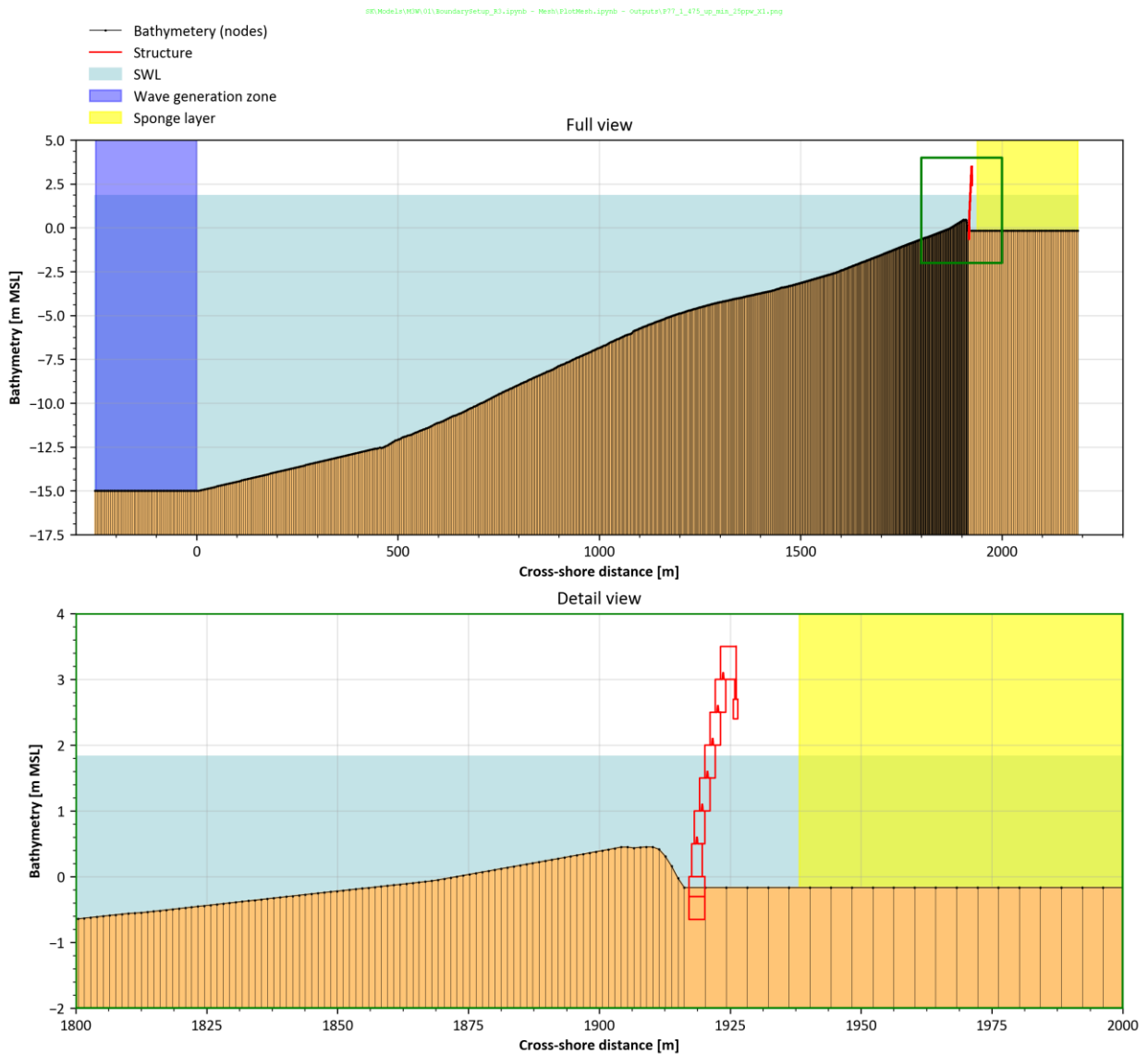


Figure 8-1: Profile 4; Example 2DV mesh for 2076, 1 y SWL, 475 y waves ($s > 1/65$). The position of the structure is shown for visual purposes only.

The model boundary conditions are the extreme unidirectional wave parameters (H_{m0} , T_p) and still water level as summarised in Table 6-3. The waves in the model were generated at the -15 m MSL contour. A JONSWAP spectrum was used with a gamma of 2.0. The specified wave parameters are used by the model to generate a sea state by applying random phases. The duration of each simulation was set to two hours excluding spin-up time.

8.3 Results

The model output was the instantaneous surface elevation across the profile over the duration of the simulation. The results from each run were processed to obtain the following outputs in front of the structures (refer to Figure 8-2):

- (a) **Total surface elevation [m MSL]:** raw time-series from model outputs.
- (b) **SWL offshore [m MSL]:** time-averaged SWL applied on the boundary.
- (c) **SWL inshore [m MSL]:** time-averaged water level in front of the structure.
- (d) **Wave time-series [m]:** time-series of surface elevation excluding SWL inshore = (a) – (c).
- (e) **Setup [m]:** increase of water level within the surf zone = (c) - (b).
- (f) **Short waves [m]:** High-pass finite impulse filter with a cut-off period of 30 s applied to (d).
- (g) **Surf beat [m]:** Low frequency waves obtained from (d) – (f).

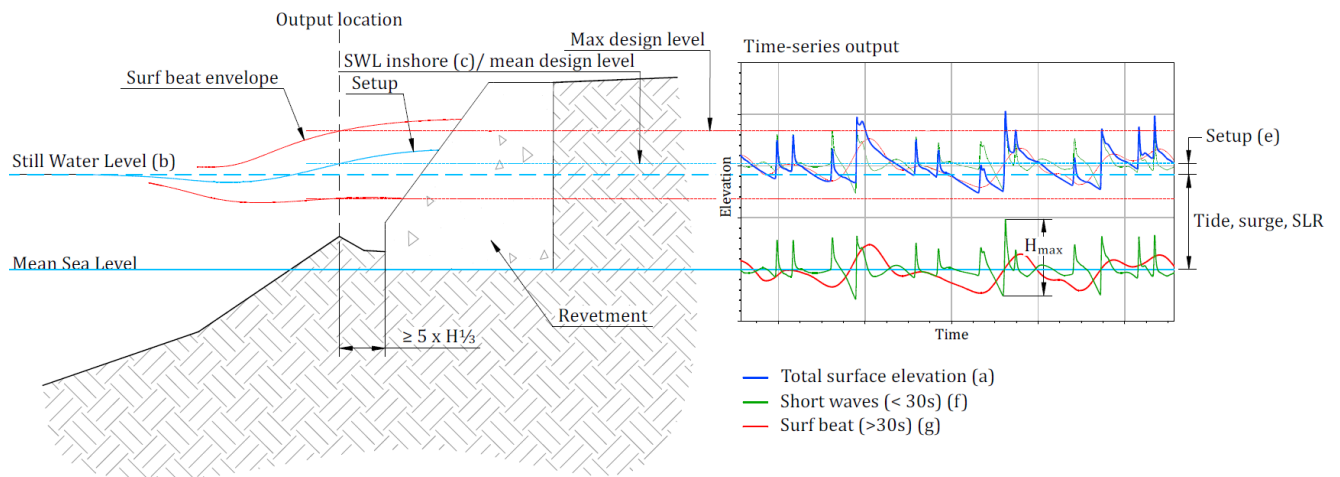


Figure 8-2: Schematic representation of modelled outputs extracted at the toe of the structure.

Figure 8-3 shows an example of the instantaneous water surface elevation at Profile 4 for a 2076 climate change scenario and a 475-year wave event ($s > 1/65$) combined with a 1-year still water level.

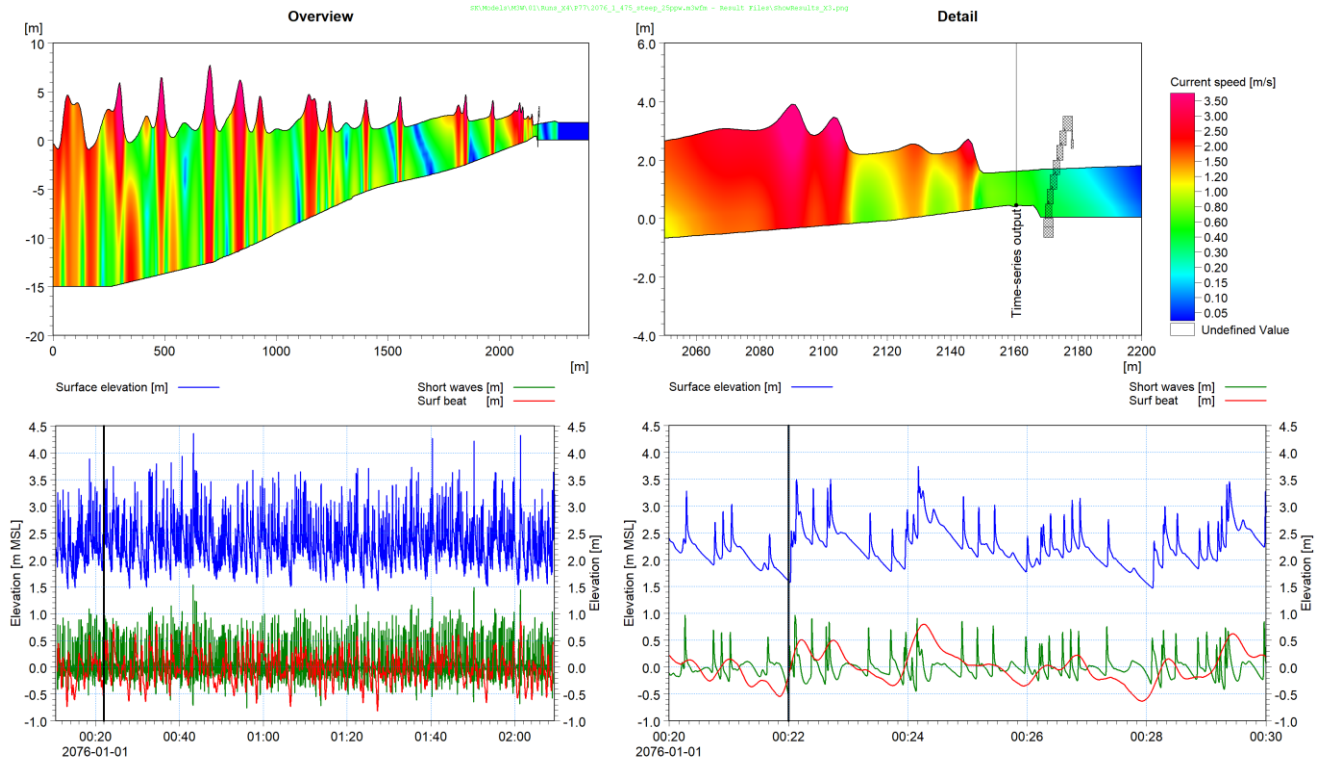


Figure 8-3: Profile 4; Example results for a 2076 climate change scenario and a 475-year wave event ($s > 1/65$) combined with a 1-year still water level. Top: cross-section of instantaneous surface elevation (the structure is shown for visual purposes only). Bottom: Time-series of surface elevation, short waves and surf beat.

A zero-crossing analysis was performed on the short wave time-series which was post-processed further to provide the required time-domain wave parameters:

- $H_{1/3}$ = time-domain significant wave height, calculated as the average of the one-third highest waves in the sea state
- H_{max} = maximum wave in the sea state
- T_s = significant wave period, calculated as the average of the periods associated with one-third highest waves in the sea state.

The down-crossing method was used as it consistently yielded larger wave heights than up-crossing due to strong non-linearity in the surf zone. For every run the final outputs are provided at the crest of the profile, where the water depth is the shallowest, or a distance of $5 \times H_{1/3}$ offshore of the wall – whichever is the greatest.

Extracting the maximum wave height from irregular wave analyses will result in different maxima depending on the random seed of the wave generation and the duration of the wave record, whereas averaged values (e.g., $H_{1/3}$) tend to provide more robust values. By convention H_{max} could be estimated from the Rayleigh distribution, but the distribution is not applicable to shallow water such as this case. Thus, the observed maxima from all runs and profiles were compared their respective $H_{1/3}$ values to determine a statistical trend for H_{max} as shown in Figure 8-4. A best estimate trendline was fitted using least squares regression and upper and lower envelopes of the scatter data were visually fitted.

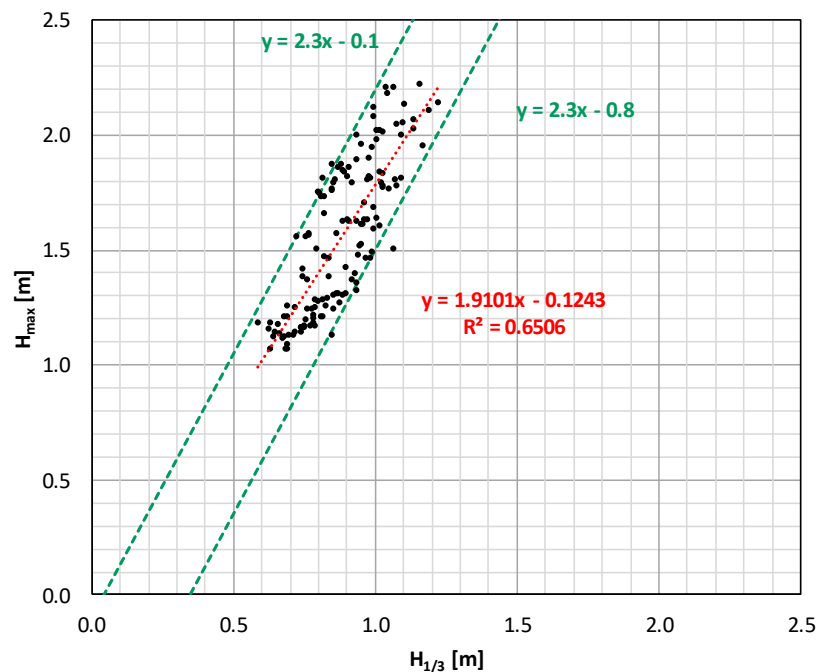


Figure 8-4: Comparison of H_{max} to $H_{1/3}$ for all profiles and cases modelled. The best estimate trendline (red) was fitted using least squares regression and the upper and lower envelopes (green) were visually fitted.

The best estimate tends to underestimate H_{max} , especially for larger $H_{1/3}$ values. It was therefore decided to use the upper envelope of the scatter data to estimate H_{max} , i.e.:

$$H_{max} = 2.3H_{1/3} - 0.1 \quad \text{Eq 8-1}$$

The low-frequency surf beat was added to the design water levels. Since the short wave heights are not strongly correlated to the surf beat a range of levels was provided (refer to Figure 8-2):

- A mean design level equal to the SWL inshore; and
- A maximum design level equal to the SWL inshore plus maximum surf beat elevation.

The extreme design conditions (bed level, mean water level, maximum water level, H_{max} , $H_{1/3}$, T_s) are summarised in Table 8-1 for Profile 4 for both joint probability combinations. The full set of tables for all the profiles are summarised in Annexure C at the end of this report. The results will be used for the structural design calculations at the toe of the structures. Where available, both joint probability combinations of wave height and water level should be tested in the design calculations. The wave results were also used to calculate the scour depth required in the design of scour protection (Section 9).



Table 8-1: Profile 4; design wave and water levels in front of stepped revetment.

Climate change horizon	Extreme condition				Bed level [m MSL]	Water level		Wave parameters					
	Joint return period [y]	Wave return period [y]	Wave steepness [-]	SWL return period [y]		Mean level [m MSL]	Max level [m MSL]	H _{max} [m]	H _{1/3} [m]	T _s [s]	No. Waves [-]		
2026	1	1	> 1/65	1	0.59	1.52	2.07	1.34	0.62	12.4	591		
		10		1	0.60	1.61	2.33	1.80	0.82	13.8	496		
	100	1		10	0.56	1.64	2.20	1.43	0.67	11.7	621		
		1		1	0.61	1.71	2.49	2.01	0.92	15.0	465		
	475	1		100	0.49	1.74	2.31	1.54	0.71	11.5	637		
		1		1	0.59	1.78	2.53	2.19	1.00	15.2	472		
	10	1		475	0.50	1.81	2.40	1.60	0.74	11.4	650		
		1		1	0.58	1.51	2.08	1.49	0.69	15.1	511		
	100	1		10	< 1/65	1	0.61	1.56	2.13	1.61	0.74	15.8	479
		1		1	10	0.56	1.63	2.21	1.62	0.75	14.8	523	
		1		100	1	0.62	1.59	2.21	1.73	0.80	15.4	461	
		1		1	100	0.51	1.73	2.34	1.77	0.81	14.3	535	
		1		475	1	0.58	1.62	2.21	1.68	0.77	14.9	466	
		1		1	475	0.51	1.80	2.41	1.86	0.85	14.3	545	
2076	1	1	> 1/65	1	0.47	1.95	2.54	1.65	0.76	11.9	641		
		10		1	0.46	2.04	2.82	2.19	0.99	13.9	520		
	100	1		10	0.43	2.07	2.68	1.77	0.81	11.7	650		
		1		1	0.46	2.15	3.04	2.38	1.08	14.6	501		
	475	1		100	0.42	2.17	2.82	2.01	0.92	12.1	656		
		1		1	0.45	2.23	3.06	2.56	1.16	14.8	497		
	10	1		475	0.42	2.24	2.90	2.10	0.96	12.2	663		
		1		1	0.43	1.94	2.52	1.78	0.82	14.0	550		
	100	1		10	< 1/65	1	0.49	1.98	2.61	2.05	0.93	15.3	510
		1		1	10	0.40	2.06	2.66	1.95	0.89	14.0	563	
		1		100	1	0.46	2.01	2.63	2.15	0.98	14.7	483	
		1		1	100	0.39	2.16	2.83	2.27	1.03	14.7	554	
	475	1		475	1	0.46	2.04	2.67	2.13	0.97	14.5	494	
		1		1	475	0.42	2.23	2.87	2.22	1.01	14.0	571	

9. LOCAL SCOUR

9.1 Introduction

This section presents estimates of the local scour in front of the proposed stepped revetment for design. Estimates are derived from empirical formulations and are considered as alternative scour estimates to those predicted by SBEACH (as presented in Section 7.4). These estimates are not additive.

9.2 Methodology

The maximum local scour depth at the toe of the structure is defined as the maximum depth below the pre-storm profile, as shown in Figure 9-1.

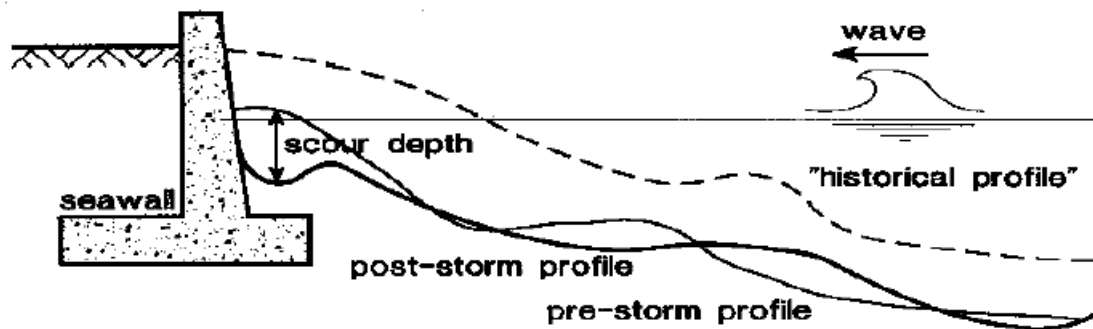


Figure 9-1: Local scour at the toe of a structure (van Rijn, L.C., 2018).

Van Rijn (2018) reviewed empirical methods to estimate the wave-related scour near the toe of a structure. A summary of the various methods, their basis and comments on their applicability are given in Table 9-1.



Table 9-1: Summary of empirical scour estimation methods.

Reference	Basis	Scour estimate	Comments on applicability
Shore Protection Manual (SPM) (CERC, 1984) and Coastal Engineering Manual (CEM) (USACE, 2002)	Thumb rule	The maximum scour depth is approximately equal to the height of the maximum wave that can be supported by the original water depth. $d_{s,max} = H_{max}$ or $d_{s,max} \approx h_{toe}$	Applies to vertical seawalls for normally incident waves with no currents.
Herbich et al (1965) as described in van Rijn (2018)	Small scale laboratory flume tests using regular non-breaking waves on a horizontal bed.	For sloped to vertical walls (30° to 90°) the observed scour depth was approximately: $d_{s,max}/H = 0.5 \text{ to } 0.6$ The upper end of the range has been used in this study.	Applies to sloped to vertical walls (30° to 90°). Applicability is questionable given the wave conditions tested (regular, non-breaking)
Steetzel (1988) as described in van Rijn (2018)	Large-scale laboratory flume test (1:5), irregular waves.	Maximum observed scour depth is approximated by: $d_{s,max}/h_{toe} = 0.75$	Applies to 1:1.8 sloped seawall, thus reasonably applicable. Based on result from one test.
Fowler (1992)	Mid-scale laboratory flume tests on initially plane slopes, irregular waves.	$\frac{d_{s,max}}{H_{s,0}} = \left(22.72 * \frac{h_{toe}}{L_0} + 0.25 \right)^{0.5}$	Applies to vertical seawalls. Scour depth is estimated as a function of deepwater wave height, resulting in very conservative estimates. Test results for profiles representative of storm conditions (seawall initially in the water) do not match the equation well (McDougal, et al., 1996).

Notes:

- $d_{s,max}$ is the maximum scour depth below the initial bed
- H_{max} is the maximum wave height near the toe of the structure
- h_{toe} is the water depth near the toe of the structure
- $H_{s,0}$ is the deepwater significant wave height
- L_0 is the deepwater significant wave height

Based on the summary given above, the methods of SPM, Herbich, and Steetzel have been applied to provide a range of estimates, noting that the applicability of the Herbich method which predicts the least amount of scour is questionable. Relating the local scour to the deepwater wave height as proposed by the Fowler method results in extreme estimates of scour depth. For example, the 475-year present-day predicted scour at Profile 4 using this formulation is approximately 3.8 m. Such estimates are not considered feasible and have not been included in this assessment.

The SPM method applies to vertical seawalls, while the proposed structure is a 1:2 slope stepped revetment. The CEM (USACE, 2002) suggests that sloped structures are expected to have less reflection which would cause somewhat less scour and suggests application of the SPM method as conservative. However, others have noted that reflection may be less important and the return flow of runup on a sloping structure may also contribute to local scour (Kraus & McDougal, 1996). In the absence of specific estimation methods for sloped or stepped revetments, the vertical wall scour is considered to provide a reasonable estimate.



9.3 Results

The three empirical methods were applied to Profiles 2 to 5 for all the return period cases and for the 2026 and 2076 climate change horizons. Since model results were not available for the 2046 climate change horizon, the scour depths for 2046 were estimated by linearly interpolating the results for 2026 and 2076.

For the application of the methods, the pre-storm beach level at the structure toe was determined at the intersection of the profiles with the proposed stepped revetment. The local water depth (h_{toe}) was calculated based on the pre-storm beach level and the local mean water level from the M3W model results presented in Section 8 including the still water level and the wave setup.

For the methods based on the local maximum wave height, detailed information is available from the M3W results, which resolves the individual wave dynamics and includes the dynamic effects of surf beat. A simpler estimate of H_{max} equal to the local water depth (USACE, 2002) is also evaluated. Figure 9-2 presents a comparison of the results from the various methods, showing results for both the simple and complex hydrodynamics where relevant.

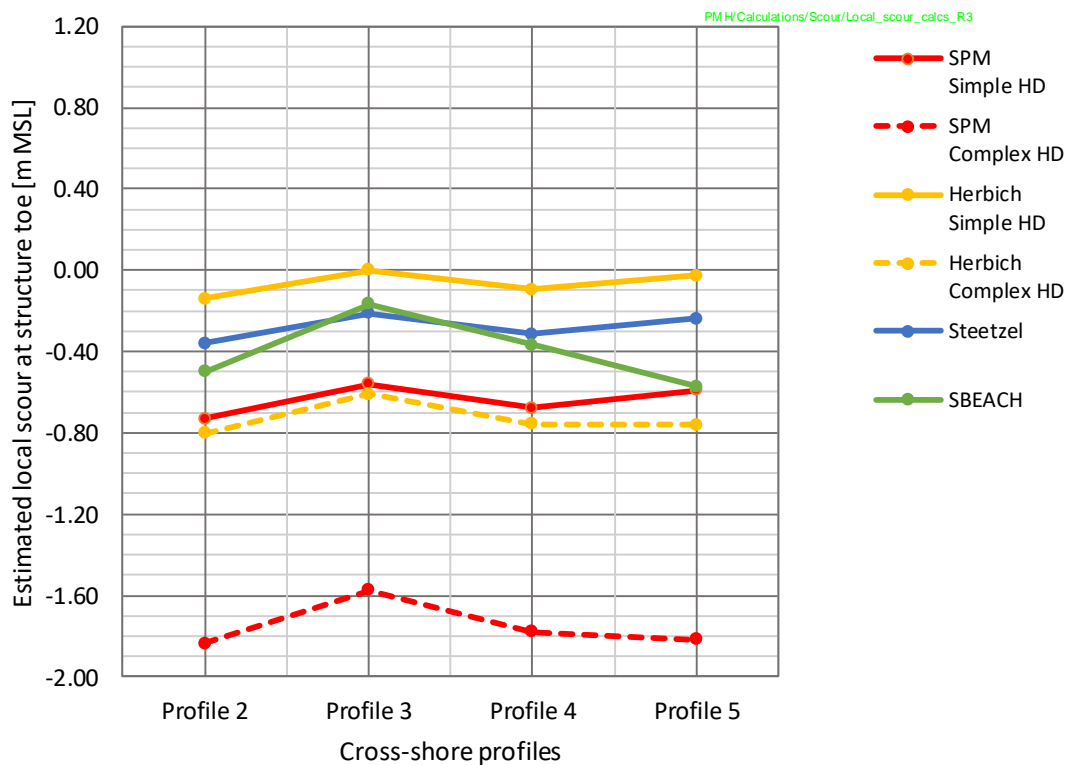


Figure 9-2: Comparison of methods for the 475-year return period in 2076.

The results using the complex hydrodynamics are substantially more conservative than the simple hydrodynamics. However, such a complex estimate of H_{max} as is available from M3W would likely not have been available in the development of the methods and is often not available for their application. Therefore, the application of these methods was based on simple hydrodynamics, where H_{max} was taken equal to the local water depth.



The local scour estimation from the empirical methods and from the SBEACH modelling were compared as shown in Table 9-2 for Profile 4 in 2026, 2046 and 2076. Annexure C contains the full set of results for Profiles 2 to 5.

Table 9-2: Pre-storm beach level and estimated local scour at the structure toe for the 1, 10, 100 and 475-year storms at Profile 4 in 2026, 2046 and 2076.

Climate change horizon	Joint return period [y]	Pre-storm beach level at structure toe [m MSL]	Maximum scour depth at structure toe [m]				Local scour level at structure toe ^(a) [m MSL]					
			SPM	Herbich	Steetzel	SBEACH	SPM	Herbich	Steetzel	SBEACH	Max scour level	Min scour level
2026	1	1.35	0.17	0.10	0.13	1.07	1.18	1.25	1.22	0.28	1.25	0.28
	10	1.35	0.29	0.17	0.22	1.17	1.06	1.18	1.13	0.18	1.18	0.18
	100	1.35	0.39	0.24	0.29	1.34	0.96	1.11	1.06	0.01	1.11	0.01
	475	1.35	0.46	0.28	0.35	1.32	0.89	1.07	1.00	0.03	1.07	0.03
2046	1	1.11	0.57	0.34	0.43	1.01	0.54	0.77	0.68	0.10	0.77	0.10
	10	1.11	0.69	0.41	0.52	1.09	0.42	0.70	0.59	0.02	0.70	0.02
	100	1.11	0.79	0.47	0.59	1.11	0.32	0.64	0.52	0.00	0.64	0.00
	475	1.11	0.86	0.52	0.64	1.11	0.25	0.59	0.47	0.00	0.59	0.00
2076	1	0.78	1.17	0.70	0.87	0.78	-0.39	0.08	-0.09	0.00	0.08	-0.39
	10	0.78	1.29	0.77	0.96	0.87	-0.51	0.01	-0.18	-0.09	0.01	-0.51
	100	0.78	1.39	0.83	1.04	1.09	-0.61	-0.05	-0.26	-0.31	-0.05	-0.61
	475	0.78	1.46	0.87	1.09	1.15	-0.68	-0.09	-0.31	-0.37	-0.09	-0.68

Notes:

(a) Based on the geotechnical information the bedrock is estimated at -1.3 m MSL.

For the 2076 horizon the scour predicted by SBEACH is within the range of predictions from the empirical methods. For the 2026 and 2046 horizons, the SBEACH results predict more scour than the empirical equations. This is due to the increased slope of the upper beach, which is realistically eroded in SBEACH, while the empirical methods do not account for varying slopes at the toe of the structure. This limits the initial water depth at the toe of the structure and thus the scour depth predicted. This may result in the empirical equations underpredicting the scour for the 2026 and 2046 horizons which have a relatively steep upper beach slope. It is therefore recommended that the minimum scour level from the four methods should be used in each case.

The geotechnical information was used to estimate the bedrock levels at the profiles as summarised in Table 7-6. The minimum and maximum scour levels and the estimated bedrock level for all four return periods are summarised in Figure 9-3, Figure 9-4, Figure 9-5 for 2026, 2046 and 2076, respectively. At Profile 2 the minimum local scour level is lower than the estimated bedrock level at -0.5 m MSL and therefore the estimated local scour level can be limited to the bedrock level.

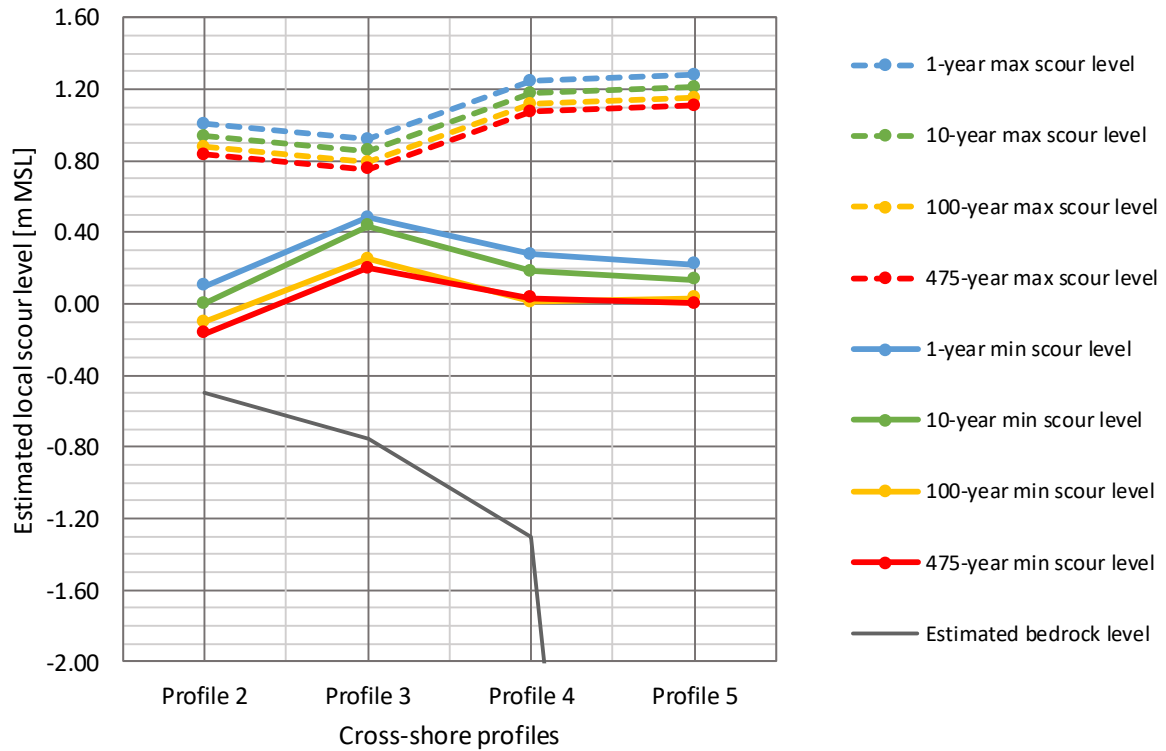


Figure 9-3: Estimated local scour at structure toe for Profiles 2 to 5 for 1, 10, 100 and 475-year return period in 2026. Minimum and maximum levels reflect the range of estimates.

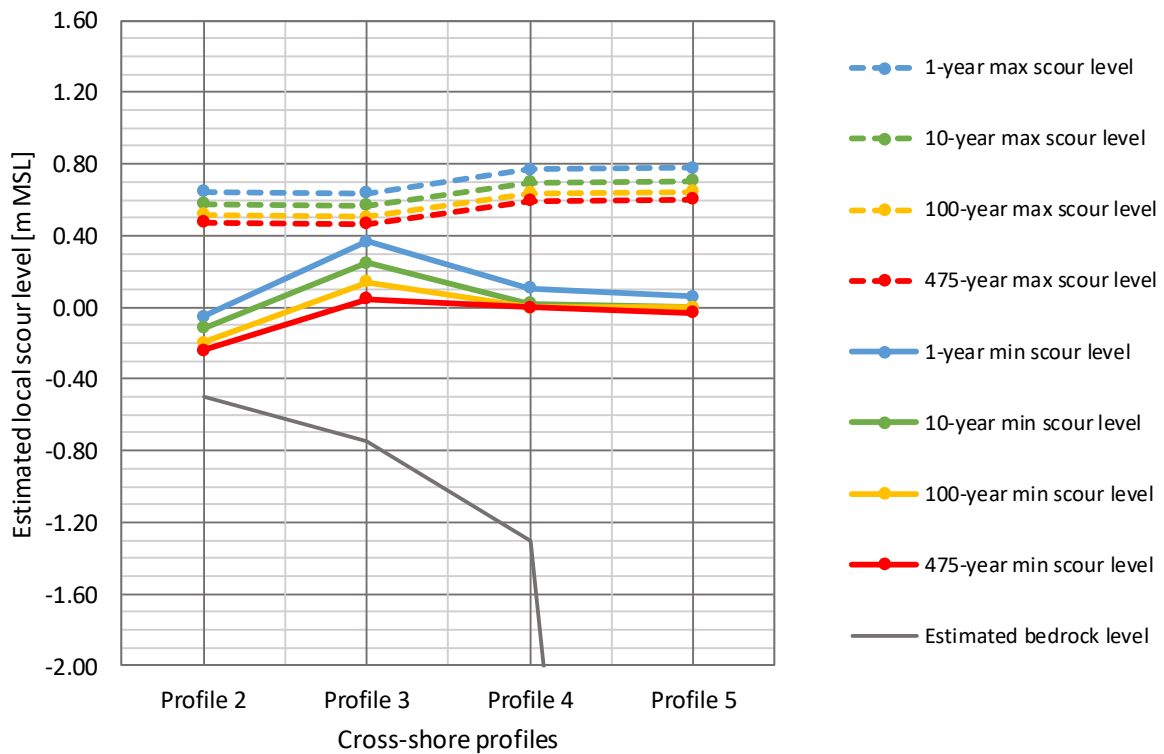


Figure 9-4: Estimated local scour at structure toe for Profiles 2 to 5 for 1, 10, 100 and 475-year return period in 2046. Minimum and maximum levels reflect the range of estimates.

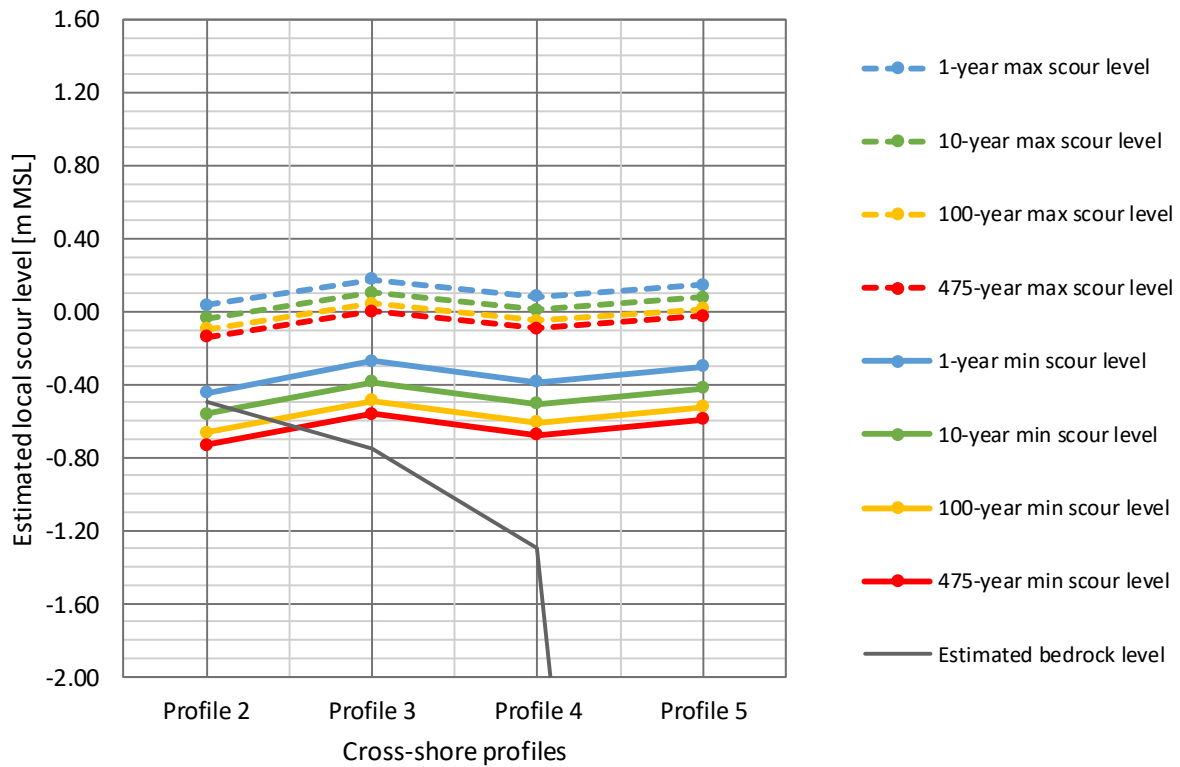


Figure 9-5: Estimated local scour at structure toe for Profiles 2 to 5 for 1, 10, 100 and 475-year return period in 2076. Minimum and maximum levels reflect the range of estimates.

The predicted 475-year minimum scour level ranges between -0.2 to +0.2 m MSL for 2026, and deepens -0.2 to 0.0 m MSL for 2046 and -0.7 to -0.6 m MSL for 2076. This trend reflects the recession of the beach profile, and the increased scour depths arising from lower bed levels, higher water levels and larger waves. For the 100-year return period, the minimum scour levels are approximately 0.1 m higher.

It is noted that none of the methods applied consider 2D effects, such as longshore currents (e.g. caused by oblique waves) which can significantly enhance scour, or beach cusps (which have been observed at Muizenberg in satellite imagery) which may locally lower the pre-storm seabed in front of the structure. Considering these unquantified effects and the uncertainty in the scour predicted by SBEACH (see Section 7.4.4), it is recommended that an allowance for an additional 0.5 m localised scour be considered in the design.

It is recommended that the minimum scour level from the four methods be used for design. The design process should consider these levels and time horizons in the scour protection design (including adaptive design approaches), and consider the proposed additional 0.5 m localised scour allowance for uncertainties in the methodologies and unquantified 2D effects. Including this allowance, the minimum scour level for the 475-year return period ranges between -0.5 to -0.7 m MSL for 2046 and -1.2 to -1.1 m MSL for 2076, noting that these will be limited by bedrock in some areas.



10. IMPACT OF CLIMATE CHANGE ON BEACH WIDTH

The impact of climate change on the dry beach width under normal conditions was assessed by estimating the variability of dry beach width on a representative profile for two sea level rise scenarios. The dry beach is defined as the beach width above the average wetted line, which corresponds to the runup level during average wave conditions and an average high tide. During low tide, the beach will be wider than this, but the sand will remain wet from the previous high tide. Note that the assessment is based on a single average runup level, whilst variations in the tides and waves will increase the natural variability of the dry beach width.

The historical measured beach profiles from Profile B (Section 7.1.4) were analysed to determine an average cross-shore profile position. Due to the alongshore uniformity of the beach the profile was assumed to be representative of the beach in front of the proposed seawall. The average beach profile, corresponding to the 8 April 2008 measurements, is shown in Figure 10-1, along with the envelope of all the measured profiles.

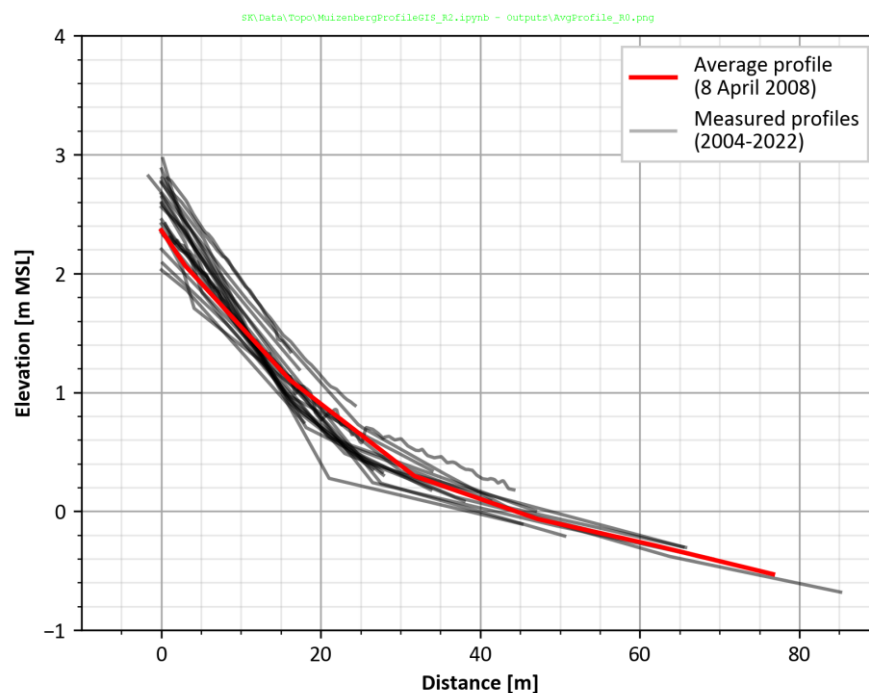
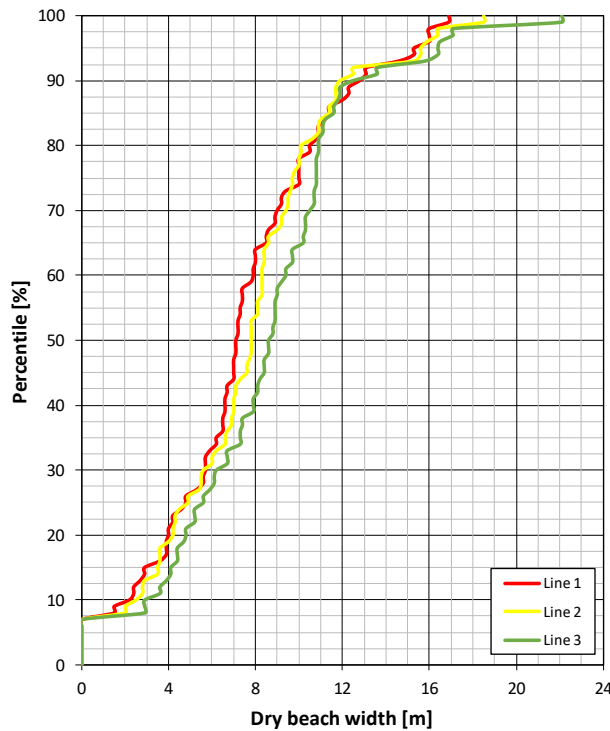


Figure 10-1: Average profile (measured on 8 April 2008) compared to the envelope of all measurements (2004 to 2022) along Profile B (refer to Section 7.1.4).

The distributions of dry beach width in front of the existing seawall were obtained from the wetted line analysis in Section 7.1.3 for the period between 2002 and 2022. Figure 10-2 presents the percentile plot of dry beach width for Lines 1, 2 and 3. The present-day average dry beach width is estimated to be 7.1 m (median dry beach width of 7.1 m for Line 1) which corresponds to a wave runup level of 1.76 m MSL on the cross-shore profile. This is supported by the wave runup levels ($R_{2\%}$), calculated for the profile for an average wave condition ($H_{m0} = 1.1$ m, $T_p = 11.1$ s) and a mean high tide water level (+0.76 m MSL) using equations from Stockdon et al. (2006) and Nielson & Hanslow (1991), which equates to 1.66 m MSL and 1.89 m MSL, respectively.



L:\H1\Analysis\Beach width\Beach_width_exceedance_R1x1xq\Summary

Percentile [%]	Dry beach width [m]		
	Line 1	Line 2	Line 3
0	0.0	0.0	0.0
5	0.0	0.0	0.0
10	2.2	2.5	2.9
20	4.0	4.2	4.8
30	5.7	5.6	6.2
40	6.6	7.0	7.9
50	7.1	7.8	8.6
60	7.9	8.3	9.4
70	9.0	9.4	10.5
80	10.5	10.1	10.9
90	12.8	11.9	12.5
95	15.3	15.6	16.4
100	16.9	18.5	22.1

Figure 10-2: Percentile plot of dry beach width in front of the existing seawall between 2002 and 2022.

The cross-shore profiles were adjusted for the long-term trend due to longshore sand supply (+0.22 m/year, see Section 7.3.5) and sea level rise for 2026, 2046 and 2076 (see Section 7.2). The median SLR projections for SSP5-8.5 (the most conservative scenario) and SSP1-2.6 (a low emissions scenario, see Figure 3-1) were considered. The average runup level was assumed to increase with sea level rise only (no adjustment for climate change-induced changes in storm surge, waves or water depth). For each scenario the dry beach width was measured between the seawall and the average runup level. Cross shore variability due to erosion and accretion was also considered by applying a horizontal offset of ± 5 m based on the envelope of observed cross-shore measurements (see Figure 10-1).

Figure 10-3 and Figure 10-4 show the existing and future dry beach variability for the SSP1-2.6 and SSP5-8.5 climate change SLR projections respectively. The temporal variation of the dry beach is shown in Figure 10-5 and summarised in Table 10-1.

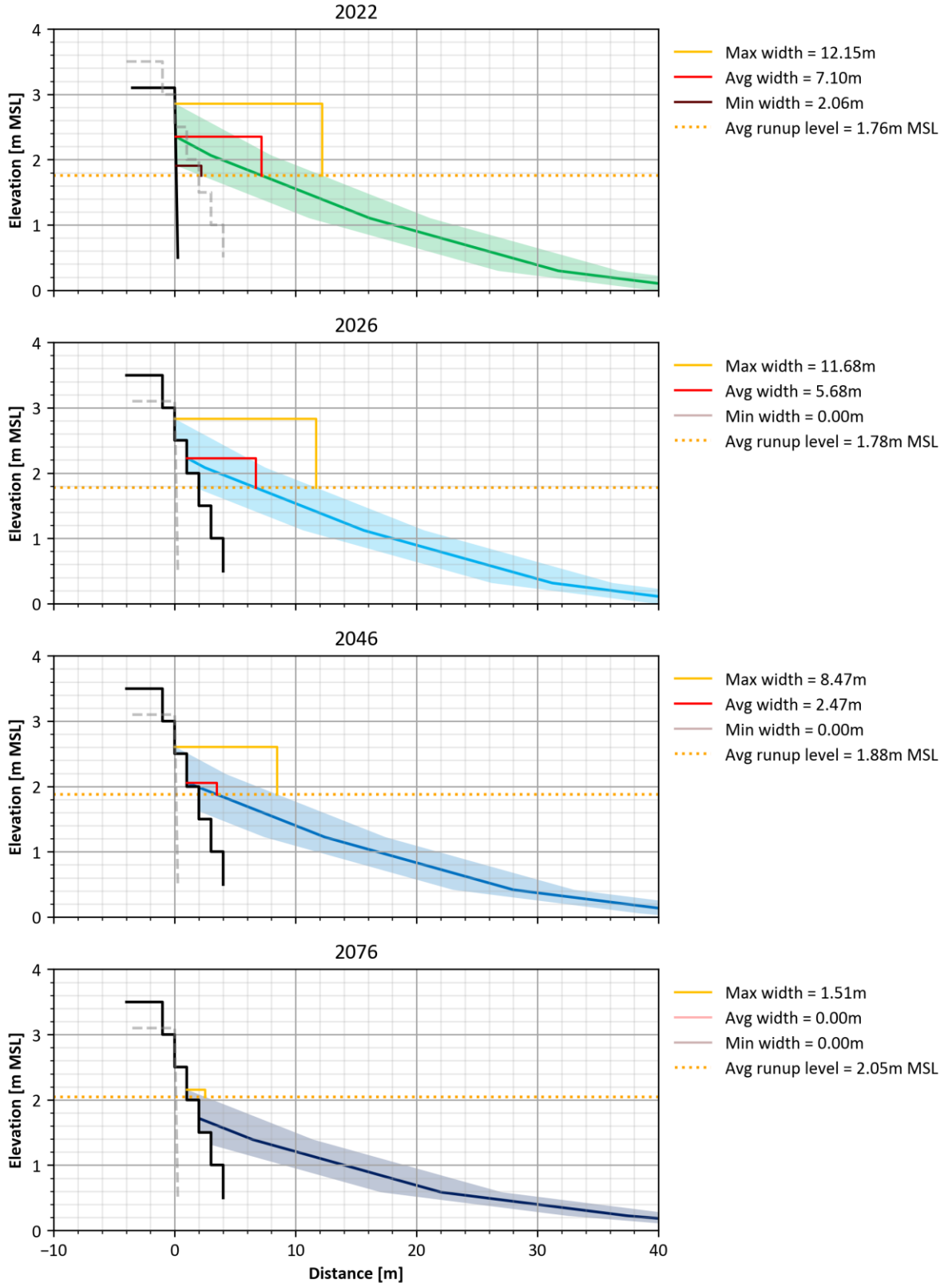


Figure 10-3: Dry beach width variability for a SSP1-2.6 median SLR scenario. Note: the dry beach width is measured relative to the existing sea wall for 2022 and the new sea wall for 2026 onward.

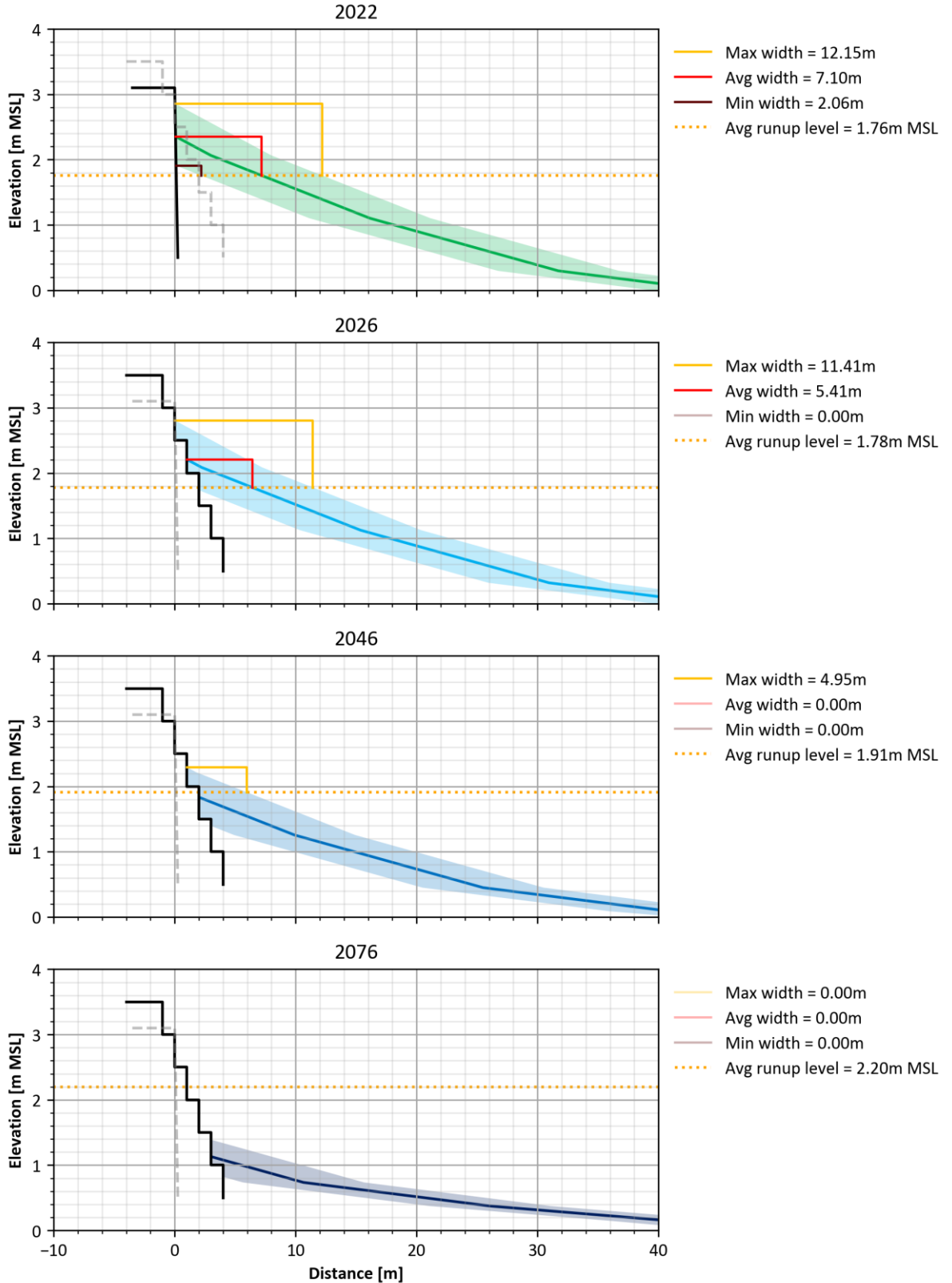


Figure 10-4: Dry beach width variability for a SSP5-8.5 median SLR scenario. Note: the dry beach width is measured relative to the existing sea wall for 2022 and the new sea wall for 2026 onward.

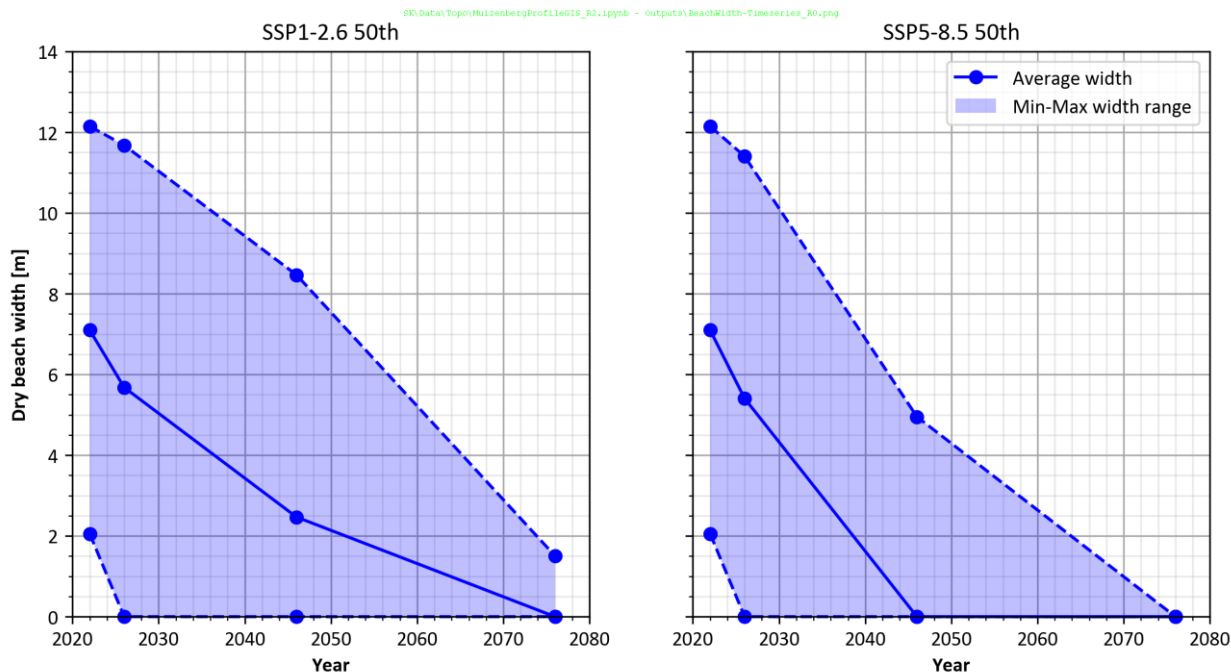


Figure 10-5: Time-series of dry beach width variability due to climate change.

Table 10-1: Summary of minimum, average and maximum dry beach widths due to climate change.

Year	Dry beach width [m]					
	SSP1-2.6 median SLR			SSP5-8.5 median SLR		
	Min	Avg	Max	Min	Avg	Max
2022	2.06	7.10	12.15	2.06	7.10	12.15
2026	0.00	5.68	11.68	0.00	5.41	11.41
2046	0.00	2.47	8.47	0.00	0.00	4.95
2076	0.00	0.00	1.51	0.00	0.00	0.00

For the SSP1-2.6 climate change projection the average beach width will reduce from 7.10 m in the present day to 5.68 m in 2026, 2.47 m in 2046 and 0 m (no dry beach) in 2076. For the more conservative SSP5-8.5 projection the average width will reduce to 5.41 m in 2026 and 0 m for both 2046 and 2076. Compared to the existing vertical wall, the proposed stepped revetment reduces the dry beach width between 1 m and 3 m depending on the vertical level of the beach and is the biggest contributor to the change in beach width between the present day and 2026.

It is noted that this assessment assumes that the longshore sediment supply has approximately balanced the erosion caused by sea level rise over the last four decades. However, due to the accelerating rate of sea level rise, this means, for example, that the predicted 33.1 m of setback in 2076 due to sea level rise under SSP5-8.5 is reduced by 12.1 m due to longshore supply (see Figure 7-25). The predicted future beach width is therefore sensitive to the assumed rate of sea level rise (as presented above) and to the longshore supply.

Projected changes in wave climate have shown a counter-clockwise rotation of the annual average mean wave direction offshore of Cape Town (Meucci, et al., 2020). For a simple wave climate and shoreline with the same orientation as False Bay, this would imply an increased westward longshore supply. However, there are factors which make the prediction of the effect on the False Bay coastline more complex.



Longshore transport at Muizenberg is governed by south-westerly swell which is dominant in winter and tends to drive the sand eastward, and south easterly waves which are dominant in summer and drive the sand westward. This can be seen in the wave roses presented in Figure 7-16, which show longer period swells from a more southerly direction and shorter period seas from a more easterly direction.

While available wave climate projections are derived from fully spectral wave models, the projections are aggregated as a change in annual average mean wave direction, i.e. all information on changes to individual components is lost. The projected rotation would reflect changes to storm tracks which are reported to shift southwards but may also include changes in other components due to changes in surface wind conditions. To conduct a proper assessment of the changes in nearshore wave climate at Muizenberg requires the effect on the individual components to be isolated, as can be done using actual wave spectra and surface wind fields.

Although the projected rotation cannot be isolated with the information available, a rotation of the south westerly swell can be assumed. The south-westerly wave energy from offshore undergoes significant wave refraction of approximately 70 degrees and is limited in direction by the shelter provided by Cape Point. Rotations in the offshore wave climate will therefore be significantly muted nearshore, limiting the associated impacts on the longshore transport, likely to within the accuracy achievable with a sand transport model. The projected effect is further complicated by wave climate studies which also project an increase in extreme storm wave heights. For the south-westerly storms which dominate the offshore extreme wave climate, this means an increased eastward transport, which is typically dominated by storm events.

The impact of climate change on the longshore transport at Muizenberg is therefore complex, and with the available information it cannot be said with certainty what the impact will be. In this study, the existing longshore supply has therefore been assumed to remain constant.



11. SUMMARY

Over 42 years of available hindcast wave data were used to model the nearshore operational and extreme wave heights. Extreme water levels were derived from measured storm surge, modelled wind set-up, sea level rise (SLR) and predicted tides. The extreme nearshore design conditions were evaluated for the 1-, 10-, 100-, and 475-year return periods, analysed as a joint probability between the waves and the extreme water level. The effect of climate change on extreme wave heights, storm surge and SLR was included for three climate change scenarios (2026, 2046 and 2076).

Analysis of the extreme wave heights showed two partitions of waves arriving at Muizenberg: larger wave heights with shorter wave periods driven by strong south-easterly winds over a long, unobstructed fetch, and smaller wave heights with longer wave periods typically associated with south-westerly swells refracting around Cape Point. The partitions were considered separately in defining the nearshore extreme wave climate.

The analysis of coastline trends from historical data showed that the beach has remained approximately stable over the long-term, even under the influence of historical sea level rise. This implies some sand supply to the beach. Longshore transport modelling was carried out to assess the supply of sand to the Muizenberg beach. The model was calibrated to the observed long-term trends, and the results were assessed to estimate the horizontal profile variability due to variations in longshore transport.

The long-term trends, horizontal variability, and coastline recession calculations using the Bruun Rule were used to estimate the horizontal and vertical profile adjustment for the three climate change horizons. Although the longshore sand supply was found to have historically balanced the expected erosion due to SLR, the accelerating rate of SLR outweighs the sand supply for the future horizons. This results in a net recession of the profiles in the future, which lowers beach levels in front of the seawall.

Cross-shore storm erosion modelling was used to simulate the erosion of the beach along the Muizenberg Beachfront during storm events. The outputs were used to set up profile models in the MIKE 3 Wave model and subsequent scour depth calculations.

The MIKE 3 Wave model was used to determine extreme wave conditions at the proposed stepped revetment and at the proposed sleeping rock revetment at the St. James walkway. The results will be used for the structural design calculations at the toe of the coastal protection structures. The full set of design conditions are presented in Annexure C. Where available, both joint probability combinations of wave height and storm surge should be tested in the design calculations.

Estimates of the local scour at the proposed structure were derived from three empirical equations and cross-shore storm erosion modelling. The results are included in Annexure C. It is recommended that the minimum scour level from the four methods should be used for design. The predicted 475-year minimum scour level ranges between -0.2 to +0.2 m MSL for 2026, and deepens -0.2 to 0.0 m MSL for 2046 and -0.7 to -0.6 m MSL for 2076. For the 100-year return period, the minimum scour levels are approximately 0.1 m higher. The design process should consider these levels and time horizons in the scour protection design (including adaptive design approaches), and consider a proposed additional 0.5 m localised scour allowance for uncertainties in the methodologies and unquantified 2D effects.

The impact of climate change on the dry beach width under normal conditions was assessed by estimating the variability of dry beach width on a representative profile. The dry beach is defined as the beach width above the average wetted line, which corresponds to the runup level during average wave conditions and an average high tide. For the SSP1-2.6 climate change projection (low emissions scenario) the average beach width will reduce from 7.10 m in the present day to 5.68 m in 2026, 2.47 m in 2046 and 0 m (no dry beach) in 2076. For the SSP5-8.5 projection (the most conservative scenario) the average width will reduce to 5.41 m



in 2026 and 0 m for both 2046 and 2076. Compared to the existing vertical wall, the proposed stepped revetment reduces the dry beach width between 1 m and 3 m depending on the vertical level of the beach and is the biggest contributor to the change in beach width between the present day and 2026. Specific consideration should be given to the usage of the area behind the proposed seawall versus the usage of the beach in front of the seawall. A landward retreat of the seawall will ensure that the beach amenity is maintained.



12. REFERENCES

- Airshed, 2021. *Proposed methodology for including Climate Change Forecasts into the Duynfontyn Site Safety Report*. [CONFIDENTIAL], Midrand: Airshed Planning Professionals.
- Allison, L. C., Palmer, M. D. & Haigh, I. D., 2022. Projections of 21st century sea level rise for the coast of South Africa. *Environmental Research Communications*, Issue 4, pp. 1-15.
- Bruun, P., 1962. Sea Level Rise as a Cause of Shore Erosion. *J. Waterways Harbors Div*, 88(1), pp. 117-132.
- CCT, 2022a. *Feasibility Report. Muizenberg Beach Front Refurbishment: Phase 1. CPX.0016740. Revision 0. 2022/04/06*, Cape Town: City of Cape Town, Coastal Management Branch.
- CCT, 2022b. *Standard Operating Procedure (SOP), Muizenberg beach lowering.*, Cape Town: City of Cape Town. Spatial Planning and Environment Directorate - Coastal Management Branch.
- CERC, 1984. *Shore Protection Manual Volume I and II*, Vicksburg, Mississippi, USA: Coastal Engineering Research Center, Department of the Army, Waterways Experimental Station, Corps of Engineers.
- DHI, 2022a. *MIKE 21 Toolbox, User Guide*, Hørsholm, Denmark: Danish Hydraulics Institute.
- DHI, 2022b. *MIKE 21 Flow Model FM, User Guide.*, Hørsholm, Denmark: Danish Hydraulics Institute.
- DHI, 2022c. *MIKE 21 Flow Model FM, Scientific Documentation.*, Hørsholm, Denmark: Danish Hydraulics Insitute.
- DHI, 2022d. *MIKE C-MAP, Extraction of World Wide Bathymetry Data and Tidal Information, User Guide*, Hørsholm, Denmark: Danish Hydraulics Institute.
- DHI, 2022e. *Extreme Value Analysis, User Guide.*, Hørsholm, Denmark: Danish Hydraulics Institute.
- DHI, 2022f. *MIKE 21, Spectral Waves FM Module, User Guide*, Hørsholm, Denmark: Danish Hydraulics Institute.
- DHI, 2022g. *MIKE 21, Spectral Waves FM Module, Scientific Documentation*, Hørsholm, Denmark: Danish Hydraulics Institute.
- DHI, 2022h. *Littoral Processes FM, User Guide*, Hørsholm, Denmark: Danish Hydraulics Institute.
- DHI, 2022i. *Littoral Processes FM, Scientific Documentation*, Hørsholm, Denmark: Danish Hydraulics Institute.
- DHI, 2022j. *MIKE 3 Wave Model FM, User Guide*, Hørsholm, Denmark: Danish Hydraulics Institute.
- DHI, 2022k. *MIKE 3 Wave Model FM, Scientific Documentation.*, Hørsholm, Denmark: Danish Hydraulics Institute.
- Esri, 2022. *Esri World Imagery Wayback*. [Online]
Available at: <https://livingatlas.arcgis.com/wayback>
[Accessed 22 04 2022].
- Fowler, J., 1992. *Scour problems and methods for prediction of maximum scour at vertical seawalls. Technical Rerport CERC 92-16.*, Vickburg, Mississippi, USA: USWES.
- Hands, E., 1983. *The Great Lakes as a Test Model for Profile Responses to Sea-Level Changes*. s.l.:CRC Press.
- Herbich, J. & Van Weele, B., 1965. *Scour of flat sand beaches due to wave action in front of sea walls*, USA: Coastal Engineering, Santa Barabara Specialty Conference, ASCE.



- HHO, 2022. *Muizenberg Beachfront Upgrade: Geotechnical Investigation Report. Report no. REP-7517-401-8001 Rev2*, Cape Town: HHO Consulting Engineers.
- IPCC, In press. *Climate Change 2021: The Physical Science Basis. Contribution of Working Group I to the Sixth Assessment Report of the Intergovernmental Panel on Climate Change.*, s.l.: Cambridge University Press.
- Kraus, N. C. & McDougal, W. G., 1996. The Effects of Seawalls on the Beach: Part I, An Updated Literature Review. *Journal of Coastal Research*, 12(3), pp. 691-701.
- Larson, M. & Kraus, N., 1989. *SBEACH: Numerical Model for Simulating Storm-Induced Beach Change, Report 1, Empirical Foundation and Model Development.*, Vicksburg, Mississippi, USA: US Army Corps of Engineers.
- Larson, M. & Kraus, N., 1998. *SBEACH: Numerical Model for Simulating Storm-Induced Beach Change. Report 5, Representation of Nonerosible (Hard) Bottoms*, Vicksburg, Mississippi, USA: US Army Corps of Engineers.
- McDougal, W. G., Kraus, N. C. & Ajiwibowo, H., 1996. The Effects of Seawalls on the Beach: Part II, Numerical Modelling of SUPERTANK Seawall Tests. *Journal of Coastal Research*, 12(3), pp. 702-713.
- Meucci, A. et al., 2020. Projected 21st century changes in extreme wind-wave events.. *Science Advances*, Issue 6, pp. 1-9.
- Morim, J., Hemer, M. & Wang, X. L., 2019. Robustness and uncertainties in global multivariate wind-wave climate projections.. *Nature Climate Change*, Issue 9, pp. 711-718.
- NCEP, 2022. *WAVEWATCH III® Hindcast and Reanalysis Archives*. [Online] Available at: <https://polar.ncep.noaa.gov/waves/hindcasts/> [Accessed 2022].
- Nielson, P. & Hanslow, D., 1991. Wave Runup Distributions on Natural Beaches. *Journal of Coastal Research*, 7(4), pp. 1139-1152.
- Petroliagkis, T. I., Voukouvalas, E., Disperati, J. & Bildot, J., 2016. *Joint Probabilities of Storm Surge, Significant Wave Height and River Discharge Components of Coastal Flooding Events. EUR 27824 EN. doi:10.2788/677778*, Italy: European Union.
- PRDW, 2022. *Sea Point Seawall Future Upgrades, Design Conditions Report. S2141-RP-CE-001-RB*, Cape Town: PRDW (Pty) Ltd..
- SANHO, 2018. *South African Tide Tables*, Tokai, South Africa: The Hydrographer South African Navy.
- Southern Oceanengineering, 2021. *The Muizenberg Beachfront Upgrade - Marine Landside Site Investigations*, Cape Town: Souther Oceanengineering.
- Steetzel, H., 1988. *Scour holes near seawalls (in Dutch), Report H298 Part 4*, The Netherlands: Delft Hydraulics.
- Stockdon, H., Holman, R., Howd, P. & Sallenger, A., 2006. Empirical Parameterisation of Setup, Swash and Runup. *Coastal Engineering*, Volume 53, p. 573–588.
- Tritan Survey, 2022. *High resolution marine site investigations in Muizenberg Beachfront, South Africa. Final Survey Report. Report No. TS10220.2*, Cape Town: Tritan Survey (Pty) Ltd..
- UHSLC, 2022. *University of Hawaii Sea Level Center*. [Online] Available at: <ftp://ftp.soest.hawaii.edu/> [Accessed 2022].



USACE, 2002. *Coastal Engineering Manual: Part IV*, Washington DC, USA: US Army Corps of Engineers.

van Rijn, L.C., 2018. *Local Scour Near Structures*. [Online]

Available at: <https://www.leovanrijn-sediment.com/papers/Localscour2013.pdf>

[Accessed 2022].



ANNEXURE A | TRITAN SURVEY REPORT



TRITAN SURVEY

3-D Laser Scanning • Engineering & Hydrographic Surveys

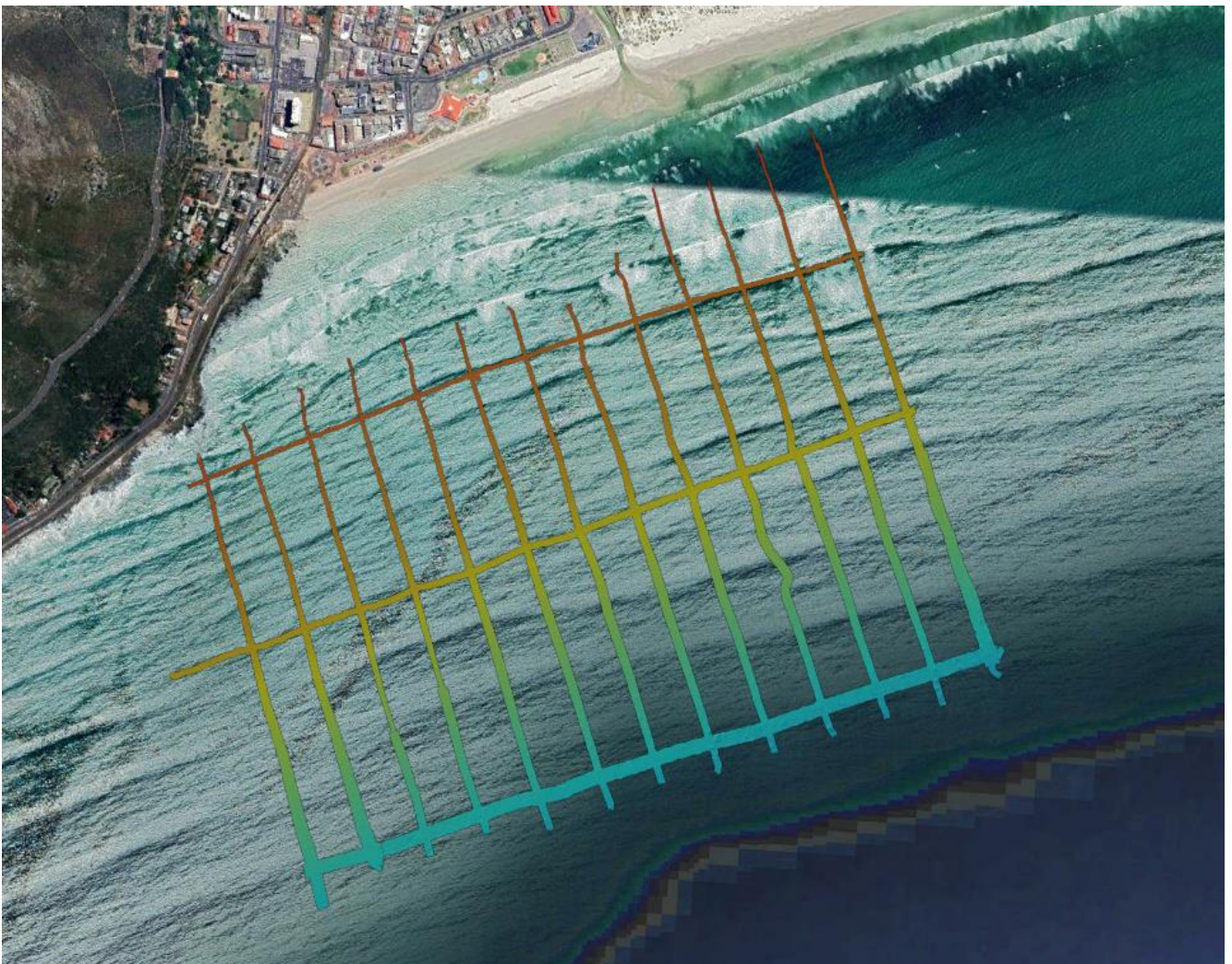
Final Survey Report

23 May 2022

HIGH RESOLUTION MARINE SITE INVESTIGATION IN MUIZENBERG BEACHFRONT, SOUTH AFRICA

For

PRDW



REPORT NO. TS10220.2

© Copyright 2021. Tritan Survey (Pty) Ltd.



CONTENTS

INTRODUCTION.....	2
Background and locality.....	2
Personnel:	3
SURVEY EQUIPMENT.....	3
Installation	3
Sensor Offsets.....	3
DATUM INFORMATION AND CONTROL.....	4
Datum level, coordinate system and control.....	4
Control	4
MULTIBEAM SURVEY (MBES).....	5
Patch Test Calibration	5
Introduction	5
Latency	5
Roll Correction	5
Pitch Correction	5
Yaw Correction.....	5
Summary of Results	5
Multi-beam Survey	6
Postprocessed Trajectory	6
BEACH CROSS SECTION SURVEY	8
Difficulties during surveys.....	8
OPERATIONS LOG.....	9
CONCLUSION AND RECOMMENDATIONS.....	9
APPENDIX.....	9
FIGURES	
Figure 1: Survey site.....	2
Figure 2 Position Standard Deviation	6
Figure 3 Attitude Standard Deviation	7
Figure 4 Example of big standard deviations due to unexpected swell	7
Figure 5 Muizenberg swell on 05/05/2022.....	8
TABLES	
Table 1 Equipment offsets Day1	3
Table 2 Equipment offsets Day2	3
Table 3 VRS shift for Beach Cross Sections	4
Table 4 Position translation for base stations	4
Table 5 Patch Test Results	5



Revision	Date	Description	Revised by
R0	2022-04-20	Report Issued	J M Christie-Smith
R1	2022-05-16	Beach Sections updated	J M Christie-Smith
R2	2022-05-23	Beach Sections 1 st survey VRS shift applied	J M Christie-Smith

INTRODUCTION

Background and locality

Tritan Survey (Tritan) was requested to conduct a nearshore bathymetric and a beach profile survey to assist PRDW and the City of Cape Town with their effort to rehabilitate and upgrade the coastal public infrastructure and services along the Muizenberg Beachfront. Figure 1 outlines the survey site and the data that was requested by the client. Additional lines were surveyed during the bathymetric survey to supply the client with the best indication of the topography of the seabed in that area.



Figure 1: Survey site



Personnel:

The survey was carried out by the following Tritan Survey personnel:

Mr James Christie-Smith- Party Chief/Skipper
Mr Barend Geldenhuys - Professional Hydrographic Surveyor

SURVEY EQUIPMENT

Instruments and equipment used:

- 2 x Trimble R4 RTK GNSS Receivers
- SBG Ekinox INS system used for navigation
- Reason 8125-HMultibeam
- Valeport Swift SVP
- 2 x Trimble R4-3 GNSS Receivers
- Data acquisition and processing done with BeamworX. Other software used include, Trimble Business Centre, Qinertia, Sonarwiz, and Microstation.

Installation

Installation of sensors, measurement of offsets and setup of the BeamworX project files were done on board the Tritan Explorer.

Sensor Offsets

The following offsets were measured and used in the BeamworX project and SBG INS:

	STBD	FRD	Up
SBG GPS 1 (Aft)	0.032	-1.556	-2.245
SBG GPS 2 (Fwd)	-0.026	1.060	-2.240
SBG IMU	0.000	-0.023	0.308
Reson 8125-H	-0.019	-0.925	-0.828
Waterline (COG)	0.000	0.000	0.000

Table 1 Equipment offsets Day1

	STBD	FRD	Up
SBG GPS 1 (Aft)	0.032	-1.556	-2.245
SBG GPS 2 (Fwd)	-0.026	1.060	-2.240
SBG IMU	0.000	-0.023	0.308
Reson 8125-H	-0.019	-0.925	-0.738
Waterline (COG)	0.000	0.000	0.000

Table 2 Equipment offsets Day2



DATUM INFORMATION AND CONTROL

Datum level, coordinate system and control

DATUM : Hartebeesthoek '94
 ELLIPSOID : World Geodetic System 1984 (WGS 84)
 GEOID MODEL : SA Geoid 2010
 CENTRAL MERIDIAN : 19°00' 00" E
 VERTICAL DATUM : LLD

Control

For the beach sections part of the survey two Trimble R4-3 receivers was utilized using its VRS function on the 19th of April 2022. A Town Survey Mark (5M32) nearby was surveyed as to accurately shift the coordinates from the ITRF2014 ellipsoid (that GPS uses) to the WGS84 ellipsoid which our destination datum (Hart94) uses. Table 3 outlines the VRS shift from both receivers as well as the average that was used.

Surveyed Town Survey Mark Coords (ITRF2014)				Published Town Survey Mark Coords (WGS84)			
	Easting	Northing	Elevation		Easting	Northing	Elevation
Receiver1	48849.40	3775062.68	1.57	5M32	48849.75	3775063.27	1.63
Receiver2	48849.38	3775062.68	1.57				
Mean VRS Shift Adopted					0.36	0.59	0.06

Table 3 VRS shift for Beach Cross Sections

The same was done for the base station that was set up on both the 12th of April 2022 as well as the 05th of May 2022 to ensure the best possible roving position data on the vessel during the bathymetric survey. During these base setups two Town Survey Marks were occupied to find the best translation in position to account for the shift when moving from ITRF2014 ellipsoid to the WGS84 ellipsoid. The two shifts are very similar in magnitude which was expected as the survey was done in the same area.

Surveyed Town Survey Mark Coords (ITRF2014)				Published Town Survey Mark Coords (WGS84)			
	Easting	Northing	Elevation		Easting	Northing	Elevation
11N30	48292.21	3773622.94	2.92	11N30	48292.59	3773623.53	2.96
5N30	48207.43	3773478.10	3.21	5N30	48207.81	3773478.71	3.23
Mean VRS Shift Adopted					0.38	0.60	0.03

Table 4 Position translation for base stations



MULTIBEAM SURVEY (MBES)

Patch Test Calibration

Introduction

To accurately measure the seafloor, the measurements made by the Multibeam sonar must be relative to true vertical and direction as reported by the inertial navigation. During installation it was not possible to obtain perfect alignment of the MBES on the measured zero axis. Therefore, a standard calibration routine was performed to obtain values for Roll, Latency, Pitch and Yaw mounting angles.

Latency

Latency is eliminated by using a PPS (Pulse per second) box. This device consistently generates a pulse every second. This pulse is recorded and is used in the processing stage to remove the latency.

A constant GPS latency can still be present because of long cables and other influences. This is eliminated by running the same line at different speeds in the same direction.

Roll Correction

Surveying one line in opposite directions, over flat seabed is performed for the roll calibration. The two profiles generated are compared and a roll offset angle correction can be derived. This procedure is then repeated, and an average angle offset is applied.

Pitch Correction

Surveying a short line, in opposite directions, over a slope feature would usually be performed to determine this correction. The two profiles generated are compared and a pitch offset angle applied.

Yaw Correction

Surveying two parallel lines in the same directions, over a slope feature so that the object appears in the swath outer beams would usually be performed to determine this correction. The two profiles generated are compared and a yaw offset angle applied.

Summary of Results

	Latency (s)	Roll(°)	Pitch (°)	Yaw (°)
12/04/2022	0.000	-0.560	1.140	0.500
05/05/2022	0.000	-1.580	1.700	5.000

Table 5 Patch Test Results



Multi-beam Survey

- The survey was conducted at no more than 4 Knots.
- A single sound velocity profile (SVP) was performed in the deepest area of the survey at the start of every survey.
- Continuous SVP data was acquired at the head to monitor surface temperature changes.
- A patch test calibration procedure was carried out to ensure the system was within the correct specification.

Postprocessed Trajectory

The GNSS base along with the logged 200kHz INS data was post processed in Qinetria software. A tightly coupled solution, where GNSS and IMU data is processed by an Extended Kalman Filter (EKF) to calculate a Smoothed Best Estimate of Trajectory (SBET) of the vessel. Standard Deviation graphs for position and attitude are below.

During the survey the team encountered unexpected, large swells whilst attempting to acquire data as shallow as possible. During one of these attempts the vessel was rocked drastically by such a swell and it can clearly be seen in the highlighted area in Figure 7 where the standard deviation for the position jumped.

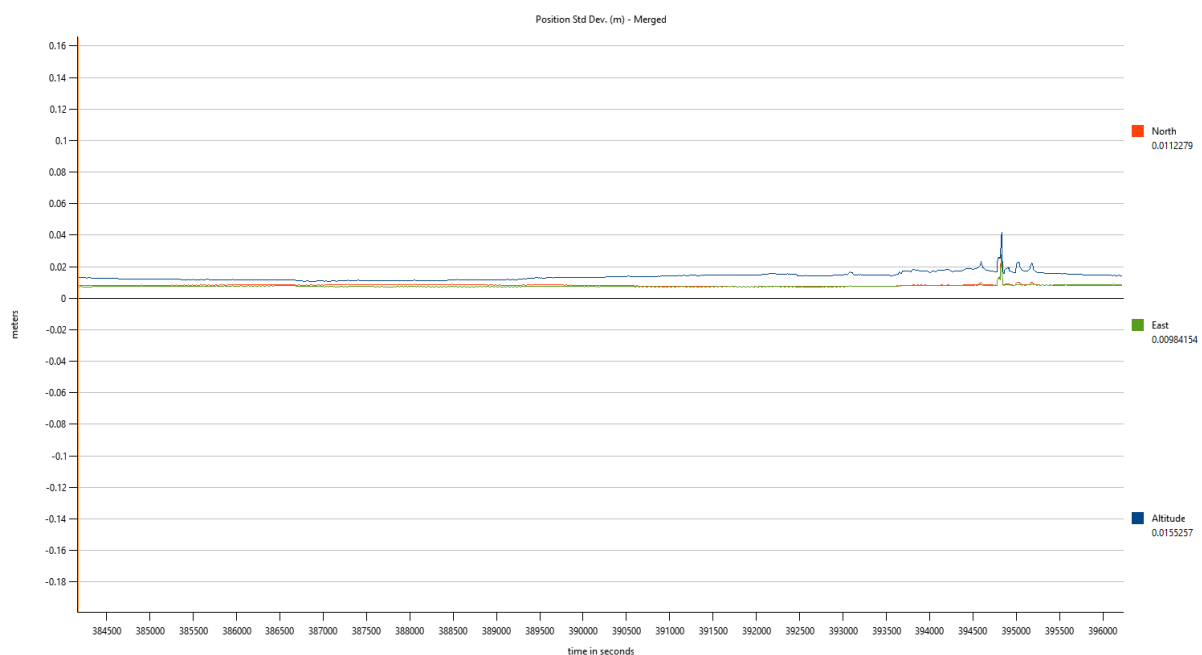


Figure 2 Position Standard Deviation

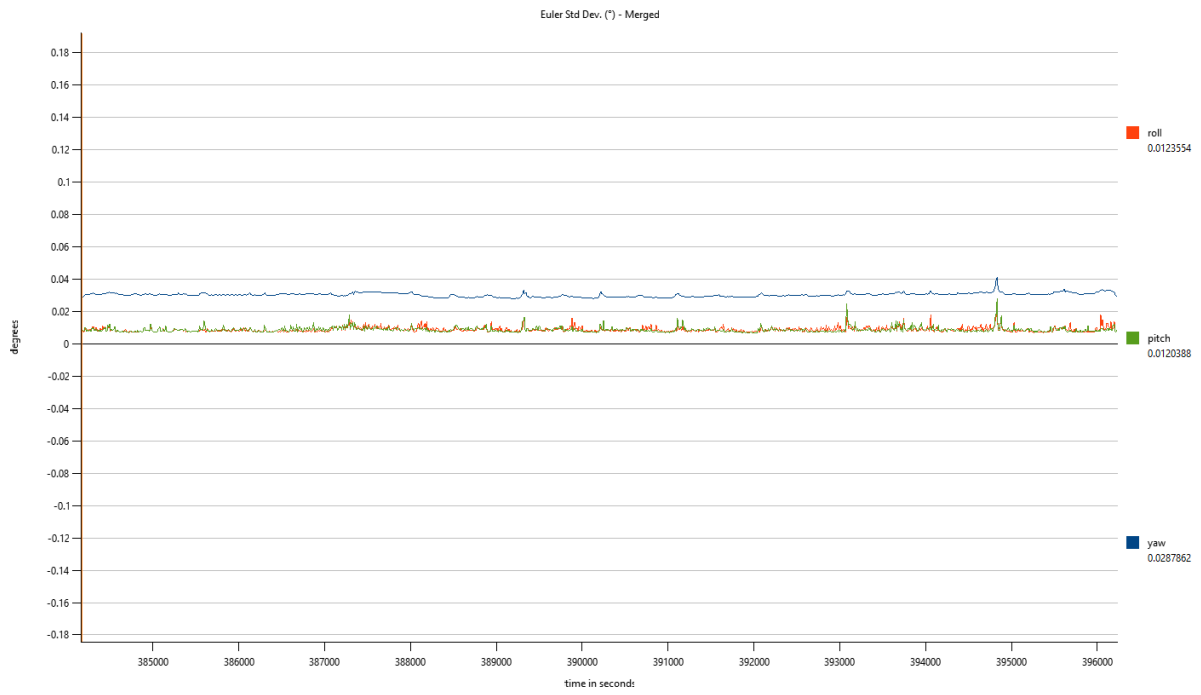


Figure 3 Attitude Standard Deviation

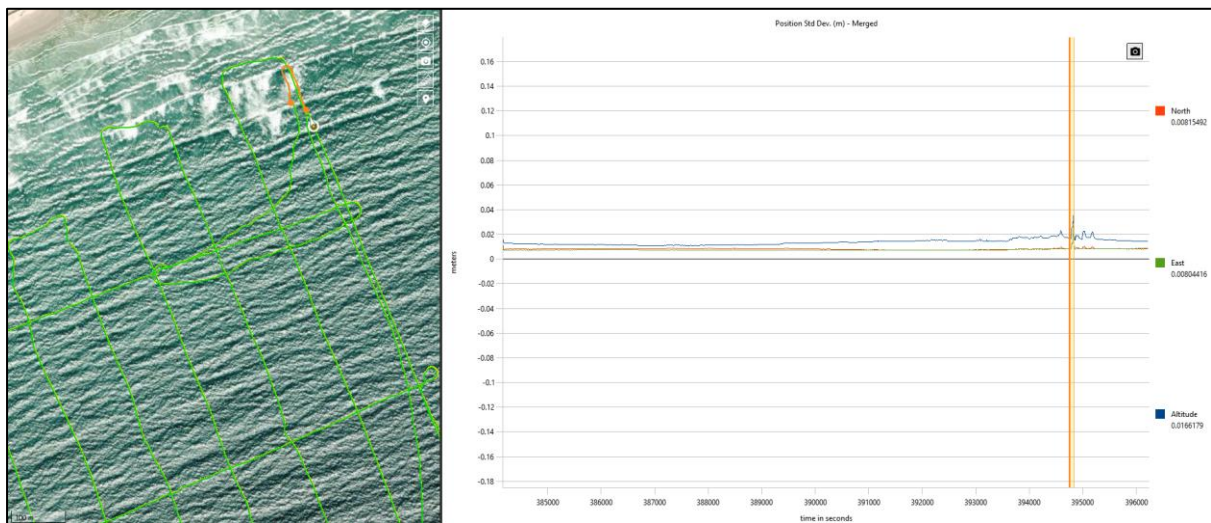


Figure 4 Example of big standard deviations due to unexpected swell



BEACH CROSS SECTION SURVEY

The Beach Cross Section phase of this survey was conducted on the 19th April 2022 during the lowest tide in the morning and the 10 May 2022 over the low tide period. This was conducted using two Trimble R4-3 receivers combined with two TSC 3 controllers as well as a Total station on the second visit, although this survey was not conducted at spring low tide, we used a prism on a three meter ranging rod to swim out to the required depth.

The cross sections were surveyed from the edge of the beach or the start of vegetation (whichever came first) into the ocean as deep as was deemed safe for the surveyors as well as the equipment that are very vulnerable to rust. An average depth of 1.5m below MSL was achieved during this survey which was expected and 1.4m below MSL on the second site visit.

As explained, VRS was used, and the shift was applied so that we were able to output the coordinates in the required datum (Hart94).

Difficulties during surveys

During the first day of the bathymetric survey on the 12th of April 2022 the water was calm but very murky closer to shore. After the patch test and initial test lines were finished, the first survey line was undertaken, running towards shore on the Western side of survey site. Whilst turning off at the end of the line the vessel had hit a rock outcrop that was not visible to the skipper in the murky conditions. Both the surveyor and the skipper thought that the motors of the vessel had hit the object, when it was in fact it was the multibeam head. Due to the impact the offsets changed, it became apparent during post processing that only the first survey line's data would be usable and that the survey team would have to return at a later date.

As also mentioned earlier, during the hydrographic survey of May 5th 2022, there were intermittent set waves that were bigger than the predicted swell. Figure 8 shows the conditions on that day. This hindered the ability of the survey team to collect data any shallower than what was acquired.



Figure 5 Muizenberg swell on 05/05/2022



The only difficulties encountered during the land surveying (beach cross sections) phase of the project was the access into the ocean from the rocky outcrop area of the survey site. This had steep drops and slippery surfaces.

OPERATIONS LOG

2022-04-12 Tue 07:00 – 11:00	Travel to site. Do Patch Test and Test lines. Hit rock outcrop @ +- 11am.
2022-04-12 Tue 11:00 – 17:00	Finish survey. Difficulties retrieving MBES head. Travel back to office.
2022-04-19 Tue 10:00 – 13:00	Beach Cross Sections Survey.
2022-05-05 Thu 10:00 – 13:00	Travel to site. Do Patch Test and Test lines.
2022-05-05 Thu 13:00 – 17:00	Survey lines. Retrieve MBES head and travel back to office.
2022-05-10 Tue 10.00 – 17.30	Beach Cross section Survey
2022-05-11 to 2022-05-16	Processing and reporting

CONCLUSION AND RECOMMENDATIONS

- No problems were encountered that we could not overcome.
- A good data set was achieved.
- Deliverables: CAD drawing with 0.5 m contours and ASCII files of the Mass Bathymetry and Beach sections.

Date: 23 May 2022

James Christie-Smith
Director

APPENDIX

CAD Drawings

- TS10220_Muizenberg.DWG



ANNEXURE B | CROSS-SHORE EROSION RESULTS



Figure B-1: Erosion results for the 1, 10, 100 and 475-year storms at Profile 2 in 2026 (top), 2046 (middle) and 2076 (bottom). 3

Figure B-2: Erosion results for the 1, 10, 100 and 475-year storms at Profile 3 in 2026 (top), 2046 (middle) and 2076 (bottom). 4

Figure B-3: Erosion results for the 1, 10, 100 and 475-year storms at Profile 4 in 2026 (top), 2046 (middle) and 2076 (bottom). 5

Figure B-4: Erosion results for the 1, 10, 100 and 475-year storms at Profile 5 in 2026 (top), 2046 (middle) and 2076 (bottom). 6

Figure B-5: Erosion results for the 1, 10, 100 and 475-year storms at Profile 6 in 2026 (top) and 2076 (bottom). 7

Figure B-6: Erosion results for the 1, 10, 100 and 475-year storms at Profile 7 in 2026 (top) and 2076 (bottom). 8

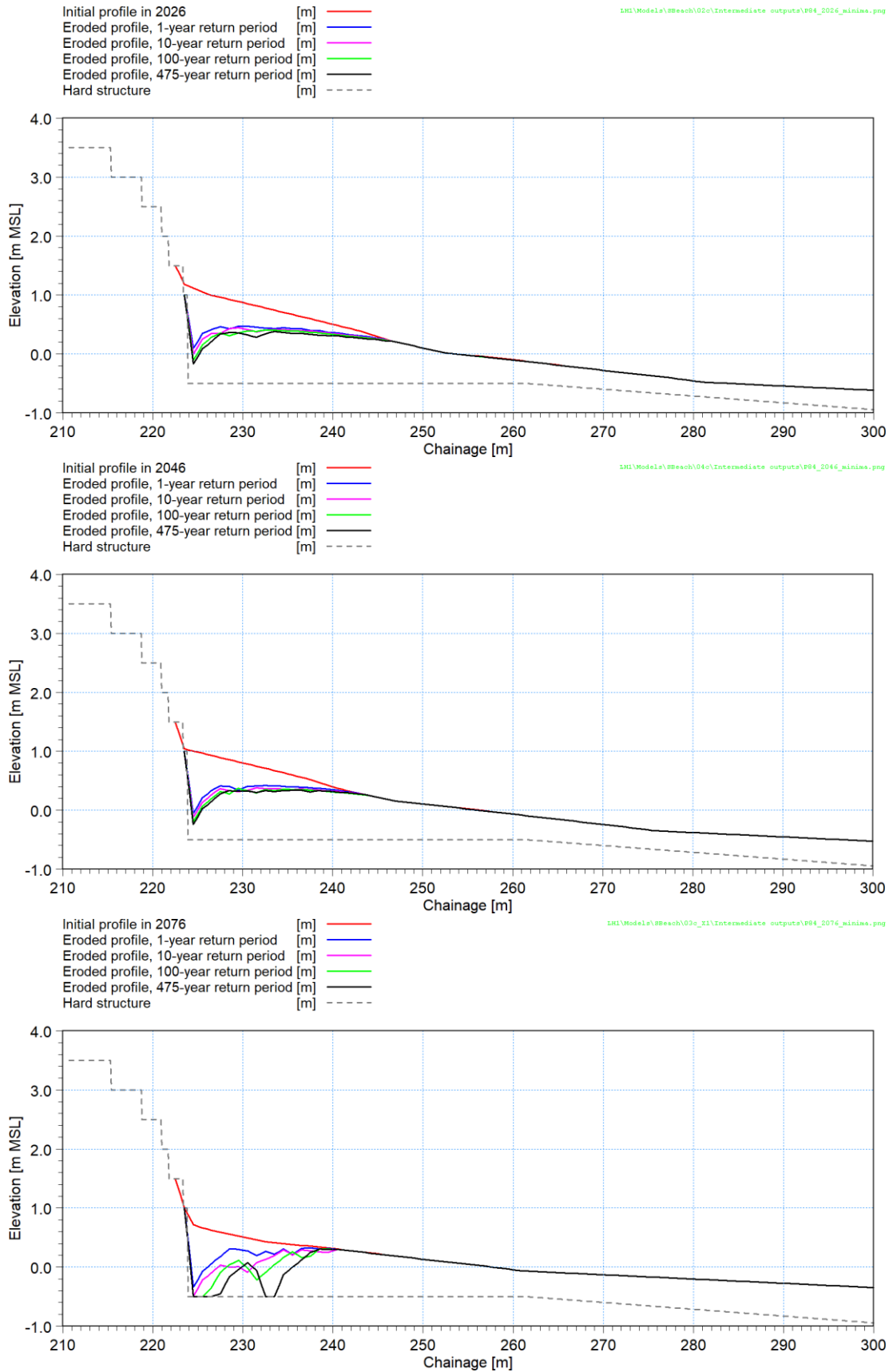


Figure B-1: Erosion results for the 1, 10, 100 and 475-year storms at Profile 2 in 2026 (top), 2046 (middle) and 2076 (bottom).

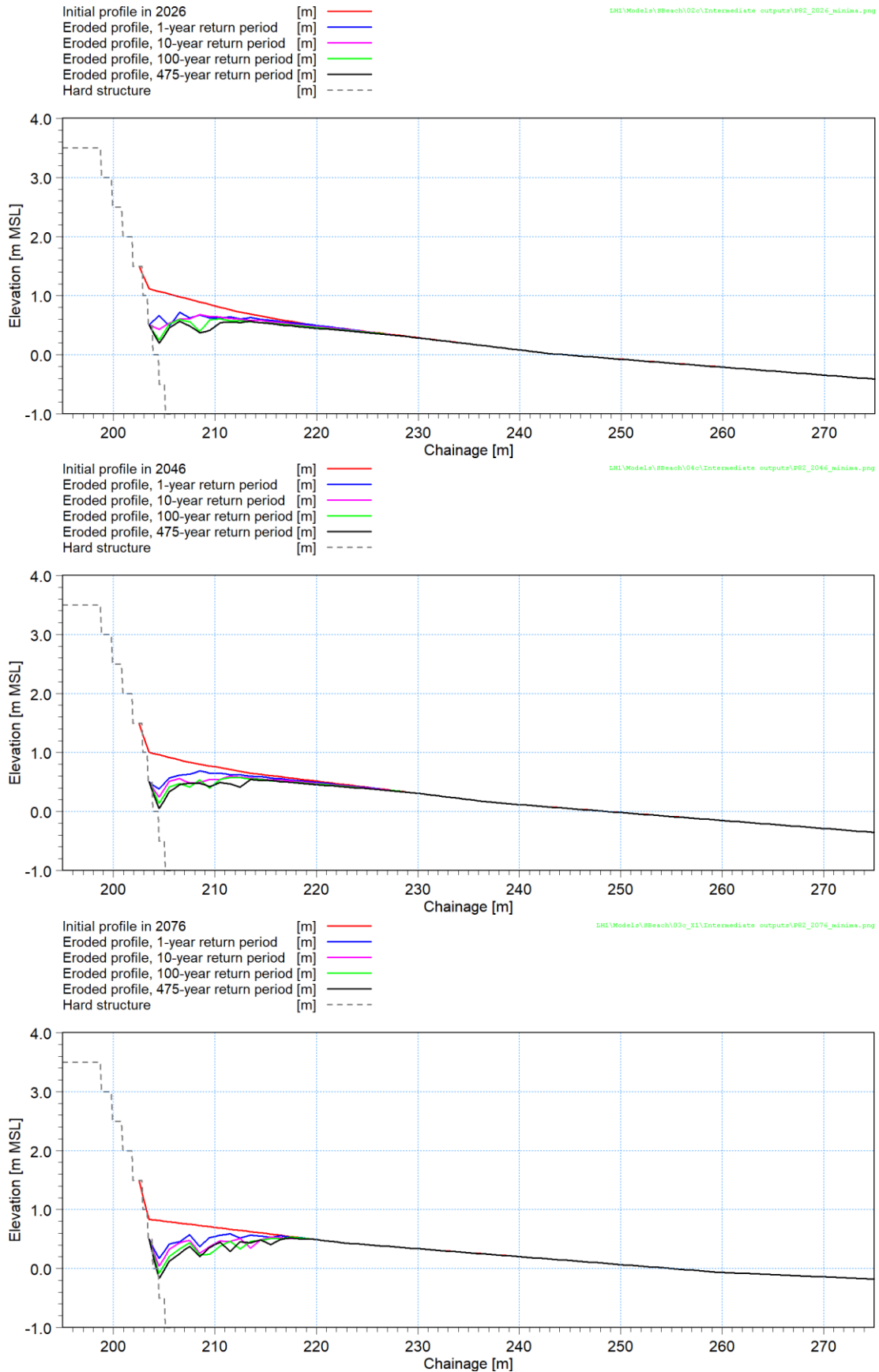


Figure B-2: Erosion results for the 1, 10, 100 and 475-year storms at Profile 3 in 2026 (top), 2046 (middle) and 2076 (bottom).

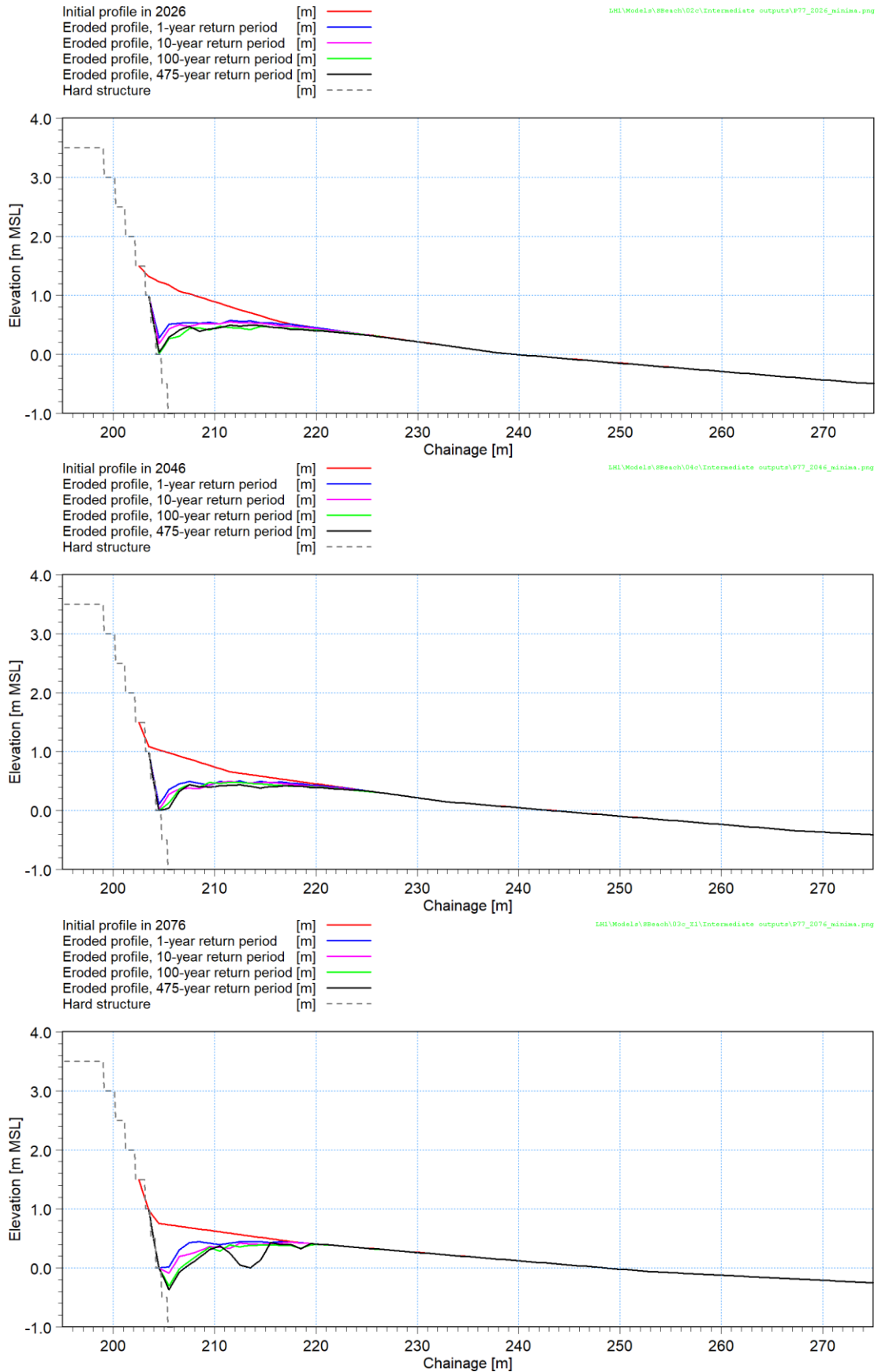


Figure B-3: Erosion results for the 1, 10, 100 and 475-year storms at Profile 4 in 2026 (top), 2046 (middle) and 2076 (bottom).

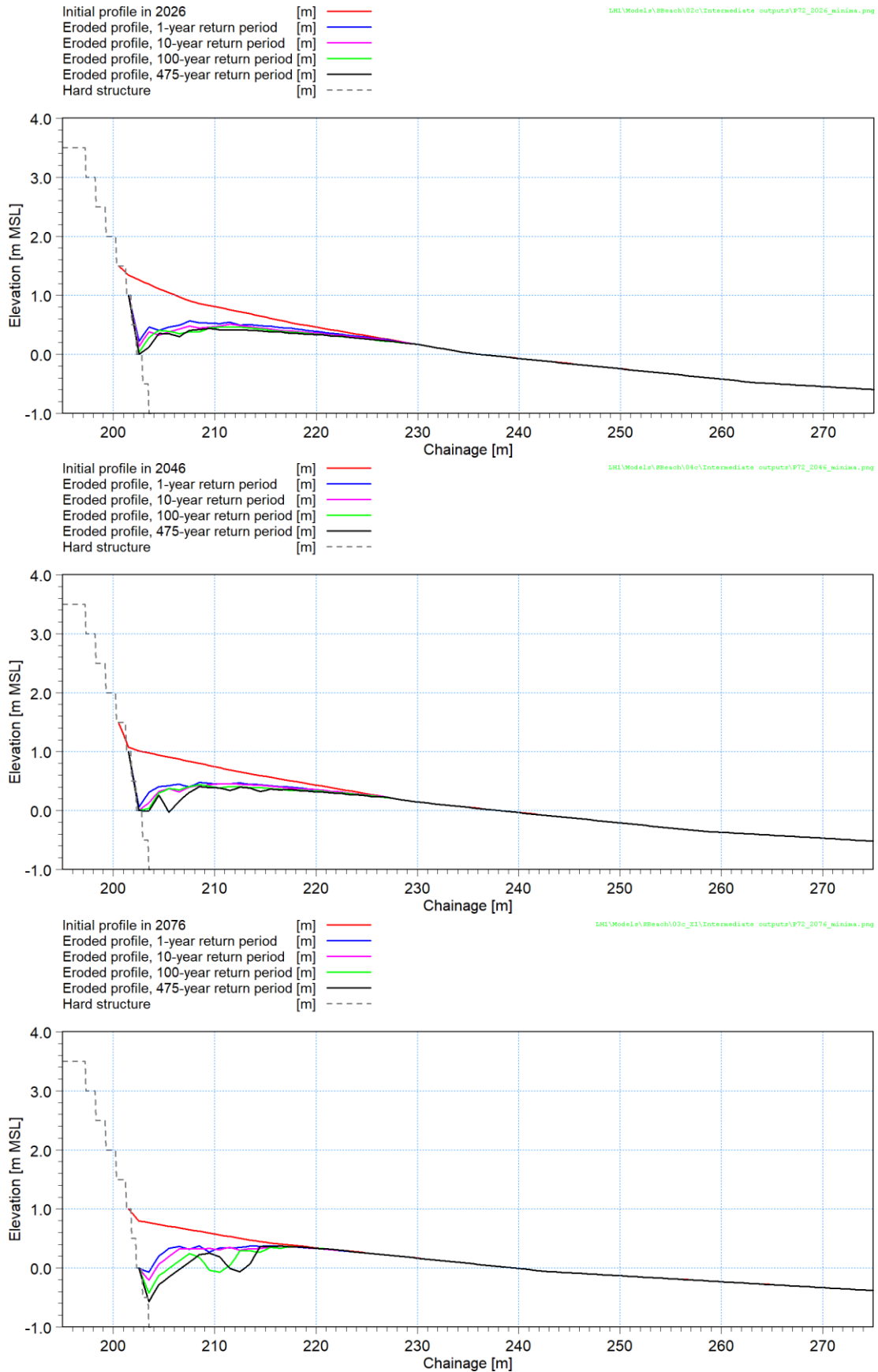


Figure B-4: Erosion results for the 1, 10, 100 and 475-year storms at Profile 5 in 2026 (top), 2046 (middle) and 2076 (bottom).

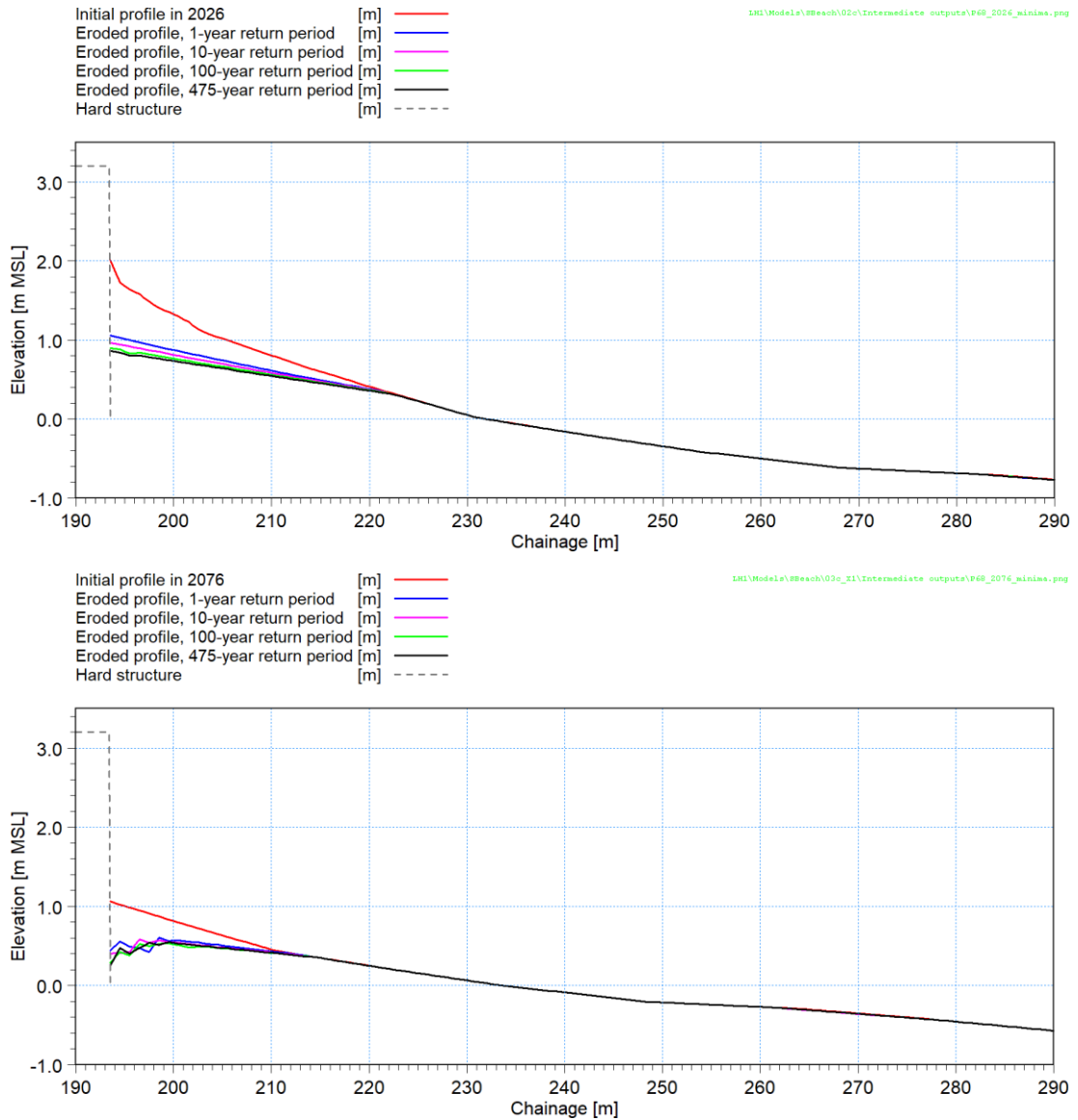


Figure B-5: Erosion results for the 1, 10, 100 and 475-year storms at Profile 6 in 2026 (top) and 2076 (bottom).

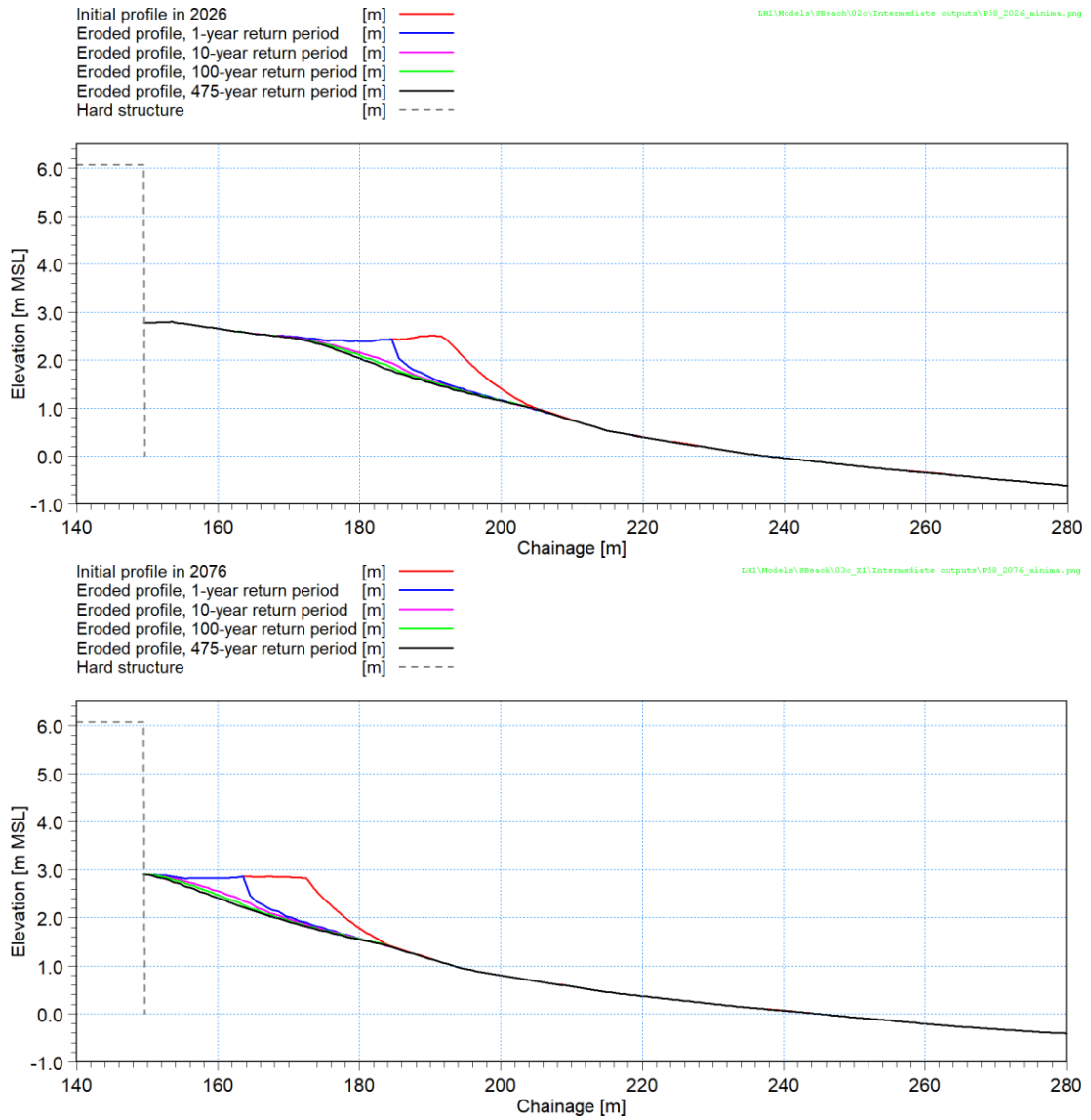


Figure B-6: Erosion results for the 1, 10, 100 and 475-year storms at Profile 7 in 2026 (top) and 2076 (bottom).



ANNEXURE C | EXTREME DESIGN CONDITIONS



TABLES

Page N°

Table C-1: Profile 1; design wave and water levels in front of rock revetment. 3

Table C-2: Profile 2; design wave and water levels in front of stepped revetment. 4

Table C-3: Profile 3; design wave and water levels in front of stepped revetment. 5

Table C-4: Profile 4; design wave and water levels in front of stepped revetment. 6

Table C-5: Profile 5; design wave and water levels in front of stepped revetment. 7

Table C-6: Pre-storm beach level and estimated local scour at the structure toe for the 1, 10, 100 and 475-year storms at Profile 2 in 2026, 2046 and 2076. 8

Table C-7: Pre-storm beach level and estimated local scour at the structure toe for the 1, 10, 100 and 475-year storms at Profile 3 in 2026, 2046 and 2076. 8

Table C-8: Pre-storm beach level and estimated local scour at the structure toe for the 1, 10, 100 and 475-year storms at Profile 4 in 2026, 2046 and 2076. 9

Table C-9: Pre-storm beach level and estimated local scour at the structure toe for the 1, 10, 100 and 475-year storms at Profile 5 in 2026, 2046 and 2076. 9



Table C-1: Profile 1; design wave and water levels in front of rock revetment.

Climate change horizon	Extreme condition				Bed level [m MSL]	Water level		Wave parameters				
	Joint return period [y]	Wave return period [y]	Wave steepness [-]	SWL return period [y]		Mean level [m MSL]	Max level [m MSL]	H _{max} [m]	H _{1/3} [m]	T _s [s]	No. Waves [-]	
2026	1	1	> 1/65	1	1.03	1.58	2.32	1.40	0.65	14.0	601	
		10		1	1.03	1.71	2.77	1.80	0.83	14.9	521	
	100	10		1	1.03	1.67	2.47	1.49	0.69	13.0	649	
		1		1	1.03	1.85	3.06	2.11	0.96	15.4	507	
	475	100		1	1.03	1.76	2.56	1.62	0.75	12.3	680	
		1		1	1.03	1.96	3.14	2.37	1.07	15.9	495	
	1	475		1	475	1.03	1.82	2.62	1.71	0.79	12.2	691
		1		1	1	1.03	1.58	2.14	1.47	0.68	16.0	525
	10	10		1	1	1.03	1.63	2.41	1.60	0.74	15.9	500
		1		10	1	1.03	1.66	2.46	1.63	0.75	15.6	538
	100	100		1	1	1.03	1.68	2.52	1.70	0.78	15.9	504
		1		100	1	1.03	1.75	2.55	1.78	0.82	15.6	552
	475	475		1	1	1.03	1.71	2.49	1.74	0.80	15.7	499
		1		475	475	1.03	1.81	2.69	1.89	0.86	15.3	560
2076	1	1	> 1/65	1	1.03	1.95	2.74	1.76	0.81	13.0	672	
		10		1	1.03	2.06	3.11	2.27	1.03	14.8	546	
	100	10		1	1.03	2.07	2.86	1.91	0.87	12.9	696	
		1		100	1	1.03	2.21	3.50	2.50	1.13	15.3	533
	475	100		1	100	1.03	2.17	2.97	2.05	0.93	12.5	707
		1		475	1	1.03	2.31	3.51	2.73	1.23	15.3	518
	1	475		1	475	1.03	2.24	3.04	2.13	0.97	12.5	716
		1		1	1	1.03	1.94	2.77	1.94	0.89	15.5	564
	10	10		1	1	1.03	1.99	2.84	2.11	0.96	15.9	533
		1		10	1	1.03	2.06	2.89	2.11	0.96	15.4	574
	100	100		1	1	1.03	2.03	2.88	2.20	1.00	15.7	505
		1		100	1	1.03	2.16	3.00	2.26	1.03	15.2	585
	475	475		1	1	1.03	2.07	2.93	2.18	0.99	15.2	520
		1		475	475	1.03	2.23	3.07	2.36	1.07	15.1	594



Table C-2: Profile 2; design wave and water levels in front of stepped revetment.

Climate change horizon	Extreme condition				Bed level [m MSL]	Water level		Wave parameters						
	Joint return period [y]	Wave return period [y]	Wave steepness [-]	SWL return period [y]		Mean level [m MSL]	Max level [m MSL]	H _{max} [m]	H _{1/3} [m]	T _s [s]	No. Waves [-]			
2026	1	1	> 1/65	1	0.48	1.53	2.09	1.39	0.65	11.7	618			
		10		1	0.50	1.62	2.36	1.86	0.85	14.0	502			
	100	1		10	0.44	1.64	2.22	1.51	0.70	11.8	643			
		1		1	0.46	1.73	2.55	2.09	0.95	14.9	480			
	475	1		100	0.40	1.74	2.34	1.63	0.75	11.6	665			
		1		1	0.45	1.80	2.51	2.24	1.02	15.1	477			
	1	1		< 1/65	1	0.50	1.51	2.11	1.57	0.73	15.1	517		
		10			1	0.52	1.55	2.16	1.70	0.78	15.5	496		
	100	1			10	0.45	1.63	2.25	1.75	0.81	14.8	534		
		1			1	0.51	1.60	2.23	1.82	0.84	15.6	467		
	475	1			100	0.44	1.73	2.36	1.87	0.85	14.2	550		
		1			1	0.51	1.62	2.22	1.80	0.83	14.8	473		
	2076	1			1	> 1/65	1	0.32	1.95	2.55	1.71	0.79	11.7	650
					10		1	0.32	2.04	2.81	2.35	1.07	14.5	521
100		1	10		0.32		2.06	2.69	1.91	0.87	12.0	671		
		1	1		0.28		2.15	3.07	2.44	1.11	14.1	516		
475		1	100		0.32		2.16	2.79	2.08	0.95	11.9	690		
		1	1		0.32		2.21	2.98	2.59	1.17	14.3	527		
1		1	< 1/65		1		0.33	1.93	2.57	1.99	0.91	14.8	557	
		10			1		0.32	1.98	2.64	2.16	0.98	15.1	527	
100		1		10	0.29		2.05	2.69	2.15	0.98	14.5	564		
		1		1	0.33		2.01	2.67	2.27	1.03	15.0	496		
475		1		100	0.31		2.15	2.79	2.31	1.05	14.4	580		
		1		1	0.33		2.04	2.69	2.24	1.02	14.4	504		
1		1		475	0.35		2.22	2.85	2.37	1.07	13.8	597		



Table C-3: Profile 3; design wave and water levels in front of stepped revetment.

Climate change horizon	Extreme condition				Bed level [m MSL]	Water level		Wave parameters						
	Joint return period [y]	Wave return period [y]	Wave steepness [-]	SWL return period [y]		Mean level [m MSL]	Max level [m MSL]	H _{max} [m]	H _{1/3} [m]	T _s [s]	No. Waves [-]			
2026	1	1	> 1/65	1	0.68	1.53	2.10	1.25	0.59	13.2	576			
		10		1	0.71	1.62	2.33	1.66	0.77	13.7	485			
	100	1		10	0.66	1.64	2.21	1.37	0.64	11.8	608			
		1		1	0.64	1.72	2.55	1.98	0.90	15.0	454			
	475	1		100	0.59	1.75	2.34	1.45	0.67	12.0	624			
		1		1	0.55	1.80	2.44	2.05	0.94	15.0	466			
	1	1		< 1/65	1	0.70	1.52	2.05	1.35	0.63	15.3	502		
		10			1	0.73	1.55	2.11	1.48	0.69	15.7	480		
	100	1			10	0.64	1.64	2.22	1.47	0.68	15.1	512		
		1			1	0.69	1.59	2.21	1.61	0.74	15.5	458		
	475	1			100	0.61	1.74	2.34	1.64	0.76	14.6	532		
		1			1	0.65	1.63	2.23	1.62	0.75	15.3	460		
	2076	1			1	> 1/65	1	0.60	1.95	2.54	1.56	0.72	11.7	622
					10		1	0.57	2.04	2.81	2.06	0.94	13.5	516
100		1	10		0.56		2.07	2.68	1.69	0.78	11.6	643		
		1	1		0.49		2.16	3.06	2.26	1.03	14.5	493		
475		1	100		0.52		2.17	2.80	1.89	0.87	12.0	650		
		1	1		0.47		2.23	3.01	2.41	1.09	14.6	498		
1		1	< 1/65		1		0.48	1.95	2.55	1.65	0.76	14.9	533	
		10			1		0.60	1.98	2.61	1.86	0.85	15.2	507	
100		1		10	0.52		2.06	2.68	1.92	0.88	14.7	542		
		1		1	0.58		2.02	2.62	1.99	0.91	14.9	478		
475		1		100	0.53		2.16	2.79	2.09	0.95	14.5	552		
		1		1	0.54		2.05	2.68	2.06	0.94	14.5	490		
1		1		475	0.52		2.23	2.87	2.18	0.99	14.5	557		



Table C-4: Profile 4; design wave and water levels in front of stepped revetment.

Climate change horizon	Extreme condition				Bed level [m MSL]	Water level		Wave parameters						
	Joint return period [y]	Wave return period [y]	Wave steepness [-]	SWL return period [y]		Mean level [m MSL]	Max level [m MSL]	H _{max} [m]	H _{1/3} [m]	T _s [s]	No. Waves [-]			
2026	1	1	> 1/65	1	0.59	1.52	2.07	1.34	0.62	12.4	591			
		10		10	1	0.60	1.61	2.33	1.80	0.82	13.8	496		
	100	1		10	0.56	1.64	2.20	1.43	0.67	11.7	621			
		100		1	0.61	1.71	2.49	2.01	0.92	15.0	465			
	475	1		100	0.49	1.74	2.31	1.54	0.71	11.5	637			
		475		1	0.59	1.78	2.53	2.19	1.00	15.2	472			
	1	1		< 1/65	1	0.58	1.51	2.08	1.49	0.69	15.1	511		
		10			10	1	0.61	1.56	2.13	1.61	0.74	15.8	479	
	100	1			10	0.56	1.63	2.21	1.62	0.75	14.8	523		
		100			1	0.62	1.59	2.21	1.73	0.80	15.4	461		
	475	1			100	0.51	1.73	2.34	1.77	0.81	14.3	535		
		475			1	0.58	1.62	2.21	1.68	0.77	14.9	466		
	2076	1			1	> 1/65	1	0.47	1.95	2.54	1.65	0.76	11.9	641
					10		10	1	0.46	2.04	2.82	2.19	0.99	13.9
		100			1		10	0.43	2.07	2.68	1.77	0.81	11.7	650
					100		1	0.46	2.15	3.04	2.38	1.08	14.6	501
475		1	100		0.42		2.17	2.82	2.01	0.92	12.1	656		
		475	1		0.45		2.23	3.06	2.56	1.16	14.8	497		
1		1	< 1/65		1		0.43	1.94	2.52	1.78	0.82	14.0	550	
		10			10		1	0.49	1.98	2.61	2.05	0.93	15.3	510
100		1			10		0.40	2.06	2.66	1.95	0.89	14.0	563	
		100			1		0.46	2.01	2.63	2.15	0.98	14.7	483	
475		1		100	0.39		2.16	2.83	2.27	1.03	14.7	554		
		475		1	0.46		2.04	2.67	2.13	0.97	14.5	494		
1		1		475	0.42		2.23	2.87	2.22	1.01	14.0	571		



Table C-5: Profile 5; design wave and water levels in front of stepped revetment.

Climate change horizon	Extreme condition				Bed level [m MSL]	Water level		Wave parameters					
	Joint return period [y]	Wave return period [y]	Wave steepness [-]	SWL return period [y]		Mean level [m MSL]	Max level [m MSL]	H _{max} [m]	H _{1/3} [m]	T _s [s]	No. Waves [-]		
2026	1	1	> 1/65	1	0.57	1.52	2.02	1.35	0.63	11.9	604		
		10		1	0.58	1.61	2.32	1.86	0.85	13.7	507		
	100	1		10	0.54	1.64	2.17	1.47	0.68	11.6	637		
		1		1	0.59	1.70	2.48	2.05	0.94	14.5	479		
	475	1		100	0.48	1.74	2.30	1.61	0.74	11.4	652		
		1		1	0.58	1.76	2.52	2.24	1.02	14.8	485		
	10	1		475	0.46	1.81	2.38	1.71	0.79	11.5	663		
		1		1	0.60	1.51	2.03	1.49	0.69	14.7	514		
	100	1		10	< 1/65	1	0.57	1.55	2.12	1.70	0.78	15.3	492
		1		10		1	0.50	1.63	2.21	1.74	0.80	14.7	523
		1		100		1	0.60	1.58	2.17	1.83	0.84	15.5	463
		1		1		100	0.48	1.73	2.34	1.88	0.86	14.3	542
		1		475		1	0.60	1.61	2.17	1.82	0.83	14.9	469
		1		1		475	0.42	1.80	2.41	1.94	0.89	14.0	550
2076	1	1	> 1/65	1	0.40	1.94	2.55	1.73	0.80	11.6	641		
		10		1	0.40	2.03	2.79	2.31	1.05	14.0	525		
	100	1		10	0.38	2.06	2.69	1.94	0.89	11.9	661		
		1		1	0.41	2.14	3.04	2.43	1.10	14.2	519		
	475	1		100	0.39	2.16	2.80	2.05	0.94	11.9	685		
		1		1	0.39	2.22	3.03	2.64	1.19	14.4	519		
	10	1		475	0.40	2.23	2.88	2.18	0.99	11.7	699		
		1		1	0.37	1.94	2.54	1.90	0.87	14.1	554		
	100	1		10	< 1/65	1	0.38	1.98	2.61	2.09	0.95	14.6	524
		1		10		1	0.37	2.05	2.70	2.21	1.00	14.5	556
		1		100		1	0.39	2.01	2.65	2.26	1.03	14.4	502
		1		1		100	0.36	2.15	2.82	2.38	1.08	14.0	565
	475	1		475	1	0.38	2.04	2.67	2.16	0.98	14.0	508	
		1		1	475	0.40	2.22	2.88	2.42	1.10	13.9	595	



Table C-6: Pre-storm beach level and estimated local scour at the structure toe for the 1, 10, 100 and 475-year storms at Profile 2 in 2026, 2046 and 2076.

Climate change horizon	Joint return period [y]	Pre-storm beach level at structure toe [m MSL]	Maximum scour depth at structure toe [m]				Local scour level at structure toe ^(a,b) [m MSL]					
			SPM	Herbich	Steetzel	SBEACH	SPM	Herbich	Steetzel	SBEACH	Max scour level	Min scour level
2026	1	1.20	0.33	0.20	0.24	1.10	0.87	1.00	0.96	0.10	1.00	0.10
	10	1.20	0.44	0.26	0.33	1.20	0.76	0.94	0.87	0.00	0.94	0.00
	100	1.20	0.54	0.32	0.41	1.30	0.66	0.88	0.79	-0.10	0.88	-0.10
	475	1.20	0.61	0.36	0.46	1.37	0.59	0.84	0.74	-0.17	0.84	-0.17
2046	1	1.05	0.67	0.40	0.51	1.10	0.38	0.65	0.54	-0.05	0.65	-0.05
	10	1.05	0.79	0.47	0.59	1.17	0.26	0.58	0.46	-0.12	0.58	-0.12
	100	1.05	0.89	0.53	0.67	1.25	0.16	0.52	0.38	-0.20	0.52	-0.20
	475	1.05	0.96	0.57	0.72	1.29	0.09	0.48	0.33	-0.24	0.48	-0.24
2076	1	0.75	1.20	0.72	0.90	1.09	-0.45	0.03	-0.15	-0.34	0.03	-0.45
	10	0.75	1.31	0.79	0.98	1.24	-0.56	-0.04	-0.23	-0.49	-0.04	-0.56
	100	0.75	1.41	0.85	1.06	1.25	-0.66	-0.10	-0.31	-0.50	-0.10	-0.66
	475	0.75	1.48	0.89	1.11	1.25	-0.73	-0.14	-0.36	-0.50	-0.14	-0.73

Notes:

(a) Based on the geotechnical information the bedrock is estimated at -0.5 m MSL

(b) It is recommended that the minimum scour level from all the methods should be used for design. The design process should also consider the proposed additional 0.5 m allowance for uncertainties in the methodologies and unquantified 2D effects and assess the associated design implications.

Table C-7: Pre-storm beach level and estimated local scour at the structure toe for the 1, 10, 100 and 475-year storms at Profile 3 in 2026, 2046 and 2076.

Climate change horizon	Joint return period [y]	Pre-storm beach level at structure toe [m MSL]	Maximum scour depth at structure toe [m]				Local scour level at structure toe ^(a,b) [m MSL]					
			SPM	Herbich	Steetzel	SBEACH	SPM	Herbich	Steetzel	SBEACH	Max scour level	Min scour level
2026	1	1.15	0.38	0.23	0.29	0.67	0.77	0.92	0.86	0.48	0.92	0.48
	10	1.15	0.49	0.30	0.37	0.72	0.66	0.85	0.78	0.43	0.85	0.43
	100	1.15	0.60	0.36	0.45	0.90	0.55	0.79	0.70	0.25	0.79	0.25
	475	1.15	0.66	0.40	0.50	0.95	0.49	0.75	0.65	0.20	0.75	0.20
2046	1	1.04	0.67	0.40	0.51	0.66	0.37	0.64	0.53	0.38	0.64	0.37
	10	1.04	0.79	0.47	0.59	0.79	0.25	0.57	0.45	0.25	0.57	0.25
	100	1.04	0.89	0.54	0.67	0.90	0.15	0.50	0.37	0.14	0.50	0.14
	475	1.04	0.96	0.58	0.72	0.99	0.08	0.46	0.32	0.05	0.46	0.05
2076	1	0.84	1.11	0.67	0.83	0.67	-0.27	0.17	0.01	0.17	0.17	-0.27
	10	0.84	1.23	0.74	0.92	0.80	-0.39	0.10	-0.08	0.04	0.10	-0.39
	100	0.84	1.33	0.80	1.00	0.92	-0.49	0.04	-0.16	-0.08	0.04	-0.49
	475	0.84	1.40	1.45	1.32	1.01	-0.56	0.00	-0.21	-0.17	0.00	-0.56

Notes:

(a) Based on the geotechnical information the bedrock is estimated at -0.75 m MSL

(b) It is recommended that the minimum scour level from all the methods should be used for design. The design process should also consider the proposed additional 0.5 m allowance for uncertainties in the methodologies and unquantified 2D effects and assess the associated design implications.



Table C-8: Pre-storm beach level and estimated local scour at the structure toe for the 1, 10, 100 and 475-year storms at Profile 4 in 2026, 2046 and 2076.

Climate change horizon	Joint return period [y]	Pre-storm beach level at structure toe [m MSL]	Maximum scour depth at structure toe [m]				Local scour level at structure toe ^(a,b) [m MSL]					
			SPM	Herbich	Steetzel	SBEACH	SPM	Herbich	Steetzel	SBEACH	Max scour level	Min scour level
2026	1	1.35	0.17	0.10	0.13	1.07	1.18	1.25	1.22	0.28	1.25	0.28
	10	1.35	0.29	0.17	0.22	1.17	1.06	1.18	1.13	0.18	1.18	0.18
	100	1.35	0.39	0.24	0.29	1.34	0.96	1.11	1.06	0.01	1.11	0.01
	475	1.35	0.46	0.28	0.35	1.32	0.89	1.07	1.00	0.03	1.07	0.03
2046	1	1.11	0.57	0.34	0.43	1.01	0.54	0.77	0.68	0.10	0.77	0.10
	10	1.11	0.69	0.41	0.52	1.09	0.42	0.70	0.59	0.02	0.70	0.02
	100	1.11	0.79	0.47	0.59	1.11	0.32	0.64	0.52	0.00	0.64	0.00
	475	1.11	0.86	0.52	0.64	1.11	0.25	0.59	0.47	0.00	0.59	0.00
2076	1	0.78	1.17	0.70	0.87	0.78	-0.39	0.08	-0.09	0.00	0.08	-0.39
	10	0.78	1.29	0.77	0.96	0.87	-0.51	0.01	-0.18	-0.09	0.01	-0.51
	100	0.78	1.39	0.83	1.04	1.09	-0.61	-0.05	-0.26	-0.31	-0.05	-0.61
	475	0.78	1.46	0.87	1.09	1.15	-0.68	-0.09	-0.31	-0.37	-0.09	-0.68

Notes:

(a) Based on the geotechnical information the bedrock is estimated at -1.3 m MSL

(b) It is recommended that the minimum scour level from all the methods should be used for design. The design process should also consider the proposed additional 0.5 m allowance for uncertainties in the methodologies and unquantified 2D effects and assess the associated design implications.

Table C-9: Pre-storm beach level and estimated local scour at the structure toe for the 1, 10, 100 and 475-year storms at Profile 5 in 2026, 2046 and 2076.

Climate change horizon	Joint return period [y]	Pre-storm beach level at structure toe [m MSL]	Maximum scour depth at structure toe [m]				Local scour level at structure toe ^(a,b) [m MSL]					
			SPM	Herbich	Steetzel	SBEACH	SPM	Herbich	Steetzel	SBEACH	Max scour level	Min scour level
2026	1	1.37	0.15	0.09	0.11	1.15	1.22	1.28	1.26	0.22	1.28	0.22
	10	1.37	0.27	0.16	0.20	1.24	1.10	1.21	1.17	0.13	1.21	0.13
	100	1.37	0.37	0.22	0.28	1.34	1.00	1.15	1.09	0.03	1.15	0.03
	475	1.37	0.44	0.26	0.33	1.37	0.93	1.11	1.04	0.00	1.11	0.00
2046	1	1.10	0.54	0.32	0.40	1.04	0.56	0.78	0.70	0.06	0.78	0.06
	10	1.10	0.66	0.39	0.49	1.10	0.44	0.71	0.61	0.00	0.71	0.00
	100	1.10	0.76	0.46	0.57	1.10	0.34	0.64	0.53	0.00	0.64	0.00
	475	1.10	0.83	0.50	0.62	1.13	0.27	0.60	0.48	-0.03	0.60	-0.03
2076	1	0.82	1.12	0.67	0.84	0.89	-0.30	0.15	-0.02	-0.07	0.15	-0.30
	10	0.82	1.24	0.74	0.93	1.03	-0.42	0.08	-0.11	-0.21	0.08	-0.42
	100	0.82	1.34	0.81	1.01	1.24	-0.52	0.01	-0.19	-0.42	0.01	-0.52
	475	0.82	1.41	0.85	1.06	1.39	-0.59	-0.03	-0.24	-0.57	-0.03	-0.59

Notes:

(a) Based on the geotechnical information the bedrock is estimated lower than -10 m MSL

(b) It is recommended that the minimum scour level from all the methods should be used for design. The design process should also consider the proposed additional 0.5 m allowance for uncertainties in the methodologies and unquantified 2D effects and assess the associated design implications.